PROCEEDINGS OF THE WORKSHOP ON HIGH TEMPERATURE SOLID OXIDE FUEL CELLS

May 5-6, 1977

Brookhaven National Laboratory
Upton, N.Y. 11973

WORKSHOP COMMITTEE AND PROCEEDINGS EDITORS
H.S. Isaacs, S. Srinivasan, and I.L. Harry

BROOKHAVEN NATIONAL LABORATORY
ASSOCIATED UNIVERSITIES, INC.
UNDER CONTRACT NO. EY-76-C-02-0016 WITH THE
UNITED STATES ENERGY RESEARCH AND DEVELOPMENT ADMINISTRATION

DISCLAIMER

BNL 50756
UC-93
(Energy Conversion - TID-4500)

PROCEEDINGS OF THE WORKSHOP ON

HIGH TEMPERATURE SOLID OXIDE FUEL CELLS

May 5-6, 1977

Brookhaven National Laboratory
Upton, N.Y. 11973

WORKSHOP COMMITTEE AND PROCEEDINGS EDITORS
H.S. Isaacs, S. Srinivasan, and I.L. Harry*

*U.S. Department of Energy, Washington, D.C.

Sponsored by the
DIVISION OF POWER SYSTEMS
UNITED STATES DEPARTMENT OF ENERGY
WASHINGTON, D.C.

BROOKHAVEN NATIONAL LABORATORY
UPTON, NEW YORK 11973

NOTICE

Printed in the United States of America
Available from
National Technical Information Service
U.S. Department of Commerce
5285 Port Royal Road
Springfield, VA 22161
Price: Printed Copy $9.25; Microfiche $3.00

April 1978 415 copies

TABLE OF CONTENTS

*Presentations given both in panel and formal sessions.

Table of Contents (Cont'd) Page

*Presentations given both in panel and formal sessions.

Table of Contents (Cont'd) Page

Table of Contents (Cont'd) Page

*Paper distributed to participants after Workshop.

FOREWORD

High efficiencies of close to 60% have been projected for the conversion of coal to electricity with solid oxide fuel cells and a bottoming cycle. The high efficiencies make these systems attractive for future coal consuming power plants and have led to renewed research and development efforts in solid oxide electrolyte fuel cells. In view of these developments, the Division of Power Systems of the U.S. Department of Energy requested that a Workshop be held to determine the state of the technology of the solid oxide electrolyte fuel cells and provide recommendations for future research and development, leading to the development of coal-based solid electrolyte fuel cells.

The emphasis of the Workshop was to determine the state of the technology and needed research of only the fuel cell and its components, i.e., the electrodes, the electrolyte, and the interconnection material. Aspects concerning coal gasifers, and the impurity levels in the gases, were not considered at this Workshop but will require future attention. The Workshop was held on May 5-6, 1977 and was attended by 55 representatives from industries and academic institutions from five countries. The first day of the Workshop was devoted to formal presentations. On the second day, panel sessions on "Electrolytes", "Interconnection Materials", and "Electrodes" were arranged to consider, in detail, the present state of understanding the deficiencies in the areas of electrodes, electrolytes, and interconnection materials. Professors A. S. Nowick, G. P. Wirtz, and T. H. Etsell served as chairmen of these three panels, respectively.

Advances in solid electrolyte fuel cell technology will require a multidisciplinary approach to produce an electrical generator with life times over 40,000 hours. Previous developments have indicated that large systems are conceivable and the shortcomings in previous designs or materials can be overcome with foreseeable technological advances.

It is hoped that the Proceedings of the Workshop will stimulate interest in research and development of solid oxide fuel cells and assist in guiding future technological investigations.

The organizers wish to acknowledge the assistance of Mrs. Virginia Sayre and Mrs. Dorothy Schroeder in making the necessary arrangements for the Workshop. Special thanks are also due to Ms. Debra Abruzzo for her devoted efforts in the organization of and during the Workshop.

THIS PAGE

WAS INTENTIONALLY

LEFT BLANK

RECOMMENDATIONS OF THE WORKSHOP

The workshop proceedings summarize the status of components technology development of high temperature solid oxide electrolyte fuel cells which show promise of being the energy conversion device in highly efficient coal-fed power plants. Many of the limitations, encountered in the past, with solid electrolyte fuel cells have been assessed and materials and processes are available for the fabrication of interconnected fuel cells. Areas identified, during presentations and panel discussions, for specific future developments and investigations yield the basis for the recommendations of the workshop. The recommendations are presented below by subject matter and are not intended to reflect specific orders of priority.

1. Future work should emphasize electrolytes supported on a porous substrate. The increase in efficiency of the fuel cells depends on reducing the resistance of the electrolyte, which can be accomplished by using thinner electrolytes. The use of supported electrolytes with thicknesses below 50 μm can be used, whereas unsupported or free-standing cells will require significantly thicker electrolytes to maintain mechanical strength.

2. There is a need to determine the factors which will lead to higher conducting electrolytes including the role of dopant valency, ionic size, and concentrations on the resistivity of the electrolyte.

3. The most successful method for producing the supported electrolyte layers has been by electrochemical vapor deposition. Investigations should be carried out to characterize the minimum thickness of a pore-free electrolyte, the dependence on surface properties of the substrate, and development of defects during operation. Other methods of producing electrolyte layers plasma spraying, ion implantation, and sintering techniques will also have to be examined.

4. The effects of electronic conduction in the electrolytes (notably for CeO_2-based ceramics) on the fuel-cell efficiencies, kinetics, and losses require further consideration. Theory should be compared with experimental observations in integrated solid electrolyte fuel cells, incorporating a fuel and air electrode where direct testing of the influence of electronic conduction can be carried out.

5. Methods to reduce polarization overvoltages at the electrode/electrolyte interface should be developed. At present, even with relatively thick electrolyes (~0.5 mm), the polarization losses are

about 30% of the total voltage losses. The relative contribution of the interfacial losses, which are independent of electrolyte thickness, will increase as the electrolyte thickness decreases and could dominate the loss in efficiency of the cells. A wide range of cathode materials has been considered and future work should characterize these materials and determine the factors which will reduce the overvoltage.

6. Techniques for depositing interconnection materials will require further development. Long-term studies should be started on multicell structures to test the stability of the materials in an actual environment in addition to the methods of production.

7. There is a definite lack of information on diffusion rates of cations and anions in the interconnection materials or cathodes. The information is required to determine material migration with pore formation or increased interfacial resistances and compatibility of components. Oxygen diffusion rates in the cathode material will influence the electrode kinetics.

8. Compatibility of the electrodes, electrolytes, and interconnection materials, should be determined under potential gradients with current fluxes to determine any tendency for induced migration.

9. The effects of impurities, in coal-derived fuels, on fuel cell performance should be investigated. Sulfur containing impurities and ash could lead to degradation of the nickel fuel electrodes and sealing of pores in a porous substrate.

I. PANEL SESSION SUMMARIES AND PRESENTATIONS

THIS PAGE

WAS INTENTIONALLY

LEFT BLANK

A. ELECTROLYTES

1. Summary of Panel Session on Electrolytes
   A. S. Nowick, Columbia University

2. A Review of Experimental Electrical and Electrochemical Methods
   R. A. Rapp, Ohio State University

3. A Useful Model for Understanding the Performance Characteristics of Oxide Solid Electrolyte Fuel Cells
   J. W. Patterson, Iowa State University

4. Phase Relationship and Ordering in ZrO_2-CaO and ZrO_2-Y_2O_3 Systems
   S. P. Ray, V. S. Stubican, Pennsylvania State University

5. Defect Interactions
   A. S. Nowick, Columbia University

6. Other Oxide Electrolytes
   M. P. Anderson, Columbia University

SUMMARY OF PANEL SESSION ON ELECTROLYTES

A. S. Nowick, Panel Chairman
Columbia University

The exploration of this topic of solid oxide electrolytes presupposes that we are not completely satisfied with ZrO_2:Y_2O_3 as a solid electrolyte for fuel cells and are interested in seeking different materials which will show higher conductivities, or at least, make it possible to attain the same conductivities at lower temperatures. The benefits of dropping the operating temperature of a high temperature fuel cell to the range 500°-700°C are quite considerable, as has often been pointed out in the literature. For one thing, it can ease some of the demands on electrode and interconnection materials.

In order to determine in which directions to go for better electrolytes, we need to know what are the factors that control the conductivity. A number of these factors have been discussed by members of this panel. Some of the important questions that we cannot yet answer completely are:

a) Why is the conductivity generally higher for trivalent dopants, e.g. Y^{3+}, than for divalents, e.g. Ca^{2+}?

b) What role is played by the ionic size of the dopant, and is there any other factor than the size and valence of the dopant that determines the electrical properties?

c) What is the defect structural unit or interaction effect that is responsible for the existence of a maximum in conductivity as a function of dopant concentration?

A broader question is whether we can apply what we have learned about fluorite-type oxides to select possible oxygen-ion conductors from among other oxide materials.

Perhaps the most controversial question arising at this meeting concerns the role of electronic conduction in limiting fuel-cell behavior, and just how much electronic conduction can be tolerated. It appears that this question is first beginning to be examined with care, and for the first time, the arbitrary requirement of an ionic transference number, t_i, of 0.99 over all oxygen partial pressures is being questioned. Thus, Dr. Patterson in the present panel, has suggested that lower t_i values might be acceptable as a trade-off against other favorable properties.

In a recent (unpublished) paper, D.S. Tannhauser has arrived at a similar conclusion from a somewhat different viewpoint. This conclusion has been challenged, however, by other members of this workshop, and a final resolution of the question remains to be achieved.

As various members of the panel have shown; the techniques for the study of solid oxide electrolytes are quite numerous and varied, and involve much more than the mere measurement of conductivity at one frequency or under d-c conditions. It is only by applying these varied techniques that we can understand the defect chemistry of these materials. It is clear from what we have heard that there is much good science in such studies, as well as the potential practical achievement of improved electrolytes for fuel cells.

A Review of Experimental Electrical and Electrochemical Methods

Robert A. Rapp
Ohio State University

A knowledge of the partial ionic and electronic conductivities, and their component carrier concentrations and mobilities as a function of the oxygen partial pressure, dopant concentration, and temperature represents a minimum "classical" description of an oxide electrolyte conductivity (1). For sufficiently high temperatures, a P_{O_2}-independent a.c. total conductivity may be independent of frequency for two, three, or four electrode arrangements of noble metal electrodes in a defined gaseous environment. This P_{O_2}-independent ionic conductivity measurement, however, masks the lower-magnitude p- and n-type partial electronic conductivities. These electronic conductivities are separately established through a Hebb-Wagner d.c. polarization measurement, involving a reversible electrode to define a known P_{O_2} and an ion-blocking (non-reversible) electrode. A stagnant liquid metal, enclosed in an electrolyte tube represents an excellent blocking electrode (2). The resulting polarization data of steady-state electronic current vs applied voltage are best treated by a Patterson-plot (3) which allows the simultaneous determination of both the p-type and n-type conductivity at the oxygen activity corresponding to the reference electrode. A three-dimensional drawing of the "electrolytic domain"(4) assists the classical description of electrolyte conductivity. The study of the kinetics of relaxation of a polarized electrolyte is limited by the diffusion of electrons and holes and can be used to establish the electron and hole mobilities and therefore their concentrations (5).

Open-circuit measurements of the voltage of galvanic cells for electrodes with differing oxygen chemical potentials should be consistent with Wagner's classic theory (6) and Schmalzried's evaluation of the transference number as a function of oxygen activity (7). Again, liquid metals polarized to steady-state by applied voltages provide electrodes of known oxygen activity for a measurement of open-circuit voltages by a third reference electrode. In

a gaseous environment, the relaxation of the potential of a polarized point electrode will identify the electrode potentials where redox reactions are possible (8).

To discern further information about the equivalent electrical circuit of an electrolyte/electrode combination, the trace of the complex impedance (or admittance) diagram introduced by Bauerle (9), may provide a separation of processes inherent to the electrode and those specific to the electrolyte. In this method, by variation of the temperature, of electrode materials and gaseous environments, and by the study the aging behavior of the sytem, a more refined electrochemical description of the system can result (10).

References

1. R.A. Rapp and D.A. Shores, "Solid Electrolyte Cells", Ch. in Techniques of Metals Research, Vol. IV, part 2, R. Rapp Ed., Wiley Publ., (1973).

2. L.M. Friedman, K.E. Oberg, W.M. Boorstein and R.A. Rapp, Metall. Trans. 4, 69 (1973).

3. J.W. Patterson, E.C. Bogren, and R.A. Rapp, J. Electrochem. Soc. 114, 752 (1967).

4. J.W. Patterson, "Ionic Conductivity and Electrochemistry of Crystalline Ceramics", Ch. in Electrical Conductivity in Ceramics and Glasses, N. Tallan Ed., Dekker Publ. (1971).

5. K. Weiss, Z. physik. Chem. N.F., 59, 242 (1968).

6. C. Wagner, Z. phys. Chem. B21, 25 (1933).

7. H. Schmalzried, Z. phys. Chem. 38, 87 (1963).

8. P. Fabry, M. Kleitz and C. Deportes, J. Sol. State Chem. 5, (1972).

9. J.E. Bauerle, J. Phys. Chem. Solids 30, 2657 (1969).

10. E. Schouler, M. Kleitz and C. Deportes, J. Chim. Phys. 70, (1973) 923.

A USEFUL MODEL FOR UNDERSTANDING THE PERFORMANCE CHARACTERISTICS OF SOLID OXIDE ELECTROLYTE FUEL CELLS

John W. Patterson
Engineering Research Institute
Professor of Materials Science & Engineering
Iowa State University
Ames, Iowa 50010

I. Introduction

The purpose here is to describe a simple model for an oxide solid electrolyte which demonstrates its most important features in relation to fuel cell performance. The model also divides these considerations into different regimes which can in large measure be addressed separately. The result is a view of fuel cells that facilitates an organized approach to assessing the performance of existing systems and bringing more clearly into focus the areas in which future research should be dedicated.

Some of the "knotty" questions that can be clarified by the approach outlined below are the following:

A) What would be the effect on the performance of an oxide fuel cell if hydrogen (1,2) or some other foreign ingredient were to become incorporated in the electrolyte as a mobile charged species?
B) To what extent will the inherent electronic conductivity of oxide electrolytes compromise the performance of a fuel cell system? Internal electronic conduction is ordinarily neglected in analyses of fuel cell and battery systems even though its existence has been documented (3).
C) What is the maximum power that can be delivered by a given oxide electrolyte; how does this depend on the ionic and electronic transport properties of the electrolyte and what is the efficiency when operating under maximum power?
D) How do electrode polarization losses enter into the evaluation of cell performance?
E) How can one calculate the efficiency of a fuel cell for a given dc load condition and what is the maximum efficiency that can be achieved by a given solid electrolyte?
F) How would the foregoing factors affect the process by which an oxide electrolyte fuel cell can be driven backwards (in the charging mode) in order to extract pure oxygen and generate hydrogen gas from steam as in the GE electrolysis process?

The dc analog circuit to be described below is an extension of the one given by Choudhury and Patterson (4,5) and of that inherent in the Hoar-Price(6) "electrochemical interpretation" of Wagners theory of

tarnishing reactions (7). Before going into those matters, however, it is appropriate to outline some of the basic concepts involved and some of the underlying assumptions.

II. Basic Concepts

Consider the generalized electrochemical cell shown in Figure 1 in which electrons e in addition to the k ionic species i = 1,2,3,...,k are all considered to be mobile. The chemical potentials of these species (in joules/mol) are represented by μ_i; i = 1,2,3,...k, e with the end point values being denoted by μ_i' (I = 0) and μ_i''.

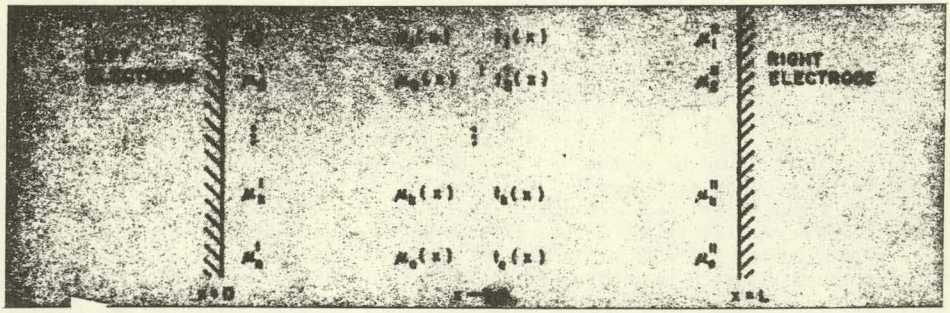

Figure 1. Schematic representation of a generalized electrochemical cell.

Following the analysis given by MacInnes (7), we arrive at the following expression for the reversible open circuit emf E which would appear over the left and right electrodes:

$$E = \sum_{i=1}^{k,e} \int_{\mu_i' (I=0)}^{\mu_i'' (I=0)} \frac{t_i^\circ}{(-Z_i \mathfrak{F})} \, d\mu_i \qquad [1]$$

where Z_i is the valence of the i th species ($Z_i < 0$ for anions and electrons and $Z_i > 0$ for cations), the Faraday $\mathfrak{F}$ is 96,500 coul and t_i° is the open circuit transference number (fractional conductivity) for species i and is dimensionless. To expedite simple interpretations, the mean value theorem of integral calculus is invoked to recast equation [1] into the following "weighted average" format:

$$E = \sum_{1}^{k,e} \langle t_i^\circ \rangle \; V_i^\circ \qquad [2]$$

Each V_i° plays the role of a thermodynamic (open circuit) voltage whose value in volts is given by

$$V_i^\circ = \int_{\mu_i' \; (I=0)}^{\mu_i'' \; (I=0)} \frac{d\mu_i}{(-z_i \mathfrak{F})} = \frac{\mu_i'' - \mu_i'}{(-z_i \mathfrak{F})} \qquad [3]$$

and clearly each $\langle t_i^\circ \rangle$ is simply the open circuit transference number of the i th mobile species averaged over the entire electrolyte.

To be sure, equation [1] - on which equations [2] and [3] are based - was derived by contemplating the reversible passage of $\mathfrak{F}$ = 96,500 coulombs through the cell. It is postulated here, however, that the same kind of relation can also be used to characterize the chemical forces which drive cells under non-reversible conditions - such as prevail when an external current flows. Under these circumstances, of course, the values of μ_i'' and μ_i' may be somewhat altered (electrode polarization effects, etc) and this should be emphasized by replacing the effective open circuit voltages V_i° in equations [2] and [3] with the altered values V_i where the super "zero" has been deliberately dropped. Similarly, the transference numbers t_i° should be replaced by (non-superscripted) t_i's in case loading inflicts a significant perturbation on the various partial conductivities. Accordingly, the following expression is proposed to characterize the active driving forces in cells operating under non-reversible conditions (load or charging)

$$V = \Sigma t_i V_i = t_1 V_1 + t_2 V_2 + \ldots t_k V_k + t_e V_e \quad . \qquad [4]$$

In this equation, the contributing voltages V_i are given by

$$V_i = \frac{\mu_i'' - \mu_i'}{(-z_i \mathfrak{F})} \qquad i = 1,2,3, \ldots k,e \quad . \qquad [5]$$

They represent the thermochemical driving force acting on each mobile species. Under load conditions these voltages will drop a bit from their respective open circuit values because polarization effects at the electrodes will cause the chemical potentials μ_i'' and μ_i' to shift slightly toward each other. Thus, in the present picture, electrode polarization effects only serve to influence the value of V that prevails in a given situation and hence are considered as a totally separate issue. By using the perturbed value of V in the analysis, the results remain valid for any V that may eventuate. That way, polarization effects can be incorporated at some later time when their impact on V can be characterized quantitatively.

In accordance with the traditional definition of transference numbers as fractional conductivity ratios, we may represent t_i with any one of the following equivalent formulas:

$$t_i = \sigma_i / \sum_{1}^{k} \sigma_i = \sigma_i / \sigma_T \qquad [6]$$

$$= G_i / \Sigma G_i = G_i / G_T \qquad [7]$$

$$= \frac{1}{R_i} / \Sigma \frac{1}{R_i} = \frac{1}{R_i} / \frac{1}{R_T} \qquad [8]$$

where the usual interrelationships relate the specific conductivity σ, conductance G and resistance R as follows:

$$R \equiv \frac{1}{G} \equiv \frac{1}{\sigma} \frac{L}{A} \qquad [9]$$

III. Equivalent Circuit Analysis

The value of the proposals put forward in Section II is that the essence of equations [2], [4], and [7] or [8] can be portrayed in terms of the very simply equivalent circuit shown in Figure 2.

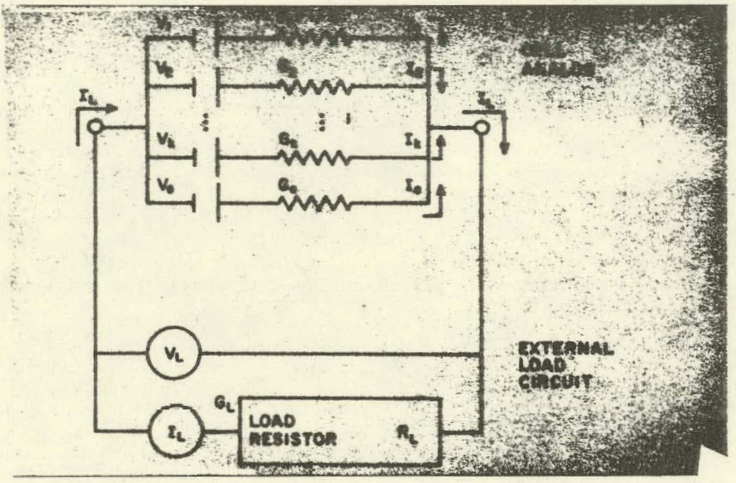

Figure 2. Equivalent circuit for fuel cell system (load mode).

Kirchhoff's law relates the load current I_L to that flowing in each branch of the equivalent circuit as follows:

$$I_L = I_1 + I_2 + \cdots I_k + I_e \ . \qquad [10]$$

But since the load voltage V_L - whatever it turns out to be - is necessarily impressed over every one of the parallel branches, we have the k + 1 relations:

$$I_i = \frac{V_i - V_L}{R_i} = G_i[V_i - V_L] \quad i = 1,2,\ldots k,e \ . \qquad [11]$$

Inserting these results into [10] and then invoking the definition of t_i from equation [8], there results

$$I_L = \Sigma G_i[V_i - V_L] = \Sigma G_i V_i - V_L \Sigma G_i = \Sigma G_i V_i - V_L G_T = G_T[\Sigma t_i V_i - V_L] \ .$$

But this is equivalent to

$$I_L = G_T[V - V_L] \qquad [12]$$

where V is the fundamental emf quantity defined by equation [4] above. Finally, inspection of the external load circuit also provides the Ohms relation

$$I_L = G_L V_L \qquad [13]$$

Equations [12] and [13] imply the following three very important relations

$$V_L = \frac{G_T}{G_L + G_T} V \ , \qquad [14]$$

$$I_L = \frac{G_L G_T}{G_L + G_T} V \ , \qquad [15]$$

and

$$W_L = \frac{G_L G_T^2}{[G_L + G_T]^2} V^2 \qquad [16]$$

and again the quantity V in all three cases is simply the emf quantity of equation [4].

These equations are of very general applicability for electrochemical systems. For example by merely setting $G_L = 0$ ($R_L = \infty$), the open circuit mode is described because I_L and W_L both vanish. Emf sensors such as the oxide probes used to measure P_{O_2} in high temperature environments operate in this mode in which case equation [14] reduces to equation [2]. The lower temperature so-called ion selective electrodes can be described in this way and equation [2] is the simplest way to interpret the emfs they exhibit. Specifically, an ion selective electrode is simply a membrane (often of "doctored" glass) for which the transference number of only one ionic species dominates equation [2].

To analyze any other situations (such as, for example, the process for generating hydrogen from steam by driving an oxide fuel cell backwards) one can simply insert an external dc supply in series with R_L and proceed accordingly.

However, in connection with fuel cell applications, we are interested in examining the implications of equations [14], [15] and [16] under load conditions. For example, equation [16] can be differentiated to determine the maximum possible power $\tilde{W}_L$ that can be delivered to load by the cell in question (fuel cell, battery, etc). The result is found to be simply

$$\tilde{W}_L = V^2/4R_T = V^2 G_T/4 \ , \qquad [17]$$

where V is again given by equation [4]. This occurs at a load resistance such that $G_L = G_L = G_T$ and amounts to impedance matching with the electrolyte. Clearly one wishes to shoot for systems with the lowest possible values of R_T (largest G_T's) consistent with the largest possible V values. As one might expect, this amounts to electrolytes with high ionic conductance and very low, or no, electronic conductance. Also, the electrodes should be capable of supporting large chemical potential differences without causing the electrolyte to decompose. Actually, halide ion conductors would be the best for getting high V values because Z would be in unity in equation [4]. However, oxides can be considered in this connection and it is therefore worthwhile to specialize the general theory to those materials.

III. Implications for Oxide Solid Electrolytes

The foregoing equations and considerations become substantially simplified when we specialize to the oxide electrolytes. In these materials the lattice cations are purported to exhibit negligible mobility and, as with all transport media (electrolyte or otherwise) there seems to be no known way to establish a non-zero value for V_e. Consequently, equations [4] and [5] simplify to

$$V = t_o V_o + t_e\, 0 = [1 - t_e]\, V_o \qquad [18]$$

because $t_o + t_e = 1$ with

$$V_o = \frac{\mu''_{O_2} - \mu'_{O_2}}{(-2Z_o\mathcal{F})} = \frac{RT}{4\mathcal{F}} \ln \left| P''_{O_2}/P'_{O_2} \right| \qquad [19]$$

However, if the electrolyte is exposed to, say, hydrogen gas on one side and if it can indeed diffuse through the oxide as a mobile ion (e.g., as protons), then another term would simply have to be added to equation [18] above to yield

$$V = t_o V_o + t_H V_H \ (+ t_e \cdot 0) \qquad [20]$$

where now

$$t_o + t_H + t_e = 1 \qquad [21]$$

and where V_H would be given by

$$V_H = \frac{\mu''_{H_2} - \mu'_{H_2}}{-2Z_H\mathcal{F}} = -\frac{RT}{2\mathcal{F}} \ln \left| P''_{H_2}/P'_{H_2} \right| \qquad [22]$$

Ordinarily, the high and low P_{O_2} sides of the electrolyte will correspond to the low and high P_{H_2} sides. Hence, both the operative thermodynamic voltages will tend to act in consort in the sense of wanting to drive electrons in the same direction through the external circuit.

Note, however, that in principle one of these two voltages could overpower the other to such an extent that the latter might be forced to run backwards. For example, if the voltage due to oxygen chemical potential difference is not exactly balanced by that due to the hydrogen, some of the oxygen flow will be consumed by driving hydrogen backwards (charging mode) through the cell. This amounts to a new kind of internal shorting process - an ion short. It can cause inefficiencies which are similar in some respects to the inefficiencies that are known to result from internal electronic shorting.

It is of interest to note that maintenance of identical H_2O pressures on both sides of the cell would help to ensure that the O_2 and H_2 voltages will be properly balanced - but only if the dissociating reactions $H_2O(g) \rightarrow H_2(g) + 1/2O_2(g)$ are in equilibrium on both sides and if electrode polarization corrections can be neglected.

In any event, this serves to demonstrate the way to handle the incorporation of extraneous substances when they can permeate the electrolyte as mobile ions. Other species could also be considered simply by contemplating other parallel branches in the equivalent circuit for the electrolyte. The major difficulties will have to do with determining the constraints which may relate the corresponding thermodynamic voltages to one or more of the others operating in the cell and also there may be considerable uncertainty as to the magnitude of the conductivity or transference number associated with the new migrant species (2).

From here on, we will neglect the effect of extraneous impurities to focus attention on certain other matters of importance, such as the role of internal electronic conduction.

As mentioned earlier, there seems to be no obvious means for establishing a non-zero value for V_e over an electrolyte system. Consequently, we will always keep V_e set to zero. This means that the rightmost term $t_e V_e$ of equation [4] will always vanish, and hence the voltage V cannot be augmented by electronic effects. Moreover, if we examine the maximum power formula equation [17] in conjunction with equation [18] for V, we see that the maximum deliverable power is also compromised by the presence of mobile electronic carriers. In particular, equation [17] can be combined with [18] to yield

$$\tilde{W} = \frac{V_o^2}{4} G_T [1 - t_e]^2 = V_o^2 \frac{A}{L} \frac{\sigma_o^2}{\sigma_o + \sigma_e} = \frac{V_o^2}{4} \frac{A}{L} \sigma_o [1 - t_e] \qquad [23]$$

Thus, for a given geometry (A/L), a given oxygen pressure driving force ($RT \ln P''_{O_2}/P'_{O_2}$) and oxygen ion conductivity; the parameter $\tilde{W}$ decreases regularly as σ_e increases from zero. On the other hand, the fall-off with t_e or σ_e is not too severe so that one might be able to gain some benefit from dopant additions which increases σ_e so long as they also increase σ_o and do so to a great enough extent.

Incidentally, equation [23] shows the benefit that can be derived by changing geometry. If the electrolyte is in the form of cylindrical tubes instead of a planar geometry, one merely replaces A/L by $2\pi L/\ln |r_o/r_i|$ where L is the length of the tube and the r's are the outside and inside radii. Not too much can be gained this way, at least as concerns the matters of interest in this paper.

The usual agreement for evaluating the efficiency of an operating cell is to divide the power delivered to load by the enthalpy consumption rate due to fuel oxidation. Thus, the denominator amounts to a ΔH_{RxN} factor multiplied by the flux of ions in moles per unit time, i.e., $I_o/[-Z_o \mathfrak{F}]$ in the present context. Thus, the conventional expression for cell efficiency ϕ for an oxide electrolyte under load takes the following form

$$\phi(G_L) = \frac{W_L}{\Delta H_o [2I_o/4\mathfrak{F}]} = \frac{4\mathfrak{F} V_o}{\Delta H_{O_2}} \frac{G_L G_o}{(G_L+G_e)(G_o+G_e+G_L)} \qquad [24]$$

where ΔH_{O_2} means the amount of enthalpy associated with the cell reaction for one mole of O_2 (two moles of O).

It is a relatively simple matter to determine the maximum possible efficiency for an electrolyte by merely differentiating equation [24]. The result can be written explicitly in terms of the electronic transference number as follows:

$$\phi^* = \frac{4\mathfrak{F} V_o}{\Delta H_{O_2}} \frac{1 - t_e}{(1 + \sqrt{t_e})^2} \qquad [25]$$

This max occurs at the relatively low load situation in which

$$G_L = G_L^* = \sqrt{G_e[G_o + G_e]} = G_T \sqrt{t_e} \qquad [26]$$

where G_T is the total conductance of the electrolyte, i.e., $G_o + G_e$. The power being delivered during max efficiency is found by substituting [26] into

$$W^* = V_o^2 G_T \sqrt{t_e} \left[\frac{1 - t_e}{1 + \sqrt{t_e}}\right]^2 \qquad [27]$$

Another use of the power-efficiency formulas is to determine the efficiency that prevails when the cell is operating at maximum power (i.e., in the impedance matched mode). This occurs when $G_L = G_T$ and then equation [24] becomes

$$\phi = \tilde{\phi} = \frac{4\mathfrak{F} V_o}{\Delta H_{O_2}} \quad \frac{1 - t_e}{[1+t_e][2-t_e]} \qquad [28]$$

IV. Summary

Because of space restrictions it is not possible to delve into a more meaningful discussion of all the results that can be developed by the method proposed in this paper. However, it is believed that the proposed model and the results which issue therefrom can provide very valuable guidlines for assessing the performance of electrochemical devices in general - and oxide solid electrolyte fuel cells in particular - for a wide variety of hypothetical and actual applications.

ACKNOWLEDGMENTS

The author wishes to acknowledge the Iowa State University Engineering Research Institute for the financial support to carry out this analysis, to Dave Martin for very helpful contributions, and to Mr. Patrick Henely for assistance with the final preparations.

REFERENCES

1. S. Stotz, and C. Wagner, Ber. Bunsenges, Phys. Chem, 70:781 (1966).

2. D.A. Shores, and R.A. Rapp, J. Electrochem. Soc, 119:300 (1972).

3. J.W. Patterson, E.C. Bogren, and R.A. Rapp, J. Electrochem. Soc., 114:7, (1967).

4. N.S. Choudhury, and J.W. Patterson J. Electrochem. Soc, 118:1399 (1971).

5. J.W. Patterson, Chapter 8 in N.M. Tallan, "Electrical Conductivity in Ceramics and Glass," Part B, Marcel Dekker, New York (1974).

6. T.P. Hoar and L.E. Price, Trans. Faraday Soc., 34:867 (1938).

7. C. Wagner, Z Phys. Chem, B21:25 (1933).

8. D. MacInnes, "The Principles of Electrochemistry," p 220-233, Dover Publications, New York (1961).

PHASE RELATIONSHIP AND ORDERING IN ZrO_2-CaO AND ZrO_2-Y_2O_3 SYSTEMS

S. P. Ray and V. S. Stubican
Department of Material Sciences
The Pennsylvania State University
University Park, PA 16802

The phase diagrams for the systems ZrO_2-CaO and ZrO_2-Y_2O_3 have been revised. Despite numerous previous works, a number of questions in relation to phase equilibria and ordering phenomena remained to be answered.

1. ZrO_2-CaO System:

Duwez et al. (1) reported that the cubic field in the ZrO_2-CaO system was between 16 and 30 m/o CaO at 2000°C. According to their work, the fluorite type cubic phase, usually called stabilized zirconia (CSZ), is stable from room temperature to the liquidus line. Dietzel and Tober (2) reported an eutectoid in the ZrO_2-$CaZrO_3$ composition region which indicated that the fluorite type solid solution of CaO in ZrO_2 is unstable below ~1220°C. Roy, Miyabe and Diness (3) used hydrothermal techniques to find an eutectoid below 800°C. Fernandes and Beaudin (4), who used $CaCO_3$ and ZrO_2 powders as starting materials also formed fluorite type solid solution unstable below ~800°C. Garvie (5) on the other hand claimed ~1230°C as the eutectoid temperature.

Order disorder transition in CSZ has been the subject of several studies. Tien and Subbarao (6) reported that a solid solution $Zr_{0.80}Ca_{0.20}O_{1.80}$ samples sintered at 2000°C for 2 hours annealed at 1400°C for one week showed only fluorite phase while the sample annealed at 1000°C for one week developed extra diffraction lines. Carter and Roth (7) by use of x-ray and neutron diffraction experiments and long annealing treatments also concluded that one or more ordered compounds are formed in this system. Michel (8) claimed that at 20 m/o CaO, two ordered compounds (Φ_1) and Φ_2 exist. From electron diffraction of fragments of 20 m/o CSZ Allpress, Rossel and Scott (9) suggested that $CaZr_4O_9$ is probably isostructural with $CaHf_4O_9$; the existence of ordered compounds at 22 and 24 m/o CaO was still in question.

In the present work, we have redetermined the extent of the cubic solid solution field by using high temperature x-ray camera, precise lattice parameter measurements and a hydrothermal technique. The cubic solid solution was found to decompose by an eutectoid reaction at 850° ± 100°C. A

reasonable agreement for the position of the eutectoid in this system was obtained by comparison of extrapolated data from high temperatures with the data obtained by the hydrothermal technique. Long range annealing of samples containing 15-24 m/o CaO-ZrO_2 in the temperature range 950-1360°C showed that only one ordered compound, $CaZr_4O_9$ is present in this system. Liquidus line has been determined with the help of a microoptical pyrometer and a strip furnace. Determination of the liquidus line indicated an eutectic at 40 m/o CaO and at 2250 ± 20°C which has been incorporated in the revised phase diagram. The revised phase diagram is shown in Fig. 1.

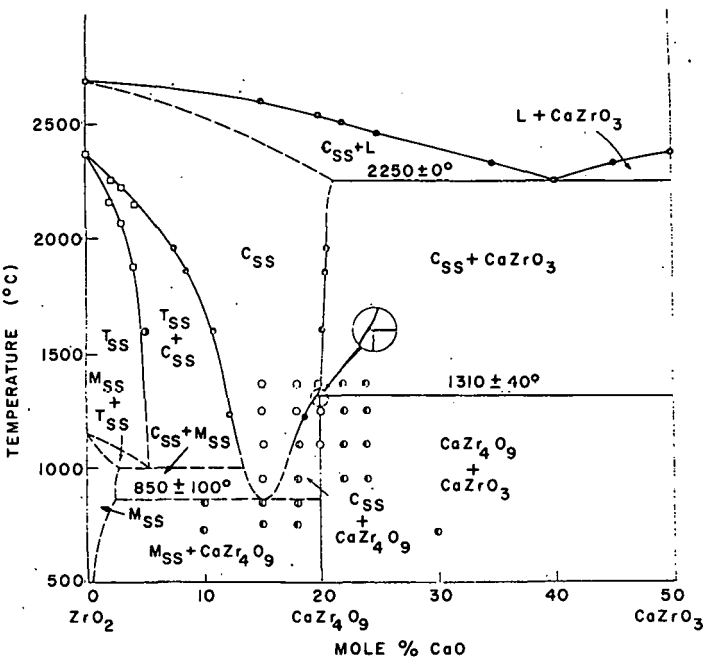

Figure 1. Phase diagram for the system ZrO_2-CaO.

2. ZrO_2-Y_2O_3 System:

The first reported phase diagram for the zirconia-yttria system was by Duwez, Brown and Odell (10). Despite numerous subsequent investigations, there is no general agreement between the proposed phase diagrams.

Fan, Kuznetsov and Keller (11) have indicated the existence of a pyrochlore type compound $Y_2Zr_2O_7$. Smith (12) could not confirm the presence of the pyrochlore phase. Srivastava et al. (13) have incorporated the tetragonal ⇄ cubic transformation in ZrO_2 found by Smith and Cline (14) into the revised phase diagram. Recently Scott (15) has proposed the existence of a miscibility gap closed below the solidus temperature in the yttria rich solid solution region. Scott's (15) diagram also includes the formation of hexagonal yttria above ~2300°C. The liquidus of the system has been studied by Noguchi and Skaggs. The present study included determination of (i) the extent of the zirconia and yttria solid solution fields, (ii) the existence and stability of ordered phases, and (iii) liquidus boundary. Fig. 2 shows the results of the findings.

The maximum solubility of Y_2O_3 in tetragonal ZrO_2 was found to be less than 2 m/o at 1650°C and 1900°C. Cubic yttria solid solution field was found to extend from pure yttria to 24 m/o ZrO_2 at 2150°C. Long range ordering was found to occur at 40 m/o Y_2O_3 corresponding to the compound $Zr_3Y_4O_{12}$. The compound has a rhombohedral symmetry and decomposes above 1250 ± 60°C.

Using a high temperature x-ray camera, the cubic ⇄ hexagonal inversion was located at 2280 ± 50°C. An eutectic was located at 83 ± 1 m/o Y_2O_3 and 2360 ± 20°C from the studies on liquidus and a study of the morphology of the directionally solidified sample. The diagram also incorporates a peritectic at 76 m/o Y_2O_3.

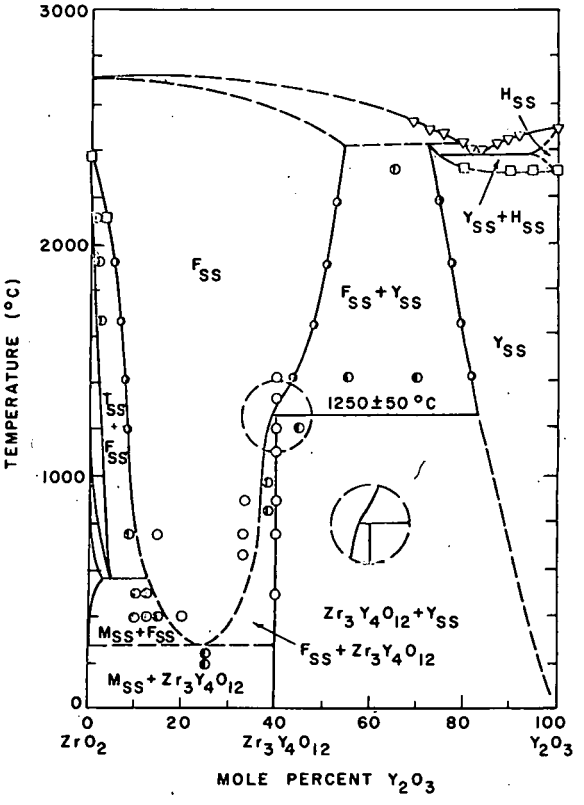

Figure 2. Phase diagram for the system ZrO_2-Y_2O_3.

References

1. P. Duwez, F. Odell and F. H. Brown, Jr., "Stabilization of Zirconia with Calcia and Magnesia", J. Am. Ceram. Soc., 35 [5] 107-13 (1952).

2. A. Dietzel and H. Tober, "Zirconium Dioxide and Binary Systems with Zirconia as Component", Ber. Deut. Ceram. Ges., 30 [4] 71-82 (1953).

3. R. Roy, H. Miyabe and A. M. Diness, "Subsolidus Decomposition of CaO-Stabilized ZrO_2", Am. Ceram. Soc. Bull., 43 [4] 255 (1964).

4. S. Fernandes and L. Beaudin, "Subsolidus Equilibria in the $CaO-ZrO_2$ System", presented at the 21st Annual Pittsburgh Diffraction Conference, Carnegie-Mellon Institute, Pittsburgh, Pa., 1963.

5. R. Garvie, "The Cubic Field in the System $CaO-ZrO_2$", J. Am. Ceram. Soc., 51, 553-556 (1968).

6. T. Y. Tien and E. C. Subbarao, "X-ray and Electrical Conductivity Study of Fluorite Phases in the System ZrO_2-CaO", J. Chem. Phys., 39 [4] 1041-1047 (1963).

7. R. E. Carter and W. L. Roth, "Conductivity and Structure in Calcia-Stabilized Zirconia", in Electromotive Force Measurements in High Temperature Systems, edited by C. B. Alcock, Institution of Mining and Metallurgy, 1968, pgs. 125-144.

8. D. Michel, "Ordered States in the Fluorite Type Solid Solution in the System Zirconia-Calcia for the Composition $4ZrO_2$-CaO", Mat. Res. Bull., 8, 943 (1973).

9. J. G. Allpress and H. J. Rossel, "A Micro-domain Description of Defective Fluorite Type Phases $Ca_xM_{1-x}O_{2-x}$ (M = Zr, Hf; x = 0.1-0.2)", J. Solid State Chem., 15, 68-78 (1975).

10. P. Duwez, F. H. Brown and F. Odell, "The Zirconia-Yttria System", J. Electrochem. Soc., 98 [9], 356-362 (1951).

11. F. Fan, A. K. Kuznetsov and E. K. Ketler, "Phase Relations in the $Y_2O_3-ZrO_2$ System: I", Izv. Akad. Nauk., SSSR Otd. Khem. Nauk., 114-116 (1962); Part II, ibid, 601-610 (1963).

12. D. K. Smith, "The Nonexistence of Yttrium Zirconate", J. Am. Ceram. Soc., 49 [11] 625-26 (1966).

13. K. K. Srivastava, R. N. Patil, C. B. Choudhary, K. V. G. K. Gokhale and E. C. Subbarao, "Revised Phase Diagram of the System ZrO_2-$YO_{1.5}$", Trans. J. Brit. Ceram. Soc., 73, 85-91 (1974).

14. D. K. Smith and C. F. Cline, "Verification of Existence of Cubic Zirconia at High Temperature", J. Am. Ceram. Soc., 45 [5] 249-250 (1962).

15. H. G. Scott, "Phase Relationships in the Zirconia-Yttria System", J. Mat. Sci., 10, 1527-2535 (1975).

DEFECT INTERACTIONS

A.S. Nowick
Columbia University

It is now widely recognized that the basic compensating defect when oxides of the fluorite structure are doped with di- or tri-valent cations, is the oxygen-ion vacancy, V_O. Further, it is established that the ionic conductivity of these materials is due to the migration of V_O defects. (1,2) Thus, if there were no defect interactions, one would predict a) that the conductivity, σ, will be proportional to the dopant concentration and b) that the magnitude and activation enthalpy, H, of the conductivity will be independent of the type of dopant. These predictions are contradicted by observations that σ goes through a maximum as a function of $[V_O]$, that it is dependent on the type of dopant, and that H increases sharply with dopant concentration, in some systems at least. (1)

The simplest type of interaction is pairing between dopant cations and V_O defects as a consequence of their Coulombic interactions. Such a concept leads to the prediction that the conductivity curves ($\ln \sigma T$ vs T^{-1}) will show three regions: region I (intrinsic), which would occur at temperatures too high to observe in these oxides, region II (extrinsic, dissociation) where V_O's are primarily dissociated and $H = H_m$, the migration energy of a V_O defect, and region III (extrinsic, association) where $H = H_m + H_B/2$ (where H_B is the binding enthalpy of an impurity-V_O pair). Examination of conductivity data shows that most measurements below 1000°C fall in region III or in the transition between regions II and III. (3) Direct observation of dielectric realxation effects due to Ca^{2+}-V_O pairs in CeO_2 at lower temperatures shows that practically all of the vacancies are bound up as pairs. Such measurements show a single Debye peak for $\lesssim$ 1% CaO, and that the peak broadens as the Ca^{2+} concentration goes beyond 2%. Relaxation measurements therefore provide a more sensitive indication of interaction effects than do conductivity data. In the case of Y_2O_3 doped CeO_2, the results are different. A double peak is obtained in the dielectric relaxation for low Y_2O_3 concentrations. At the same time, the conductivity measurements show that, while H is constant at a value of 0.78 eV for compositions up to $\sim$ 4% Y_2O_3, it rises sharply beyond this concentration, to reach values as high as 1.1-1.2 eV near 15% Y_2O_3. It is this increase in

activation energy that appears to be the major factor in the conductivity, since σ goes through a sharp maximum as a function of Y^{3+} doping in the composition range where H is rising most sharply. The exact nature of the interaction effects which give rise to this sharp increase in H is not yet understood, but further experiments are aimed at achieving such an understanding.

Diffraction studies, particularly neutron and electron scattering, give considerable information about interaction effects on a coarser scale, as already reviewed by Dr. Ray. For example, basic unit of a "Bevan cluster", i.e. a 6-coordinated cation surrounded by a sheath of 7-coordinated cations, has provided a very useful concept in the interpretation of various ordered structures.(4) However, the Bevan cluster is not an electric dipole and therefore cannot account for the large dielectric relaxation effects already mentioned. Further, dielectric relaxation involves the reorientation of a dipolar defect through the migration of oxygen vacancies and not through cation migration (since the activation energies for relaxation are always in the range 0.7-0.8 eV). A defect involving a pair of Y^{3+} ions in CeO_2, of the type suggested by Fender(5) based on his neutron scattering work, would not meet this requirement.

In summary, it is interesting to note that, while it is clear that the electrical properties are controlled in a large measure by defect interactions, the types of interactions postulated thus far by various investigators have usually been based on a single technique, which tends to give a very limited picture. A more comprehensive study of interaction problems, involving the application of several techniques to the same material over a range of compositions, should lead to a more complete understanding of these interaction phenomena.

References

1. T.H. Etsell and S.N. Flengas, Chem. Revs. 70, 339 (1970).
2. T. Takahashi, in Physics of Electrolytes, Vol. 2, J. Hladik, Academic Press, N.Y., 1972, p. 989.
3. A.S. Nowick and D.S. Park, in Superionic Conductors, ed. G.D. Mahan and W.L. Roth, Plenum Press, N.Y. 1976, p. 395.
4. S.P. Ray, this conference.
5. B.E.F. Fender, in Chemical Applications of Thermal Neutron Scattering, ed. B.T.M. Willis, Oxford Press 1973, p. 250.

OTHER OXIDE ELECTROLYTES

M.P. Anderson
Columbia University

Many investigations into the use of solid electrolytes for high temperature fuel cells have dealt almost exclusively with the stabilized zirconias having the fluorite structure, such as zirconia-calcia and zirconia-yttria. These have proved to be somewhat inconvenient for commercial application due to an insufficiently high conductivity; in order to increase fuel cell efficiency it has either been necessary to operate at high temperature (1000°C) or to use thin oxide layers, both of which involve technical difficulties.

Takahashi and coworkers in Japan have attempted to expand the base of materials exhibiting oxide ion conduction by turning to oxides with different crystal structures. (1-3) He has had partial success with a number of systems, notably:

(a) Certain Perovskite oxide solid solutions
(b) Bi_2O_3 - Y_2O_3
(c) Bi_2O_3 - WO_3

Conduction enhancement in the Perovskite solid solutions occurs via the same mechanism as for the quadrivalent fluorites, viz., the substantial replacement of the host cation by a metallic ion of lower valence, with the consequent creation of an oxygen vacancy. Conductivity at 1000°C is on the order of 10^{-2} $(ohm\text{-}cm.)^{-1}$, equivalent to ZrO_2 - 8% Y_2O_3. Enhancement for Bi_2O_3 - Y_2O_3 and Bi_2O_3 - WO_3 occurs via the stabilization of a cubic phase having a defect fluorite structure. Conductivity in this case is at least one order of magnitude larger than for the optimum stabilized zirconia in the range 500-800°C.

Since these materials exhibit such enticing properties, there are two areas which require further investigation:

(1) Because of possible problems with electronic conduction in reducing environments, the characteristics of Bi_2O_3 - Y_2O_3 and WO_3 need to be examined under actual fuel cell conditions.

(2) The structural characteristics of the stabilized cubic phase (and the kinetics involved) need to be determined. Since it appears that vacancy ordering may be a key aspect in these materials, this will require careful neutron diffraction work.

References

1. T. Takahashi, H. Iwahara and Y. Nagai, J. Appl. Electrochem. 2, 97 (1972).
2. T. Takahashi and H. Iwahara, ibid 3, 65 (1973).
3. T. Takahashi, H. Iwahara and T. Arao, ibid 5, 187, 197 (1975).

THIS PAGE

WAS INTENTIONALLY

LEFT BLANK

B. INTERCONNECTION MATERIALS

1. Summary of Panel Session on Interconnection Materials
   G. P. Wirtz, University of Illinois

2. Conduction Model for Rare Earth Perovskites
   G. P. Wirtz, University of Illinois

3. Compositional Dependence of Thermal Expansion, Lattice Parameters, Volatilization Rate and Electrical Conductivity of $LaCrO_3$ Based Oxides
   H. U. Anderson, R. Murphy, A. K. Fox, University of Missouri; B. Rossing, Westinghouse Electric Corporation; A. Aldred, Argonne National Laboratory

4. Highly Conducting Oxide Materials
   P.E.D. Morgan, University of Pittsburgh

5. Interconnection Materials for Thin Layer Zirconia Electrolyte Fuel Cells
   R. J. Ruka, Westinghouse Electric Corporation

SUMMARY OF PANEL SESSION ON INTERCONNECTION MATERIALS

G. P. Wirtz, Panel Chairman

University of Illinois at Urbana-Champaign, Urbana, IL 61801

The highlight of the discussion of interconnection materials was the virtual unanimity of opinion that $LaCrO_3$, modified by various dopants, will be the choice of material for the interconnection in the high temperature, thin-film, fuel cell.

The chromium ion is unique among transition elements of the third period in that it is stable in the trivalent state over the 18 orders-of-magnitude difference in oxygen fugacity required in this application. The perovskite structure lends itself better than other chromium compound structures to the formation of partially filled collective electron bands, yielding high conductivity. Doping with strontium or magnesium improves the electrical conductivity while varying thermal expansion. Aluminum as a dopant increases the thermal expansion markedly, although decreasing the conductivity. $LaCrO_3$, therefore, provides us with a material which can be "engineered" to a remarkable extent to meet exacting requirements for electrical conductivity and thermal and mechanical properties. Life tests reported by Rohr of Brown, Boveri and Cie in West Germany indicate that lifetimes of 5 years or more should be readily achieved. The outlook for high-temperature fuel cells from the standpoint of the interconnection material is therefore very optimistic.

While the materials selection seems to be essentially accomplished, there is work yet to be done on processing or device fabrication. The primary techniques which have been used to fabricate thin-films of the interconnection material on the porous substrate have been: a) sintering, b) chemical vapor deposition, and c) r.f. sputtering. Due to the volatility of the chromium ion, fabricating temperatures must be kept as low as possible, which favors the latter two fabrication techniques. Completely gas-tight films to date have only been claimed by the Westinghouse group for their chemical vapor deposition process. It seems clear that there is a definite art involved in fabricating gas-tight films over porous substrates. With the materials selection accomplished then, there appears to be three major steps yet to be taken before the interconnection material hurdle can be said to be completely overcome:

1. Development of technology for fabrication.
2. Building of hardware.
3. Performing necessary life-tests.

On the more basic side, there are two major areas in which knowledge of the properties of lanthanum chromite seems to be still inadequate. Most immediate is the question of what exactly are the anion and cation diffusion rates in the chromite. Of particular interest and concern is the question of hydrogen or proton diffusion through the structure. Apparently no data is available in this area. Secondly, our knowledge of the

defect structure of the rare earth perovskites is very sketchy. As pointed out by Anderson, divalent dopants may be compensated ionically by oxygen vacancies, under certain conditions, as well as electronically. Ionic compensation results in decreased electrical conductivity, but would almost certainly increase the anion diffusion rate. Defect structures and their relation to transport properties in the rare earth perovskite systems clearly warrants further research.

CONDUCTION MODEL FOR RARE EARTH PEROVSKITES

G. P. WIRTZ

Department of Ceramic Engineering

University of Illinois at Urbana-Champaign

Urbana, Illinois 61801

Other papers (1,2,3) in this conference have presented a wealth of data on the properties of rare earth perovskites and their use as interconnection materials for high-temperature fuel cells. Modification of the base material by appropriate dopants has been shown to vary both electrical conductivity and thermal expansion in these materials. The primary purpose of this paper is to provide a qualitative, phenomenological, explanation for the variation of the electrical properties with various dopants, which might serve as a basis for further "engineering" of these materials for this application.

Modern discussion of highly conductive oxide materials begins (and often ends) with the Goodenough "one-electron" energy band scheme (4). The basic premise of this theory is that knowing the crystal structure of an oxide, one can apply molecular orbital theory to come up with one or more possible energy level diagrams consistent with the known crystal structure. The conservation of electronic states is basic to chemical bonding theory. Knowing the composition, therefore, one knows the number of electrons per unit cell, and by simply starting at the lowest energy state and filling

them with available electrons one can determine the position of the Fermi level relative to the energy bands for each of the possible energy level diagrams. From this one can predict whether the material will be an insulator--semiconductor, or conductor, and whether the majority carriers will be electrons or holes. Experimental confirmation of the correctness of a model is required.

To a first-order approximation, the perovskite structure is a primitive cubic structure with one formula unit of ABO_3 per unit cell. In the present case, B is a transition metal ion and A is a rare earth ion. The unit cell may be pictured as in Figure 1 with the B atoms at the cube corners, the oxygen atoms at the centers of the cube edges, and the rare earth atom at the body centering position. For most cases the A atom may be seen as a donor which merely gives up its valence electrons to the bands formed by the BO_3 sublattice. The outer s and p states of the transition metal cations form sigma bonds with the s and pσ orbitals of the oxygen ions; however, the unfilled d levels in the cation are also available for bonding. The octahedral coordination of the transition metal site will split the five d states into the doubly degenerate e_g states and the triply degenerate t_{2g} states, the orientations of which are partially shown in Figure 1. The e_g orbitals point along the cube edges and are similarly available for σ bonding with the 2s and 2p oxygen orbitals. The t_{2g} orbitals are directed at an angle from the cube edges but may form π bonds with the pπ orbitals of the oxygen.

Whether chemical bonding leads to localized electron states (Mott insulators) or collective electron bands is primarily a matter of the degree of overlap of bonding orbitals. The greater the overlap, the broader the band will be. It can be easily seen that the degree of overlap is greatest between s and pσ orbitals, somewhat less between e_g and pσ orbitals, and even less between t_{2g} and pπ orbitals. The outer electrons therefore will always form collective electron σ and σ*, or bonding and anti-bonding, bands. The e_g and t_{2g} electron states may or may not form collective electron bands, but if only one does it will be the e_g σ bonds which form collective electron bands due to greater overlap.

To a first approximation then, assuming all d electrons are in collective electron bands, the flat band energy level diagram for a perovskite would be as shown in Figure 2. The number of electron states available in each band are shown in the square brackets with the multiplier of two representing the spin multiplicity. For a trivalent A ion there are 3 electrons per A atom, 6 electrons per oxygen atom and 2 plus the number of d electrons per B atom. Considering the B atom as a trivalent atom there would be then 24 outer electrons associated with the oxygen ions per unit cell. This will exactly fill the bonding states and the non-bonding pπ states shown in Figure 2, which would be associated with the oxygen atom. Additional d electrons would then go into the π* band. The degree to which the π* band would be filled will vary from half full for Cr to completely filled for Co,

to an excess of one electron which must spill over into the σ^* state for Ni. The π^* and σ^* bands are shown separated but they may in fact be close or even overlap.

Immediately and most importantly this model predicts that with the possible exception of the nickel compound, the majority carriers in the rare earth perovskites should be holes. This seems consistent with available experimental data and allows one to make predictions about the effects of dopants on conductivity.

The most common dopants to increase the conductivity of these materials are strontium and magnesium. The strontium is believed to substitute for the rare earth element on the A site, but controversy exists over whether the magnesium occupies an A or B site. The effect of substituting a divalent cation for a trivalent cation on the A site is to decrease the number of electrons in the system by one. In a p-type conductor this will increase the number of carriers, thereby increasing the conductivity. While the majority of other data seems to indicate magnesium occupies the B site, the electrical conductivity indicates that it most probably occupies an A site.

As pointed out by Anderson, et al. (2), aluminum has the very desirable effects of increasing the thermal expansion coefficient and depressing the orthorhombic to rhombohedral phase transition to below room temperature in $LaCrO_3$. At the same time, however, it decreases the electronic conductivity

of the material. It is agreed that aluminum occupies a B site in this material. It's effect on conductivity can be predicted from the fact that it contributes three fewer electrons than the chromium which it replaced, but it contributes 10 fewer states (the d electron states) for these electrons to occupy. The net result is an increase in the Fermi Level relative to the conduction band and a decrease therefore in the number of holes in the conduction band. Magnesium on the B sites should have a similar but less marked effect on conductivity.

Finally, since these materials are asked to function over a wide range of oxygen fugacity, the effect of non-stoichiometry on their electrical conductivity is important. For p-type conducting oxides a decrease in oxygen content must yield a decrease in electrical conductivity. An oxygen vacancy removes 8 electronic states from the band structure but only 6 electrons, again giving rise to an increase in the Fermi Level and a decrease in the number of conduction holes. A cation interstitial would have a similar effect. Figure 3 shows the effect of reduction in forming gas on the conductivity of $LaCoO_3$ and $La_{1-x}Sr_xCoO_3$ (5). The predicted effect is observed; however, note that at temperatures approaching the operating temperature for the fuel cells in question the conductivities are very similar. Hence, it must be remembered that these materials will be asked to perform at high temperatures, and predictions of the effect of any dopant on the carrier concentrations may be outweighed by changes in the temperature dependence of the conductivity.

References

1. R. J. Ruka: "Interconnection Materials for the Thin-Layer Zirconia Electroylte Fuel Cell," This volume.
2. H. U. Anderson et al., "Compositional Dependence of Thermal Expansion, Lattice Parameters, Volatilization Rate and Electrical conductivity on $LaCrO_3$ Based Oxide," ibid.
3. P. E. D. Morgan, "Highly Conducting Oxide Materials," ibid.
4. J. E. Goodenough, "Metallic Oxides," Prog. in Solid State Chem. 5, 145-399 Ed. H. Reiss, Pergamon Press, New York (1971).
5. L. B. Sis, "Physical Properties and Catalytic Activity of Lathanum Cobaltate," Ph.D. Thesis, University of Illinois at Urbana-Champaign (1972).

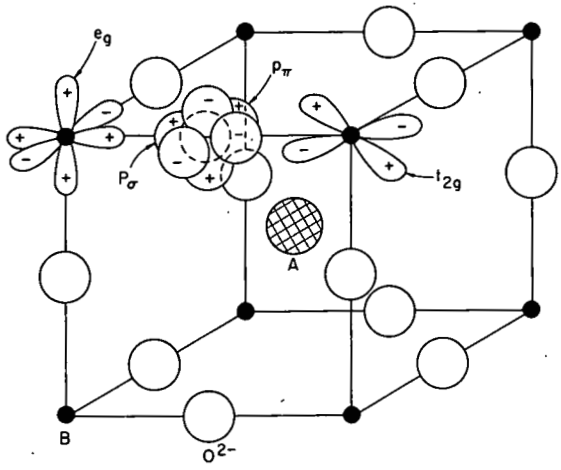

Figure 1. The perovskite unit cell for compound ABO_3.

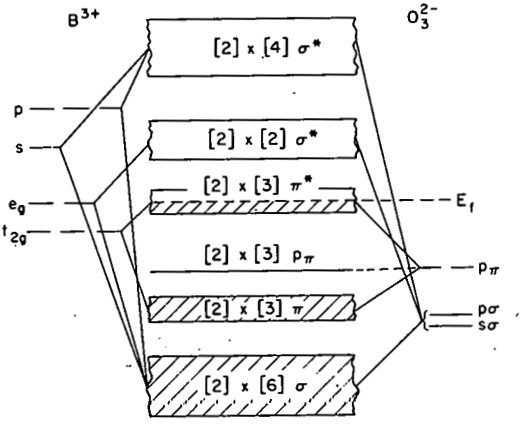

Figure 2. One-electron energy band diagram for the perovskite structure assuming de-localization of all d-states.

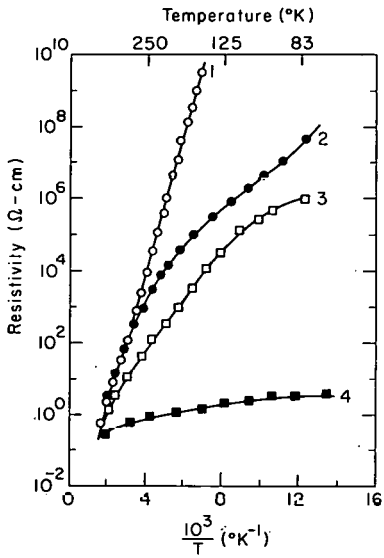

Figure 3. Electrical resistivity of $LaCoO_3$ and $Sr_{0.15}La_{0.85}CoO_3$.

1. $Sr_{0.15}La_{0.05}CoO_{3-x}$ Reduced 4.2 w/o.
2. $LaCoO_{3-x}$ Reduced 1.2 w/o.
3. $LaCoO_3$.
4. $Sr_{0.15}La_{0.85}CoO_3$.

COMPOSITIONAL DEPENDENCE OF THERMAL EXPANSION, LATTICE PARAMETERS, VOLATILIZATION RATE AND ELECTRICAL CONDUCTIVITY OF $LaCrO_3$ BASED OXIDES

H.U. Anderson, R. Murphy, and A.K. Fox
University of Missouri-Rolla
Rolla, Missouri 65401

B. Rossing
Westinghouse Electric Corporation
Pittsburg, Pennsylvania 15235

A. Aldred
Argonne National Laboratory
Argonne, Illinois 60439

Introduction

The rare earth and alkaline earth chromites are unique in combining high melting points (> 2000°C) and high electronic conductivity. Of the chromites investigated to date, acceptor doped $LaCrO_3$ appears to be best in fulfilling most high temperature electrode requirements with the exception of volatilization and possibly corrosion. Weight loss measurements indicate that volatilization limits the temperature which it can be used as an electrode to about 1750°C. In order to achieve higher operating temperature the volatilization rate of the electrode material needs to be reduced by one to two orders of magnitude.

In an earlier investigation $La_{.95}Mg_{.05}Cr_{1-x}Al_xO_3$ specmens were prepared in which up to 100% of the Cr was replaced by Al (1). The results of this study are tabulated in Table I and illustrated in Figures 1 and 2. As can be seen in Table I the replacement of Cr by Al in $La_{.95}Mg_{.05}Cr_{1-x}Al_xO_3$ reduces the volatility of the oxide both in dry and moist atmospheres. An extrapolation of the data indicates that volatilization will not limit the use of these compositions for temperatures as high as 2000°C. The electrical conductivity measurements (Figure 1) show that up to 50% of the Cr can be replaced by Al before the conductivity is too low for MHD electrode application. It was also observed that the thermal expansion increases as the Al content is increased (Figure 2). In addition, the orthorhombic

TABLE I

Measured Rate of Weight Loss at 1740°C

atm A - $P_{O_2} = 10^{-3}$ atm

atm B - $P_{O_2} = 10^{-3}$ atm + 10^{-1} atm H_2O

Gas Flow Rate = 1 linear cm/sec

Specimen	Weight Loss* $\mu g/cm^2/hr$ atm A	atm B
$La_{.95}Mg_{.05}CrO_3$	2	10-44
$La_{.95}Mg_{.05}Cr_{.95}Al_{.05}O_3$	4.4	16
$La_{.95}Mg_{.05}Cr_{.9}Al_{.1}O_3$	5.1	7-24
$La_{.95}Mg_{.05}Cr_{.85}Al_{.15}O_3$	6.2	19-24
$La_{.95}Mg_{.05}Cr_{.8}Al_{.2}O_3$	10.3	16-34
$La_{.95}Mg_{.05}Cr_{.75}Al_{.25}O_3$	0	0-16
$La_{.95}Mg_{.05}Cr_{.5}Al_{.5}O_3$	0-1	0-9
$La_{.95}Mg_{.05}Cr_{.25}Al_{.75}O_3$	0	0
$La_{.95}Mg_{.05}Cr_{.1}Al_{.9}O_3$	-	0-8
$La_{.95}Mg_{.05}AlO_3$	0	0-9

* Uncertainty in measurement = $\pm$ $\mu g/cm^2/hr$

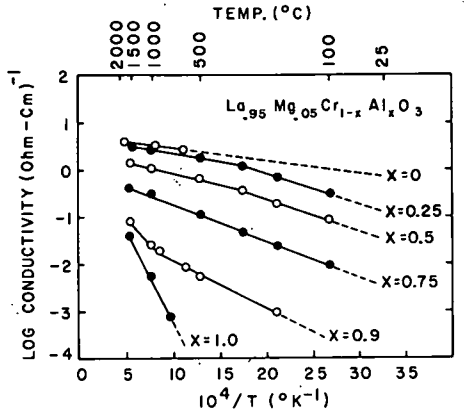

Figure 1. Electrical conductivity of $La_{.95}Mg_{.05}Cr_{1-x}Al_3O$.

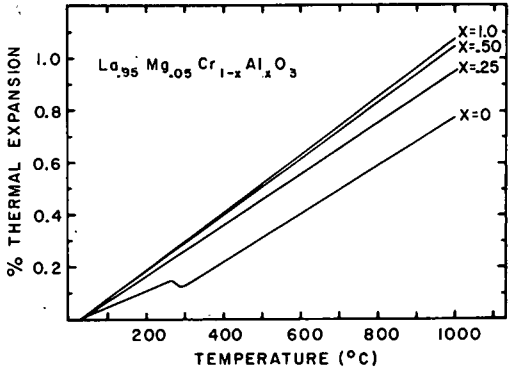

Figure 2. Thermal expansion of $La_{.95}Mg_{.05}Cr_{1-x}Al_xO_3$.

to rhombohedral transition is depressed to below room temperature when the Al content exceeds 20%.

Since these data showed that properties could be controlled in a very reproducible manner an investigation of the $LaCrO_3$-$LaAlO_3$ system was initiated with the objective of obtaining more detailed information on the interrelation between the composition and properties.

To make this study, a number of compositions based on $La_{.95}Mg_{.05}CrO_3$ were prepared with Al substituted for Cr from 0 to 100%. The influence of cation stoichiometry was determined on the base compositions $La_{1-x}(Mg_{.05}Cr_{.5}Al_{.5})_{.95}O_3$ and $La_{1-x}CrO_3$. The ratio of La to $(Mg_{.05} + Cr_{.5} + Al_{.5})$ or La to Cr was varied from 0.8 to 1.1.

Experimental

The required compositions were prepared with a chemical preparation technique which allowed precise compositional control and produced highly sinterable powders of < 0.1 μm crystallite size. The compositions were then dry pressed and sintered into disc-shaped test specimens whose densities all exceeded 93% of theoretical density with no surface porosity. X-ray diffraction analysis showed that all of the compositions were single phase with essentially complete solid solution between $LaCrO_3$ and $LaAlO_3$. Thus it was felt that the preparation technique was such that property measurements should reflect variation in either Al content or cation stoichiometry rather than extraneous influences which result from the preparation process.

The volatilization rates were determined by measuring the weight changes occuring on sintered specimens after heating to 1740 $\pm$ 15°C in a controlled atm Mo tube furnace in flowing atmospheres of either N_2 + 10^{-3} atm O_2 or N_2 + 10^{-3} atm O_2 + 10^{-1} atm H_2O for times up to 48 hours. A flow rate of 1 linear cm/sec was maintained throughout the experments. The oxygen pressure was determined by sampling the gas stream with a solid state electrolytic cell. The water content was maintained at 10^{-1} atm by bubbling the gas through a 46°C water bath.

Both thermal expansion and electrical conductivity measurements were made on sintered specimens in air atm at temperatures to 1500°C. Some electrical conductivity measurements were made at 10^{-4} atm O_2, but they were found to dif-

fer from those measured in air by only 10% so no more measurements as function P_{O_2} were made.

Results

The volatilization rates as function of Al content and cation stoichiometry are listed in Tables I and II. As can be seen the rate of volatilization decreases as Al and La increases.

Electrical conductivity measurements were made both as a function of Al and La content. Figure 1 shows that the electrical conductivity is very dependent upon Al content. Typically the room temperature electrical conductivity varies from 1 to $< 10^{-13}$ $(\Omega cm)^{-1}$ as the Al content increases from 0 to 100%. No systematic relationship between La content and electrical conductivity was observed. All of the measurements are in agreement with those shown in Figure 1 even though the La content was varied from 10 m% excess to 10 m% deficit.

The thermal expansion as function of Al content is shown in Figure 2. As can be seen the addition of Al does two things: 1) increases the thermal expansion coefficient of the rhombohedral phase from 9.1×10^{-6} m/m/°C to 11.3×10^{-6} m/m/°C as it increases from 0 to 100 m% and 2) shifts the orthorhombic to rhombohedral transformation temperature to lower temperatures. Figure 3 illustrates the temperature shift of the transformation temperature. No measurements were measured below room temperature so only specimens containing less than 15 m% Al could be measured. An extrapolation of the data suggests that 13 m% of Al is sufficient to shift the transformation temperature to room temperature.

The influence of La content or cation stoichiometry on thermal expansion was investigated. As can be seen in Figure 4, the thermal expansion is little influenced by La content. Both the rhombohedral phase and orthorhombic phase have expansion coefficients similar to those reported in Figure 1, 9.2×10^{-6} m/m/°C and 6.7×10^{-6} m/m/°C respectively. However, as can be seen in Figure 5, the temperature over which the orthorhombic to rhombohedral transformation occurs is dependent upon La content. The onset temperature of the transformation ranges from 240°C to 251°C for La/Cr ratios of 0.9 and 1.1 respectively. The transformation is somewhat sluggish, it is small ($< 2 \times 10^{-2}$%) and occurs over about a 10°C temperature range. Upon cooling,

TABLE II

Measured weight loss after 48 hours in $P_{O_2} = 10^{-3}$ atm, $P_{H_2O} = 10^{-1}$ atm at 1740°C

Specimen	Initial Wt	ΔW(g)	Δw/hr/cm² x 10⁶*
$La_{.8}B^{**}O_3$	4.1007	-0.0141	35
$La_{.85}BO_3$	4.0324	-0.0082	20
$La_{.90}BO_3$	3.8334	-0.0022	9
$La_{.92}BO_3$	7.2734	-0.0071	14
$La_{.96}BO_3$	5.0733	-0.0002	0
$La_{.98}BO_3$	4.7580	-0.0056	20
$La_{1.00}BO_3$	10.8134	-0.0094	12
$La_{1.04}BO_3$	4.1585	-0.0029	7
$La_{1.06}BO_3$	3.5519	+0.0028	gain
$La_{1.10}BO_3$	5.1644	+0.0036	gain

* $\pm$ 5 μg/cm²/hr

** $B = (Mg_{.05}Cr_{.5}Al_{.5})_{.952}$

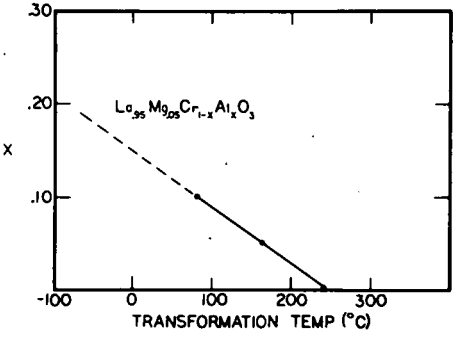

Figure 3. Temperature of onset of orthorhombic-rhombohedral transformation.

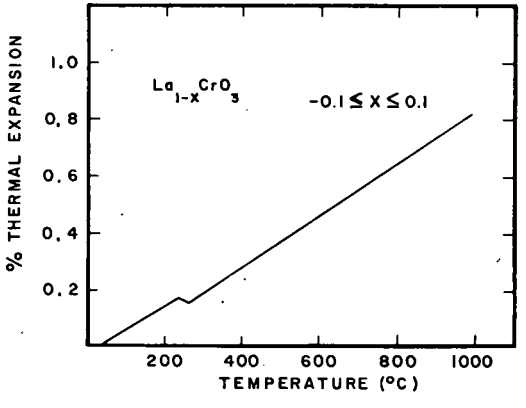

Figure 4. Thermal expansion of $La_{1-x}CrO_3$.

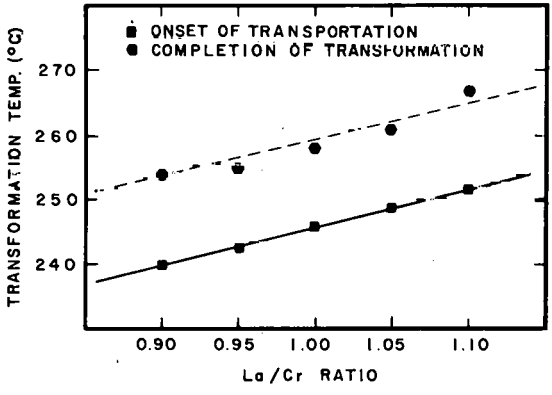

Figure 5. Dependence of orthorhombic-rhombohedral transformation upon La/Cr ratio.

the onset of the transformation is depressed by about 10°C. The extent of hysteresis does not appear to be dependent upon either La or Al content.

Room temperature lattice parameter and crystal structure determinations were made both as function of La/Cr ratio and Al content. The results are listed in Tables III and IV. As can be seen in agreement with the thermal expansion the crystal structure changes from orthorhombic to rhombohedral for Al content greater than 10 m%.

The rhombohedral lattice parameter a and angle α decrease smoothly as the Al content increases from 10 m%. For 100 m% Al the crystal structure is very nearly cubic with an angle of about 60.1°.

It is evident from Table IV that the room temperature of a crystal structure of $La_{1-x}CrO_3$ is orthorhombic over the ranges $-.1 \leq x \leq .1$ with no measureable changes in lattice parameters.

Discussion and Conclusions

It is apparent that both the thermal expansion and electrical conductivity of $LaCrO_3$ can be controlled by substitution of either aliovalent or isovalent ions into the structure. The substitution of an isovalent ion, Al^{+3} increases the thermal expansion coefficient, depresses the orthorhombic-rhombohedral phase transition and decreases the electrical conductivity. The substitution of the acceptor-type ion, Mg^{+2} greatly increases the electrical conductivity. No attempts were made to study the influence of Mg content upon the electrical conductivity since this has been reported elsewhere (2). All of the compositions with Mg additions contained a constant level of Mg (5 m%).

The influence of La content upon thermal expansion, electrical conductivity and crystal structure is essentially insignificant. However, the temperature of the orthorhombic-rhombohedral phase transition does show a sufficiently strong dependence that we should be able to use it as a way of determining cation stoichiometry. For example, for the composition $La_{.95}Mg_{.05}CrO_3$ the question arises as to whether the Mg substitutes for La or Cr. The transformation temperature is 239°C, which indicates a A/B ratio for ABO_3 of 0.9 which is what results if Mg substitutes on the Cr(B) lattice. A transition temperature of 246°C should be expected if Mg

TABLE III

Lattice Parameters for $La_{.95}Mg_{.05}Cr_{1-x}Al_xO_3$

x	a, (Å)*	b (Å)	c (Å)	Remarks
0	5.4910	5.5176	7.7466	(ortho)
.05	5.4868	5.5176	7.7763	(ortho)
.10	5.4789	5.115	7.7664	(ortho)
.15	5.4495			α = 60·62 (Rh)
.2	5.4454			α = 60·60 (Rh)
.25	5.4404			α = 60·52 (Rh)
.35	5.4334			α = 60·52 (Rh)
.5	5.4230			α = 60·46 (Rh)
.75	5.3882			α = 60·28 (Rh)
1.00	3.7967			cubic

* ± .005 Å

TABLE IV

Lattice Parameters for $La_{1\pm x}CrO_3$

Composition	a (Å)*	b (Å)	c (Å)
$La_{.9}CrO_3$	5.4908	5.5180	7.7834
$La_{.95}CrO_3$	5.4916	5.5216	7.7666
$La_{1.00}CrO_3$	5.4923	5.5207	7.7703
$La_{1.05}CrO_3$	5.4936	5.5228	7.7700
$La_{1.10}CrO_3$	5.4900	5.5180	7.7734

* $\pm$ .005 Å

substitutes on the La(A) lattice. Therefore, we conclude that Mg does substitute on the Cr lattice in agreement with Brodmann and Morgan (2).

The combination of the continuous changes in lattice parameters, crystal structure, thermal expansion and electrical conductivity with Al content offers strong evidence that the $LaCrO_3$-$LaAlO_3$ system forms complete solid solution. The lack of detection of second phases by x-ray diffraction in any of the compositions prepared also supports our conclusion that complete solid solutions exist in this system.

In conclusion, some of the significant results of this investigation are:

1) The substitution of Al for Cr substantially decreases the volatilization rate of $La_{.95}Mg_{.05}Cr_{1-x}Al_xO_3$.

2) The room temperature electrical conductivity of $La_{.95}Mg_{.05}Cr_{1-x}Al_xO_3$ varies systematically from 1 (ohm cm)$^{-1}$ for x = 0 to about 10^{-13} $(\Omega cm)^{-1}$ for x = 1.

3) The thermal expansion coefficient of rhombohedral $La_{.95}Mg_{.05}Cr_{1-x}Al_xO_3$ varies from 9.1 x 10^{-6} m/m/^oC for x = 0 to 11.3 x 10^{-6} m/m/^oC for x = 1.

4) The room temperature crystal structure of $La_{.95}Mg_{.05}Cr_{1-x}Al_xO_3$ is orthorhombic for x < .15 and is rhombohedral for x > .15. The system $La_{.95}Mg_{.05}CrO_3$-$La_{.95}Mg_{.05}AlO_3$ appears to form a complete solid solution series.

5) The orthorhombic-rhombohedral phase transition is sluggish, occuring over about a 10^oC temperature span and shows about a 10^oC hysteresis upon cooling.

6) Variation of the La/Cr ratio does not significantly alter the thermal expansion or the electrical conductivity.

7) The temperature of the orthorhombic-rhombohedral phase transition shows enough dependence upon the La/Cr ratio that we should be able to use it as a measure of the La/Cr ratio.

8) This study demonstrated that by careful control of preparation techniques and by the application of the "Verwey controlled ionic valency principle" the properties of $LaCrO_3$ can be altered in both a controllable and predictable manner.

References

1. H.U. Anderson, R. Murphy, S. Semachaibovorn, B. Rossing, A. Aldred, W.L. Procarione and R.J. Ackermann, "Influence of Composition and Cation Stoichiometry on the Volatility and Electrical Conductivity of $LaCrO_3$ Based Oxides" presented at Conference of High Temperature Sciences Related to Open Cycle, Coal-Fired MHD Systems at Argonne National Laboratory, Argonne, Ill., April 4-6, 1977.

2. F.J. Brodmann and P.E.D. Morgan, "Advances in Lanthanum Chromite MHD Electrode Development", ibid.

HIGHLY CONDUCTING OXIDE MATERIALS

P. E. D. Morgan
Department of Metallurgy and Materials Engineering
University of Pittsburgh
Pittsburgh, PA. 15261

Oxide perovskites such as $LnMO_3$, Ln = rare earth, alkaline earth, lead and M = chromium, manganese, iron, cobalt or nickel, are often good electronic conductors and some could find application as electrodes or interconnector materials in fuel cells.

One of the most studied, $La_{0.84}Sr_{0.16}CrO_3$ (1-4), has a resistivity, R, of 0.2 → 1 Ω,cm at room temperature dropping to a minimum ∿ 3 x 10^{-2} Ω,cm at 1000°C. Pure $LaCrO_3$ has a melting point of 2430°C, almost certainly the highest of all the conducting perovskites, and so has been the prime candidate for MHD, electrode application (5). $LaFeO_3$ has a melting point ∿ 1880°C (6) and $LaMnO_3$ is probably similar, $LaCoO_3$ and $LaNiO_3$ seem to melt at ∿ 1400°C. $La_{0.5}Sr_{0.5}CoO_3$ has metallic type conductivity* with R ∿ 1 x 10^{-4} Ω,cm at room temperature and ∿ 6 x 10^{-4} Ω,cm at 1200°C. $La_{0.5}Sr_{0.5}FeO_3$ is a semiconductor (p type) with R ∿ 7 x 10^{-2} Ω, cm at room temperature and ∿ 5.5 x 10^{-3} Ω,cm at 900°C, as is $La_{0.7}Sr_{0.3}MnO_3$, R ∿ 9 x 10^{-2} Ω,cm at room temperature and ∿ 1 x 10^{-2}Ω,cm at 1000°C.

Some dexterity is required in the air sintering of polycrystalline boules, isopressed at 50,000 psi from precalcined chemically prepared powders, for, at higher temperatures suitable for rapid sintering, some compositions also begin to decompose, depending on the relative stability of the higher valent states of M. Compositions where M = Cr, Mn and Fe are the most stable. $La_{0.5}Sr_{0.5}CoO_3$ begins to decompose in air ∿ 1200°C while the nickel composition, $La_{0.5}Sr_{0.5}NiO_3$, does not even form as a single phase. This is in accord with the known chemical stabilities $Cr^{IV} > Mn^{IV} > Fe^{IV} > Co^{IV} >> Ni^{IV}$. However, annealing treatments in air at ∿ 900°C after sintering at higher temperatures allow some polyphasic ceramic compositions to be converted to the single phase perovskite e.g., $La_{0.5}Sr_{0.5}FeO_3$; coincidentally the resistivity drops greatly, e.g., for "$La_{0.5}Sr_{0.5}FeO_3$" from 2 Ω,cm before annealing to 7 x 10^{-2} Ω,cm after the air anneal.

Especially where the higher valent states of M are less stable, we may consider another series of complex oxides of the K_2NiF_4, potassium nickel fluoride, type. Typical of this group is metallic $La_2Cu^{II}O_4$, (7) while La_2NiO_4 is metallic above 500°K. Mixed types e.g., $LaSrV^{III}O_4$ are

*Similar metallic conductivity has been known in the perovskite "tungsten bronzes", Na_xWO_3 (x = 0 → 1), for many years.

also known (8). Conductivity in this crystal type is two dimensional as opposed to the three dimensional perovskite. Sintering of the nominal composition "$La_{0.5}Sr_{0.5}NiO_3$" gave instead $LaSrNi^{III}O_4$ + excess NiO.

Nevertheless the resistivity was $\sim 3 \times 10^{-2}$ Ω,cm at room temperature and 8×10^{-3} Ω,cm at 900°C. Therefore, the pure compound $LaSrNi^{III}O_4$, with the K_2NiF_4 structure, was prepared; $R \sim 5 \times 10^{-2}$ Ω,cm at room temperature and 4×10^{-3} Ω, cm at 900°C. $LaSrFe^{III}O_4$, however, has a high resistivity.

Some of the Ln_2MO_4 compounds may well be more refractory than the corresponding $LnMO_3$ although melting points have not yet been measured.

An interesting consequence of very high electronic conductivity is the potential for increased thermal shock resistance. It has been shown (9) that for a variety of good ceramic conductors, borides, silicides, carbides, a sulphide etc., a modified Wiedemann-Franz-Lorenz equation is applicable. If this relation applies to (for example) $La_{0.5}Sr_{0.5}CoO_3$ then, at 1000°C, the predicted thermal conductivity is greater than all other known oxides, with the exception of BeO. This may well confer superior thermal shock resistance to some of these materials.

References

1. D.B. Meadowcroft,"Some Properties of Strontium-Doped Lanthanum Chromite, Brit. J. Appl. Phys., 2, 1225 (1969).

2. M. Foex, C. R. Acad. Sci., Paris, 260, 6389 (1965).

3. P.E.D. Morgan, "Sintering of Chrome Systems," in Press, Bull. Am. Ceram. Soc., May 1977.

4. U.S. 3,974,108, "$LaCrO_3$ Electrodes and Method of Manufacture," R. Staut and P. E. D. Morgan, August 10, 1976.

5. V. N. Pavlikov et al, Phase Diagrams for Ceramists III, Fig. 4397 (1975).

6. J. Cassedann See Phase Diagrams for Ceramist III, Figs. 4586, 4604, 4605. Am. Ceram. Soc. (1975).

7. P. Ganguly and C.N.R. Rao, Mat. Res. Bull., 8, 405 (1973).

8. J. M. Longo and P. M. Raccah, J. Solid State Chem. 6, 526 (1973).

9. P.E.D. Morgan, "Wiedemann-Franz-Lorenz Relation in Metallic Conducting Ceramics,"J. Am. Ceram. Soc. 58, 349 (1975).

INTERCONNECTION MATERIALS FOR THE THIN LAYER ZIRCONIA ELECTROLYTE FUEL CELL

R. J. Ruka
Westinghouse Research & Development Center
Pittsburgh, Pennsylvania 15235

In a project ending in 1972, sponsored by the Office of Coal Research, Isenberg and coinvestigators (1) at the Westinghouse Research & Development Center developed the basic components of a high temperature zirconia electrolyte fuel cell. Electrodes, electrolyte, and cell interconnections were thin layers 20-50 micrometers thick. A system combining the fuel cell with a coal gasification unit, both operating near 1000°C, was proposed. Engineering calculations suggested a possible thermal efficiency as high as 60% based on the higher heating value of the coal.

A schematic of an individual demonstration fuel cell stack built during that earlier project is shown in Fig. 1.

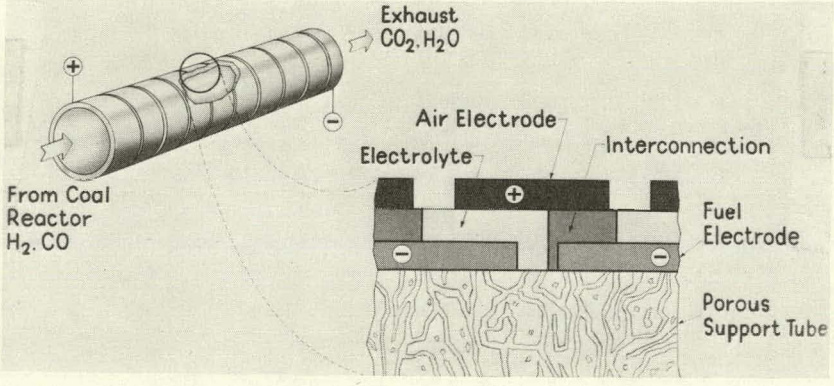

Figure 1. Cross section through the wall of a thin-film fuel-cell stack.

An experimental model of a 15 cell stack was made on that project and was leak-tight as produced, but after 100 hours operation at 1000°C was found to have developed severe cracks at the interconnections. In contrast, individual tests of the air or fuel electrodes in contact with the zirconia electrolyte had shown little deterioration in 1000 hour tests. This suggested that an improved interconnection material, or perhaps structural design or fabrication method, was needed.

Last year, work on this fuel cell design was renewed under sponsorship of ERDA (2) and work on the interconnection problem was given priority.

Our approach to the interconnection problem was to select a limited number of mixed oxide systems in which the metal ion content could be substantially altered to tailor the properties of the interconnection material to the rather severe requirements for an interconnection material. Guidelines for our selection were as follows: (1) moderate material cost, (2) nearly invariant composition in both fuel and air atmospheres, (3) non-reaction with other cell components at 1000°C, (4) resistivity of less than 50 ohm cm and nearly 100% electronic conduction at 1000°C, (5) negligible metal ion conduction, (6) thermal expansion characteristics compatible with other cell components, (7) absence of destructive phase transformations in the region from room temperature to 1000°C, (8) low volatility of oxide components in the working atmosphere, (9) fabricability as a thin, gas-impervious layer.

These stringent requirements eliminate all but a few mixed oxide systems from consideration. One of the few, the rare earth chromite system, is particularly good from the standpoint of low reactivity with other cell components, good conductivity, and composition invariance. In fact, of the various combinations of the rare earths with the 3-d transition metal oxides to form perovskite crystal structure compounds, only the rare earth chromites remain "essentially" invariant in composition in the air and fuel atmospheres typical of fuel cell operation.

We are presently concentrating our work on modifications of lanthanum chromite, lanthanum being the preferred rare earth constituent from the standpoint of cost, conductivity, and thermal expansion. An orthorhombic to rhombohedral phase transformation (3) between room temperature and 1000°C is an undesirable feature of lanthanum chromite. This transformation involves two forms of the same basic perovskite structure having different degrees of crystalline distortion from the ideal cubic. An essentially "diffusionless" transformation occurs readily in this system at the relatively low temperature

of ∿270°C. This transformation is eliminated from the 25-1000°C range by substitution for part of the Cr^{3+}, or part of the La^{3+} in the perovskite crystal structure. Thermal expansion match with the electrolyte can also be adjusted in this way.

Fabrication of interconnection films of the lanthanum chromite system is a difficult problem. Because of the low metal ion diffusion rates, these materials can't be simply sintered to form films at feasible preparation temperatures of 1200°C or below. Two methods are being investigated for this purpose: (1) chemical vapor deposition, and (2) radio frequency sputtering. The major difficulty with the former is obtaining the desired chemical composition of the oxide, while retaining non-porous films after annealing or over porous substrates is the major difficulty with the latter method.

It is anticipated that interconnection film thicknesses of 20-50 micrometers will be used in the thin-layer fuel cell stacks. At these thicknesses, the lanthanum chromite materials exhibit physical, chemical, and electrical properties that are essentially the same as the bulk oxides at the operating fuel cell temperature (∿1000°C).

Critical areas for further study and development include: (1) fabrication of films, (2) ionic conduction properties as related to possible damage to the interconnection-electrode interfaces while current is being drawn from the fuel cell, and (3) long term stability as a non-reactive, invariant composition and non-porous film under operating fuel cell conditions.

In summary, lanthanum chromite, with various substitutions which improve the thermal expansion match, conductivity, and reduce the volatility of chromium components, has the basic characteristics necessary for an interconnection material in the thin layer, zirconia-electrolyte fuel cell for use near 1000°C. Fabrication, composition optimization, and long term operational stability remain for further investigation.

References

1. Final Report - Project Fuel Cell, Research and Development Report No. 57, Office of Coal Research, Department of Interior, Washington, D.C. (1971)

2. Thin Film Battery/Fuel Cell Power Generating System, ERDA Contract No. E(04-3)-1197.

3. J. S. Ruiz, A. M. Anthony, and M. Foex, C. R. Acad. Sci. Paris, 264, Series B, 1967 (1271).

C. ELECTRODES

1. Summary of Panel Session on Electrodes
   T. H. Etsell, University of Alberta

2. Performance of Solid Oxide Fuel Cells
   T. H. Etsell, University of Alberta

3. Mechanism of Electrode Polarization in
   High Temperature Solid Electrolyte Systems
   P. J. Meschter, University of Tennessee

SUMMARY OF PANEL SESSION ON ELECTRODES

T. H. Etsell, Panel Chairman
University of Alberta
Edmonton, Canada

(a) Recommendations:

Consistent with most high-temperature systems, oxide fuel cell development is dependent upon solving materials problems. This is typified by the variety of requirements stipulated for suitable electrodes:

- Moderate cost
- Good adherence
- Thermodynamically stable
- Chemically inert
- Electrochemically active
- Minimal interdiffusion with adjacent components
- Low volatility
- Compatible thermal expansion
- Resistivity-thickness ratio $< 0.2\ \Omega$
- Ease of fabrication into thin porous layers (~ 30 μm) that resist excessive sintering
- Mechanical strength

The most successful electrode materials to date are as follows:

Anode

- Co
- Ni
- Co-stabilized ZrO_2 cermet
- Ni-stabilized ZrO_2 cermet
- CeO_2 (+ Y_2O_3 or La_2O_3)

Cathode

- $LaCoO_3$
- $LaCoO_3$ (+ Sr)
- $PrCoO_3$
- In_2O_3 (+ Sn)
- $LaNiO_3$ (+ Bi)
- $LaMnO_3$ (+ Sr)
- SnO_2 (+ Sb)

The cathode may also be supported by a stabilized zirconia matrix and may be incorporated with a current collector. Unlike the cathode, the anode materials appear widely accepted.

Further effort is required in the quest for a fully satisfactory cathode material, e.g., mixed conducting perovskite- and fluorite-type oxides should be more fully characterized. Cathodes with high oxygen ion mobility

eliminate the need for three-phase contacts. Although some single cell data for up to four years at 1000°C are available, information on the long-term behavior of electrodes in multiple cells, e.g., chemical and thermal compatibility with the interconnector and stability of their resistivity, is needed. Furthermore, the effect on the anode from using real rather than clean laboratory fuels should be determined.

As sophisticated preparation techniques can now be used to prepare very thin impervious electrolytes, knowledge of electrode polarization is more important since it represents a greater percentage of the cell losses. Unfortunately, despite a considerable effort, the polarization behavior of solid electrodes on oxide electrolytes is unclear. Take, for example, the cathode reaction

$$O_{2,g} + 4e' + 2V_O^{\cdot\cdot} \rightarrow 2\,O_O$$

Neglecting some of the transport steps, this occurs as follows on a porous Pt electrode:

$$O_{2,g}\ \text{(in bulk)} \rightarrow O_{2,g}\ \text{(in Pt pores)}$$

$$O_{2,g}\ \text{(in Pt pores)} \rightarrow O_{2,ad}\ \text{(on Pt and s.e.)}$$

$$O_{2,ad}\ \text{(on Pt and s.e.)} \rightarrow O_{2,ad}\ \text{(near tpb)}$$

$$O_{2,ad}\ \text{(near tpb)} \rightarrow 2\,O_{ad}\ \text{(near tpb)}$$

$$2\,O_{ad}\ \text{(near tpb)} \rightarrow 2\,O_{ad}\ \text{(at ers)}$$

$$2\,O_{ad}\ \text{(at ers)} + 2V_O^{\cdot\cdot} \rightarrow 2\,O_O + 4h^{\cdot}$$

$$4h^{\cdot} + 4e' \rightarrow 0$$

In this sequence, ad is adsorbed, s.e. is solid electrolyte, tpb means three-phase boundary, ers is electrochemical reaction site, $V_O^{\cdot\cdot}$ is a doubly ionized oxygen vacancy, O_O is an oxygen ion, $h^{\cdot}$ is an electron hole in the electrolyte and e' is an excess electron. Processes of gaseous diffusion, adsorption, surface diffusion, dissociation, bulk diffusion, dissolution, ionic and electronic transport, and charge transfer are involved. All the above seven steps have been advanced as rate limiting with Pt electrodes, indicative of the difficulty in obtaining and interpreting high-temperature data and the great influence of often ill-defined electrode structure.

To obtain a better fundamental understanding of

electrode processes on oxide electrolytes, careful polarization studies are needed on well-characterized Pt electrodes while appreciating the difficulties:

1) electrode structure may be time dependent
2) active electrode areas are uncertain and may change
3) Pt oxides may influence the results
4) Pt reacts with stabilized zirconia at high cathodic overpotentials (> 1 V)
5) Pt evaporation can be serious in long-term experiments.

Greater advantage should be taken of a-c impedance measurements although interpretation of the results is often difficult. For practical fuel cells, investigations should be carried out on cermet anodes and oxide cathodes, and the influence of electrolyte composition, long times (> 10,000 hr) and lower temperatures (< 900°C) should be evaluated. Determination of exchange current densities for H_2 fuel would prove interesting. Extrapolation of single cell polarization losses to fuel cell power stacks seems realistic if one is aware that operating on real rather than clean fuels could corrode or poison the electrodes.

(b) Discussions

Regarding the loss in performance after 10,000 hr at 830°C of a cell with a Pt cathode, Meschter suggested that this could be due to sintering of the electrode. However, replacing it did not help. Despite this observation, subsequent experiments revealed that Pt evaporation was the main problem rather than an increase in cell resistance. Both its tendency to evaporate and reactivity with oxygen and zirconia make Pt not as attractive a choice as an experimental electrode material.

Srinivasan wondered if any efforts had been made with H_2 as fuel to separate the ohmic contribution during discharge from activation overpotential. Etsell replied that this has been done in several instances but invariably the electrolyte resistance was large making separation of the small activation overpotential contribution very imprecise. With thin-film techniques, better polarization data for H_2 should be forthcoming.

With CO fuel, the non-ohmic contribution to the cell voltage drop is larger but considerable confusion exists as to the rate-limiting step. Tafel slopes of RT/F have often been observed. Appleby remarked that this slope cannot be interpreted by assuming charge-transfer control with two electrons involved (n=2) and the symmetry factor $\alpha = 0.5$ since modern electron transfer theory shows that it is impossible to transfer two electrons together in a packet. Instead, rate control by a chemical, diffusion or adsorption process is needed. The latter may be possible in CO and perhaps in O_2 to explain RT/F slopes. Etsell commented that it is very difficult to separate adsorption from charge transfer as part of the transfer of charge often occurs within the adsorption step, while Meschter indicated that earlier work on CO fuel suggested the two were not independent. Etsell mentioned that charge-transfer control with $n = 1$ and $\alpha = 1$ might be possible but not probable. It might also be feasible to observe an apparent two-electron process if the single electron transfer steps were not independent. Appleby remarked that the observed Tafel slope depends on the partial charge on the species involved in the slow step.

Bergmann introduced the possibility of rate control by oxygen ion transport in the electrolyte which, Appleby stated, could also give an RT/F slope as found for H_2 evolution at Pt electrodes in aqueous solution. Rotating disc electrode experiments show that H_2 diffusion is rate

determining, i.e., the reaction is under Nernstian control. A similar situation may be present in certain solid electrolyte systems. However, Meschter contended that the fuel must be involved to explain the quite different behavior of CO from H_2. Etsell remarked that, unfortunately, other possible rate-limiting steps, e.g., chemical reaction, can also yield RT/F slopes from Tafel plots. Prompted by the reaction between CO and adsorbed oxygen during isotopic exchange measurements, Appleby postulated a mechanism for the anode reaction to explain an RT/F slope consisting of electron transfer to give O^- at the electrolyte surface and chemical reaction with CO to produce CO_2^- followed by rapid discharge to CO_2. This will give the observed slope if the chemical step is rate determining. Nonetheless, such control would result in a tendency toward limiting currents which has generally not been observed.

Appleby asked if there were any data on the CO reaction order for the process thinking that it might be zero order, i.e., full surface coverage of CO at all CO/CO_2 ratios. Etsell replied that the exchange current density varies as $P_{CO}^{0.5}\ P_{CO_2}^{0.5}$. Meschter emphasized that isotopic exchange results indicate that CO is not strongly adsorbed on fairly noble metals.

Isaacs wondered about the use of Tafel plots for interpreting polarization measurements on oxide electrolytes. A large potential gradient at the interface is required to influence an activated process involving charged species. Can this be developed at a solid electrolyte interface since, unlike aqueous electrolytes, electronic conductivity is present spreading the gradient across a much greater distance? Accordingly, one might normally expect to find something more linear than logarithmic. Aqueous and solid electrolytes appear to form two different ideal systems and real solid electrolyte systems are somewhere in between.

Superior cathode materials generally are mixed oxygen and electronic conductors. In response to an inquiry about anionic mobility in In_2O_3, a distorted fluorite-type oxide with one quarter of the anions missing, Isenberg stated that the oxygen ion mobility is very low being comparable to Y_2O_3. It is a purely electronic conductor and is used as a current collector. However, $LaNiO_3$ is a reasonable mixed conductor thereby allowing two-phase reduction of oxygen (air-electrode interface) and oxygen ion migration through the electrode bulk into the electrolyte. Isenberg noted that many perovskites, e.g., $LaNiO_3$, PrO_x, $PrCoO_3$,

display good oxygen ion mobility and, therefore, function well as electrodes although they have high resistivity and cannot withstand thermal cycling. Meschter felt that the best approach appears to be a mixed conductor with a current collector.

Weppner asserted that the important parameter for mixed conducting electrodes is not oxygen ion mobility but the chemical diffusion coefficient which may be several orders of magnitude larger than the tracer diffusion coefficient as electron transport creates an electric field which enhances oxygen ion transport. Isenberg replied that this makes the situation even more favorable but, as a first approach, tracer diffusion coefficients are suitable to evaluate cathode materials. Weppner cautioned that the relationship between tracer and chemical diffusion coefficients is widely variable.

PERFORMANCE OF SOLID OXIDE FUEL CELL ELECTRODES

T. H. Etsell
Department of Mineral Engineering
University of Alberta
Edmonton, Canada T6G 2G6

Acceptable electrochemical characteristics and long-term stability of solid oxide fuel cell electrodes are limited by several problems inherent in high-temperature systems. Carbon deposition at the anode may occur if the fuel gas composition is not carefully controlled, interdiffusion between cell components can affect critical properties, temperature changes can cause cracking due to thermal expansion mismatches, hermetic seals must be maintained, and the nature of the electrodes may change due to sintering. Non-uniform current distribution resulting from small three-phase interfacial areas or high-resistivity oxide cathodes can produce hot spots and associated mechanical stress. Considerable research effort has been made towards the resolution of some of these problems although long-term performance data are often lacking.

Fuel cell electrode performance can often not be separated from overall fuel cell performance and consequently will be discussed by first briefly describing several important cell designs and the influence of critical design parameters. Cell discharge characteristics and stability will then be summarized.

Design

General Electric originally described a cell with a ZrO_2-CaO or ZrO_2-Y_2O_3 tubular or flame sprayed electrolyte, carbon anode and liquid silver cathode (impregnated in porous zirconia) operating on CH_4 fuel (1). The electrodes were subsequently replaced by a nickel anode and $PrCoO_3$ cathode (2).

Brown, Boveri and Cie developed the cell illustrated in Fig. 1 (3). Such a cell yields a power density of 250 mW/cm^3 at 900°C if the electrolyte is 0.5 mm thick. Parallel plate (4) and bell-and-spigot designs (5) were subsequently studied. The electrolyte was either ZrO_2-Y_2O_3 or ZrO_2-Y_2O_3-Yb_2O_3 while nickel and cobalt anodes, and silver, doped $LaNiO_3$, Sn-doped In_2O_3 and $LaCoO_3$ cathodes have been tried.

The Westinghouse thin-film cell in Fig. 2 (6) is

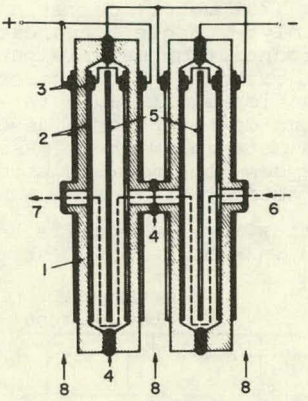

1. ELECTROLYTE
2. ELECTRODE
3. CURRENT COLLECTER
4. ENAMEL SEAT
5. REGULATOR
6. FUEL GAS INLET
7. WASTE GAS OUTLET
8. AIR

Figure 1. Brown, Boveri and Cie fuel cell.

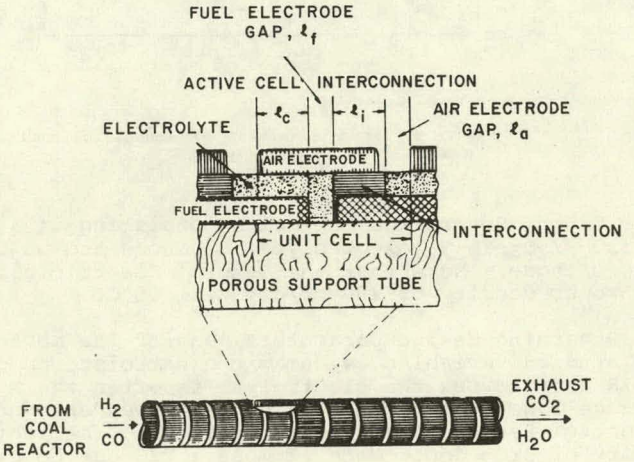

Figure 2. Westinghouse thin-film fuel cell.

built up from 20-50 μm layers (air sprayed, plasma sprayed, vapor deposited or painted) of a porous nickel- or cobalt-stabilized zirconia (70% metal) cermet anode, dense ZrO_2-CaO or ZrO_2-Y_2O_3 electrolyte, dense manganese-doped $CoCr_2O_4$ (2 atom % Mn) interconnection material and porous tin-doped In_2O_3 (2 atom % Sn) cathode. Short-circuiting is inevitable near the interconnection-electrolyte interfaces as electrons can flow from the inside to the outside of the cell through the interconnection material without passing through both electrodes while oxygen ions migrate in the opposite direction through the electrolyte.

Power densities for these cells as a function of temperature are compared in Fig. 3 (5). The three lower curves

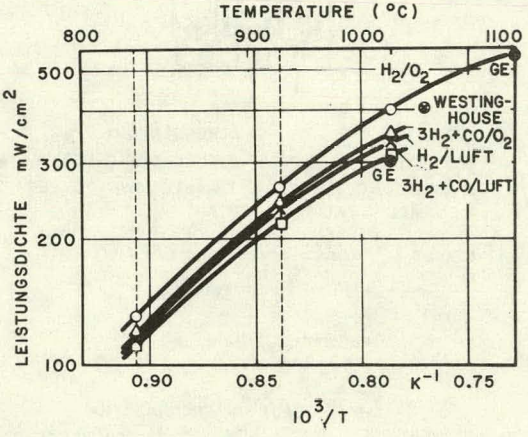

Figure 3. Power densities for industrial fuel cell designs.

are for Brown, Boveri and Cie cells consisting of a 0.5 mm thick ZrO_2-Y_2O_3-Yb_2O_3 electrolyte, Ni anode and Ga_2O_3-doped $LaNiO_3$ cathode. Note that the General Electric cell realized a power density of 400 mW/cm^2 at 1000°C.

Regarding design parameters, one of the most extensively studied variables is ceramic electrolyte composition. Since IR drop across the electrolyte is often the major source of voltage loss, performance is highly dependent on minimizing electrolyte resistivity and thickness. The ionic conductivity of ZrO_2 doped with 12 mole % CaO can be expressed as

$$\sigma = 1170\ e^{-25,200/RT} \qquad [1]$$

while that for both ZrO_2 and CeO_2 containing 9 mole % Y_2O_3 closely follows

$$\sigma = 175\ e^{-18,400/RT} \qquad [2]$$

The latter are over twice as conductive as ZrO_2-CaO at 1000°C with this factor becoming greater at lower temperatures due to the activation energy difference.

Comparing ZrO_2- and CeO_2-based electrolytes, recent work has indicated that CeO_2-Gd_2O_3 has an ionic conductivity four to five times higher than that given by Eq. [2] at 1000°C (7). However, CeO_2 is easily reduced at the fuel electrode which introduces n-type conductivity. Nevertheless, although energy efficiency is accordingly lowered going through a maximum at a certain cell current, it can easily exceed that for an electrolyte with $t_{ion} = 1$ and lower conductivity (8). Furthermore, increasing the total conductivity (constant t_{ion}) leads to larger current and, therefore, power at maximum efficiency. Early work indicated that Pt electrodes on CeO_2-La_2O_3 electrolytes are less polarizable than on ZrO_2-CaO electrolytes, especially at low temperatures ($\leq$ 800°C) (9). Further research is certainly justified as to electrochemical properties and stability of CeO_2-based electrolyte fuel cells.

To maximize the power per unit volume of the cell in Fig. 2, the product of cell resistance and overall cell length must be minimized (10). Subsequent analysis combined with selected material resistivities and cell dimensions produced the plot in Fig. 4. The resistivity-thickness products for the electrolyte and interconnection were chosen to be equal (0.04 ohm-cm^2) which led to equal active cell (section of electrolyte between both electrodes) and interconnection lengths. The maximum power of 7.8 kW/ft^3 (280 mW/cm^3) corresponds to the inflection point on the current density curve (0.66 A/cm^2). Also, the shallow minimum in the resistance curve coincides with the inflection point on the power per unit volume curve.

The optimum electrolyte and interconnection length at maximum power output increases with increasing electrolyte and interconnection resistivity-thickness products or increasing air and fuel electrode gap lengths (ℓ_a,ℓ_f,cf.

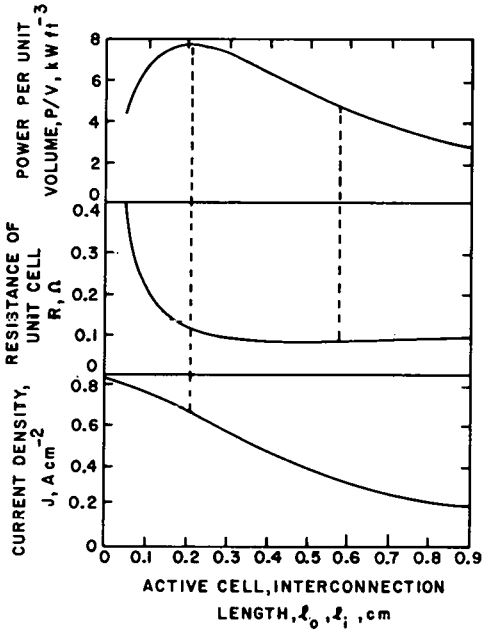

Figure 4. Parameters for the Westinghouse fuel cell.

Fig. 2), but decreases with increasing average electrode resistivity-thickness ratio (10). Changes are such as to keep the cell resistance - cell length product at its optimum value.

Recently, an analysis has been made of the performance of a cylinder type cell using H_2-H_2O fuel with the cathode and anode terminals at opposite ends (11). The cell chosen was assumed to be at 750°C with a CeO_2-Gd_2O_3 electrolyte (ρ = 20 ohm-cm), Ni anode ($\rho = 3.6 \times 10^{-5}$ ohm-cm) and $LaCoO_3$ cathode ($\rho = 10^{-3}$ ohm-cm). Results are presented in Fig. 5. Cases A and B are for the fuel entering at the cathode terminal end and anode terminal end, respectively. The fuel consumption, λ, is the fraction of H_2O in the H_2-H_2O fuel gas and the mean current density was 0.1 A/cm^2. Current density is proportional to fuel consumption rate (gradient of λ) and is, therefore, a minimum at the fuel consumption inflection point. Note the high current density at the cathode terminal in case A (since the cathode has a high resistance). However, in case B, the current distribution is approximately symmetrical since the small H_2 concentration (large λ) at the cathode terminal yields a small emf, i.e., driving force, cancelling the resistance effect.

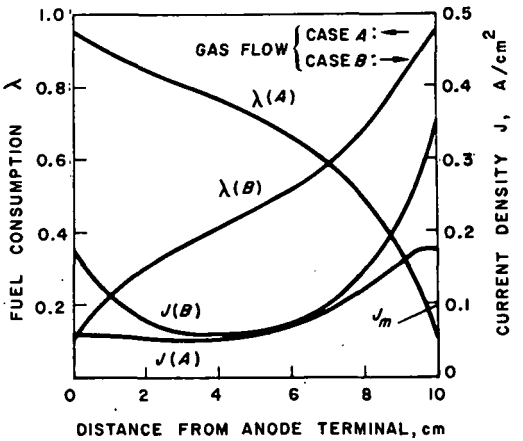

Figure 5. Influence of gas flow direction on performance of cylinder type fuel cell.

Clearly, fuel gas should be supplied from the end with the terminal of the lower resistance electrode.

As seen in Fig. 6, cell length is also a critical parameter. Stacks 20 cm long composed of 2 and 10 cells would give theoretical power densities of 55 and 217 mW/cm^2 at 750°C, respectively (11).

Discharge

Performance is most commonly categorized by discharge characteristics (E-i curves). Open-circuit cell voltages are generally reproducible and agree to within 3% of theoretical values for single or multiple cells.

Linear plots in Fig. 7 (12) for Pt electrodes in contact with O_2 or Ar-O_2 mixtures have a slope approximating the electrolyte resistance, indicative of solely resistance overpotential. This agreement may not be realized since porous electrodes only contact part of the solid electrolyte surface reducing its effective cross-sectional area for conduction (13). Alternatively, insufficient cathode porosity can cause marked polarization (14), although cathodes with suitable composition, porosity and pore size should not cause serious

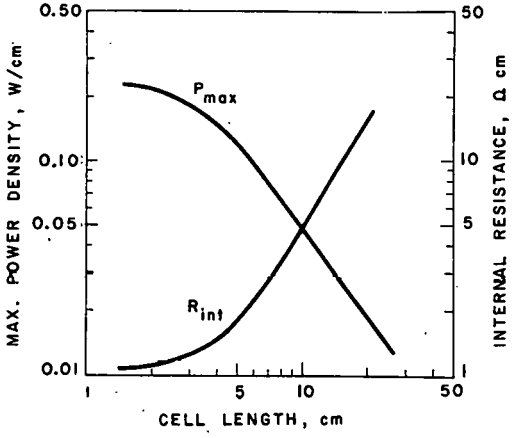

Figure 6. Influence of cell length on performance of cylinder type fuel cell.

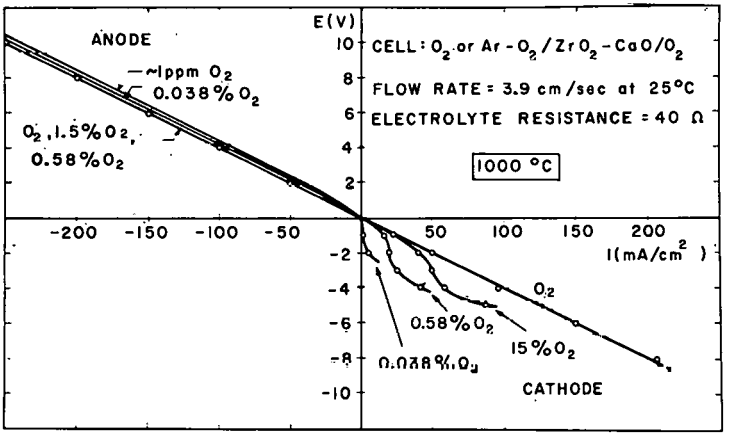

Figure 7. Pt electrode characteristics in contact with O_2 and Ar-O_2 mixtures.

losses at 900°C - 1000°C (15,16). Mixing the cathode with an oxide powder of similar composition as the electrolyte can greatly lower the polarization (14,17). Although low oxygen pressures at the cathode result in significant diffusion overpotential (12), oxygen or air is invariably the oxidant in fuel cells.

A major advantage in high-temperature operation should be rapid electrochemical reactions without the need for catalysts. However, considerable discrepancy has existed as to the presence or absence of non-ohmic polarization at the fuel electrode. In the presence of H_2, additional polarization is essentially absent in Fig. 8 (18). Reformed propane or hydrogen contacted the anode side of a 0.5-1.0 mm thick ZrO_2-CaO disc. For all gases, essentially only ohmic polarization is present (there is a small non-ohmic contribution at low i) since $H_2 + O^{=} \rightarrow H_2O + 2e$ is the overall anode reaction. Some concentration polarization is evident from the lowest curve at high current densities due to dilution with N_2.

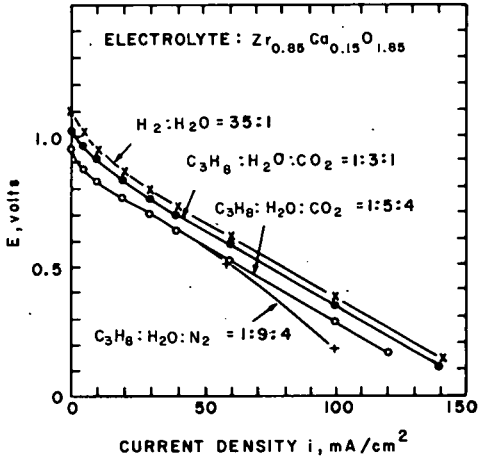

Figure 8. Discharge curves for various fuels at 1000°C. Pt electrodes.

Excellent performance for a 1.4 mm thick ZrO_2-Yb_2O_3 electrolyte cell at 800°C with either a H_2-H_2O or CO-CO_2 mixture at the anode has been reported in Fig. 9 (19).

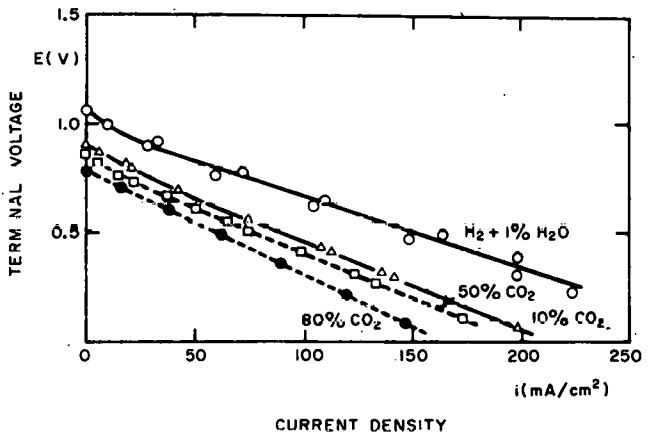

Figure 9. Discharge characteristics for a ZrO_2-Yb_2O_3 electrolyte cell at 800°C. Ni anode. Ag cathode.

For H_2 fuel, this type of behavior has been verified at 1000°C for a ZrO_2-CaO electrolyte, CeO_2-La_2O_3 or CeO_2-Y_2O_3 anode and Pt cathode (16,20), and for a ZrO_2-Y_2O_3-Yb_2O_3 electrolyte disc, Ni anode and SnO_2 + 8 atom % Sb cathode (21). However, charge transfer at the anode generally does not occur readily in dry CO-CO_2 mixtures. Considerable transition overpotential is apparent when the IR drop is subtracted from the data in Fig. 10 (22) and Fig. 11 (12) obtained from ZrO_2-CaO electrolyte tubes 0.8 and 2.0 mm thick, respectively. Exchange current densities are about 1 mA/cm^2 and decrease further as the gas mixture becomes dilute in either component.

Cell performance for single Westinghouse thin film cells has been reported (23). A cell with a 60 μm reactively sintered ZrO_2-CaO electrolyte, a cobalt-stabilized zirconia anode in contact with H_2 fuel, and a cathode consisting of $PrCoO_3$-impregnated porous ZrO_2-Y_2O_3 coated with

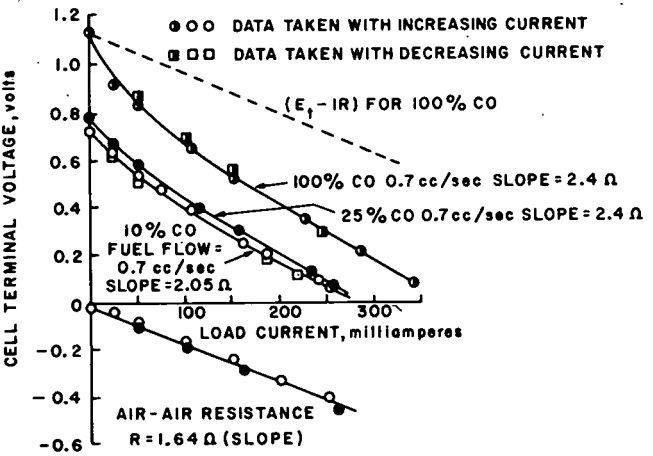

Figure 10. Discharge curves for $CO-CO_2$ mixtures at 940°C. Pt electrodes. A = 27.6 cm^2.

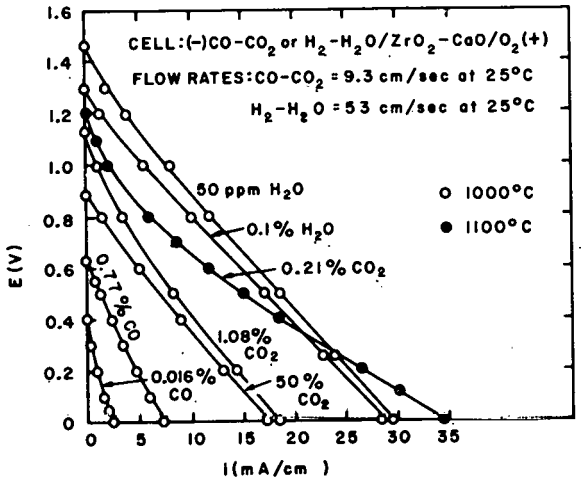

Figure 11. Discharge curves for $CO-CO_2$ and H_2-H_2O mixtures at 1000° and 1100°C. Pt electrodes.

In_2O_3 + 2 atom % Sn still maintained a terminal voltage at 960°C of 0.6 V at 150 mA/cm^2.

Westinghouse results from Fig. 10 have been extended to a stack of 20 bell-and-spigot cells in Fig. 12 (22).

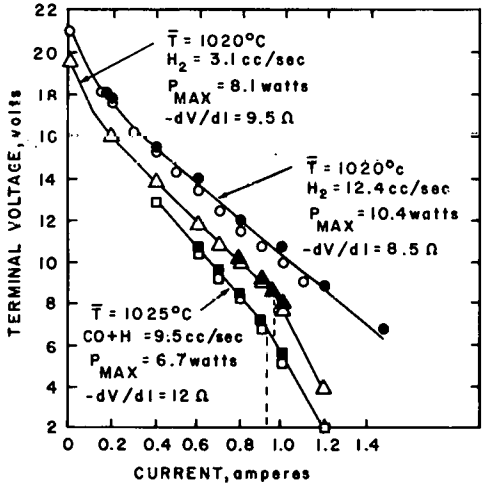

Figure 12. Discharge characteristics for a 20 cell stack. Pt electrodes. A = 13 cm^2.

Excess hydrogen has been supplied to the anode in the uppermost curve whereas complete hydrogen combustion was realized for the lower curves. Further extension to 20 stacks of 20 cells (2 groups of 200 series-connected cells in parallel) appears in Fig. 13 (22). At 1000°C using hydrogen as fuel, the maximum power of 110 W was produced at a current of 1.2 A.

From the last results, it would appear that discharge characteristics for single cells can be extrapolated to predict power system performance with some degree of confidence. However, this cannot be adequately assessed without further data.

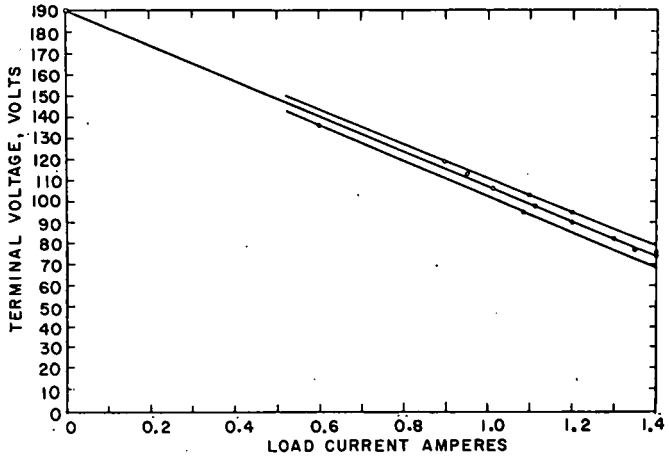

Figure 13. Westinghouse 100 W solid electrolyte fuel cell power system. Pt electrodes.

Stability

Structural changes with time in cell components at high temperatures pose many serious problems.

If not fully stabilized, zirconia will progressively destabilize on thermal cycling (24). Stabilized zirconia electrolytes tend to age due to cation and oxygen vacancy ordering leading to a decrease in conductivity. Unfortunately, aging kinetics are most rapid at the temperatures of fuel cell operation (1). Typical behavior for ZrO_2-Y_2O_3 is presented in Fig. 14 (25). Samples were held for 9 days in air and a further 16 days in H_2-H_2O. The data at the various temperatures were obtained using interpolated values from log σ vs. 1/T plots taken in the vicinity of 800°C at selected times. Electrolyte resistance increases considerably and obeyed first order kinetics given by

$$-\frac{d\sigma}{dt} = k(\sigma - \sigma_\infty) \qquad [3]$$

where σ_∞ is the final conductivity. Furthermore, aging depends on atmosphere.

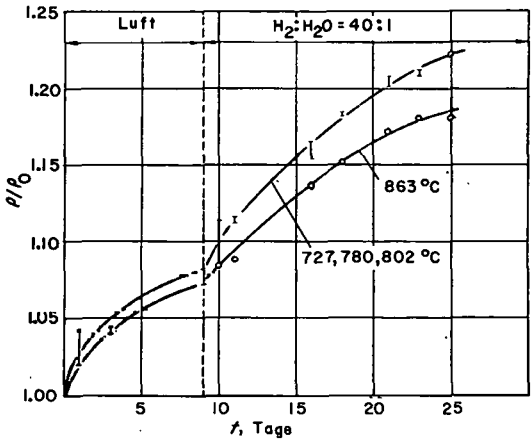

Figure 14. Aging of ZrO_2 + 9 mole % Y_2O_3 at 800°C in air and H_2-H_2O.

Anode materials must not densify and block gas channels, corrode in the fuel atmosphere or react with the electrolyte. The cobalt concentration profile in a ZrO_2-Y_2O_3-Yb_2O_3 electrolyte after cell operation for 10,000 hr at 830°C is shown in Fig. 15 (26). The cobalt diffusion coefficient was calculated to be 5×10^{-15} cm^2/sec.

Cathode materials must resist changes in their conductivity and, like the anode, must have an expansion coefficient similar to the electrolyte.

Coincident discharge curves for a cell comprised of a ZrO_2-Y_2O_3-Yb_2O_3 electrolyte and a $LaCoO_3$ cathode and Ni anode were found during 220 hr of cell operation at 1000°C (27). A power density of 202 mW/cm^2 was maintained. A similar cell with a SnO_2 + 8 atom % Sb cathode operated satisfactorily for 262 hr (21). Reasonable behavior for 1000 hr at 830°C was reported for cells with a Ni or Co anode and Ag cathode (4). Doped In_2O_3 operated successfully as the cathode for over 1100 hr at 1000°C (14). Over 300 mW/cm^2 was maintained for over 7000 hr at 1000°C in a cell with a Ni anode and $PrCoO_3$ cathode (2). However, considerable power loss was experienced with a cell involving a 0.9 mm thick ZrO_2-Y_2O_3-Yb_2O_3 electrolyte, Co + 10 atom % Fe anode in contact with H_2 fuel, and Pt cathode as indicated in Fig. 16(26). Although the open-circuit voltage was

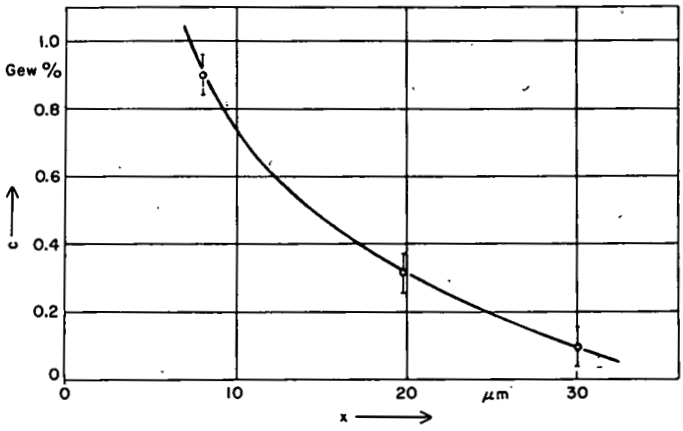

Figure 15. Diffusion of a cobalt anode into a ceramic electrolyte after 10,000 hr.

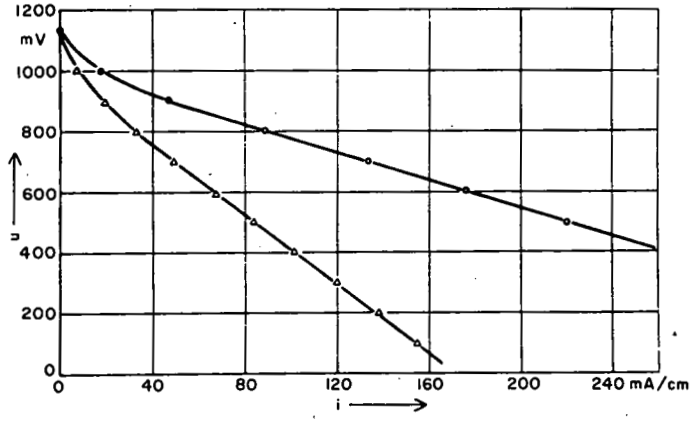

Figure 16. Cell deterioration after 10,000 hr of operation at 830°C.

unaltered, the power decreased from 105 to 45 mW/cm^2 after 10,000 hr of operation. This was attributed to an increase in electrolyte resistance. However, the necessary change would be too excessive to account for the entire performance loss. Vaporization of the Pt cathode is most probable although cooling the cell and replacing the electrodes did not help.

More research is definitely needed on the long-term changes (5000-10,000 hr) in oxide cell components at about 1000°C as a function of time, atmosphere, current and electrolyte composition. Emphasis should be placed on thin-film materials. Secondly, more long-term cell performance information is needed. In this case, great care must be exercised in extrapolating single cell results to power stacks.

References

1. D.W. White, "A Zirconia Electrolyte Fuel Cell" in Proc. Internat. Symp. Fuel Cells, Vol. III, pp. 10-18, S.E.R.A.I., Brussels(1966).

2. D.W. White, GE Rept. 69-C-05, Jan. 1969.

3. O. Antonsen, W. Baukal and W. Fischer, "High-Temperature Fuel Cells with a Ceramic Electrolyte", Brown Boveri Rev., 53, 21-30 (1966).

4. H.J. Boehme and F.J. Rohr, "Disc-Shaped Solid Electrolytes for Construction of High-Temperature Fuel Cells" in Proc. Third Internat. Symp. Fuel Cells, pp. 120-24, Presses Académiques Européennes, Brussels (1969).

5. W. Fischer, H. Kleinschmager, F.J. Rohr, R. Steiner, and H.H. Eysel, "High-Temperature Fuel Cells with Ceramic Electrolytes for the Conversion of Inexpensive Fuels. Part II", Chem.-Ing.-Tech., 44, 726-32 (1972).

6. E.F. Sverdrup, C.J. Warde, and A.D. Glasser, "A Fuel-Cell Power System for Central-Station Power Generation Using Coal as a Fuel" in From Electrocatalysis to Fuel Cells, G. Sandstede, Editor, pp. 255-77, Univ. of Washington Press, Seattle (1972).

7. T. Kudo and H. Obayashi, "Oxygen Ion Conduction of the Fluorite-Type $Ce_{1-x}Ln_xO_{2-x/2}$ (Ln = Lanthanoid Element)", J. Electrochem. Soc., 122, 142-47 (1975).

8. T. Takahashi, K. Ito and H. Iwahara, "The Efficiency of Solid-Electrolyte Fuel Cells", Electrochim. Acta, 12, 21-30 (1967).

9. T. Takahashi, K. Ito and H. Iwahara, "The Fuel Cell With a New Type Solid Electrolyte" in Proc. Internat. Symp. Fuel Cells, Vol. III, pp. 42-48, S.E.R.A.I., Brussels (1966).

10. E.F. Sverdrup, C.J. Warde and R.L. Eback, "Design of High-Temperature Solid-Electrolyte Fuel-Cell Batteries for Maximum Power Output per Unit Volume", Energy Conv., 13, 129-41 (1973).

11. T. Kudo and H. Obayashi, "Performance of Cylinder Type High Temperature Solid Electrolyte Fuel Cell", Energy Conv., 15, 121-25 (1976).

12. T.H. Etsell and S.N. Flengas, "Overpotential Behavior of Stabilized Zirconia Solid Electrolyte Fuel Cells", J. Electrochem. Soc., 118, 1890-1900 (1971).

13. H. Tannenberger and H. Siegert, "The Behavior of Silver Cathodes in Solid Electrolyte Fuel Cells", Adv. Chem. Series, 90, 281-300 (1969).

14. E.F. Sverdrup, D.H. Archer and A.D. Glasser, "Stannic Oxide and Indium Oxide Films as Air Electrodes for High Temperature Coal Reacting Fuel Cells", Adv. Chem. Series, 90, 301-14 (1969).

15. C.S. Tedmon, Jr., H.S. Spacil and S.P. Mitoff, "Cathode Materials and Performance in High-Temperature Zirconia Electrolyte Fuel Cells", J. Electrochem. Soc., 116, 1170-75 (1969).

16. T. Takahashi, H. Iwahara and Y. Suzuki, "Electrode Materials for High Temperature Solid Electrolyte Fuel Cells" in Proc. Third Internat. Symp. Fuel Cells, pp. 113-19, Presses Académiques Européennes, Brussels (1969).

17. H. Eysel and H. Kleinschmager, "Electrode Behavior in High-Temperature Fuel Cells with Oxygen-Ion Conducting Solid Electrolytes", ibid., pp. 92-96.

18. H. Binder, A. Koehling, H. Krupp, K. Richter and G. Sandstede, "Electrochemical Oxidation of Hydrocarbons in a Solid Electrolyte Fuel Cell at Temperatures of 900-1000°C, Electrochim. Acta, 8, 781-93 (1963).

19. H. Schachner and H. Tannenberger, "Behavior of Nickel Anodes in Solid Electrolyte Fuel Cells" in Proc. Internat. Symp. Fuel Cells, Vol. III, pp. 49-55, S.E.R.A.I., Brussels (1966).

20. T. Takahashi, H. Iwahara and I. Ito, "Solid Solutions of Ceria as an Anode Material for Solid Electrolyte Fuel Cells", Denki Kagaku, 38, 509-13 (1970).

21. R. Boehm and H. Kleinschmager, "Tin Dioxide Layers on Stabilized Zirconia as Cathodes in High-Temperature Fuel Cells", Z. Naturforsch., 26a, 780-82 (1971).

22. D.H. Archer, L. Elikan and R.L. Zahradnik, "The Performance of Solid-Electrolyte Cells and Batteries on CO-H_2 Mixtures; A 100-Watt Solid-Electrolyte Power Supply" in Hydrocarbon Fuel Cell Technology, B.S. Baker, Editor, pp. 51-75, Academic Press, New York (1965).

23. N.J. Maskalick and C.C. Sun, "Sintered Zirconia Electrolyte Films in High-Temperature Fuel Cells", J. Electrochem. Soc., 118, 1386-91 (1971).

24. J.D. Buckley and H.H. Wilson, "Destabilization of Zirconia by Cyclic Heating", J. Amer. Ceram. Soc., 46, 510 (1963).

25. W. Baukal, "Aging Kinetics of a ZrO_2 - Solid Electrolyte as a Function of Oxygen Partial Pressure", Electrochim. Acta, 14, 1071-80 (1969).

26. R. Steiner, "The Long-Term Behavior of High-Temperature Fuel Cells", Energy Conv., 12, 31-35 (1972).

27. W. Fischer, H.Kleinschmager, F.J. Rohr, R. Steiner and H.H. Eysel, "High-Temperature Fuel Cells with Ceramic Electrolytes for the Conversion of Inexpensive Fuels. Part I", Chem.-Ing.-Tech., 43, 1227-32 (1971).

MECHANISMS OF ELECTRODE POLARIZATION IN HIGH-TEMPERATURE SOLID ELECTROLYTE SYSTEMS

Peter J. Meschter
Department of Chemical, Metallurgical, and Polymer Engineering
The University of Tennessee
Knoxville, TN 37916

Possible atomistic mechanisms of cathodic and anodic polarization in electrochemical cells with solid oxide electrolytes are reviewed. Polarization phenomena have been investigated by d.c. and complex admittance techniques. Rate limiting electrode processes are identified from the variation of limiting current I_{lim} and electrode resistance R_e with temperature, P_{O_2}, composition of electrode and electrolyte, and electrode geometry.

The cathode or air electrode may be either an electronic conductor (typically Pt, $PrCoO_3$, In_2O_3-SnO_2) or a mixed ionic and electronic conductor (pure ZrO_2 or PrO_{2-x}). In the former case, incorporation of oxygen into the electrolyte requires three-phase gas-electrode-electrolyte contact. Thus the porosity of the supporting electrode becomes critical, and pore diffusion a likely rate-limiting step. Polarization data obtained on microporous electrodes (1-4) are evaluated on the basis of a pore-diffusion formalism presented by Schwerdtfeger and Turkdogan (5). Pore diffusion control predominates for small (< 1μ) pore sizes; small (< 0.02) values of P_{O_2} ; and high temperatures. For this case, $I_{lim} \propto P_{O_2}$.

Polarization studies on macroporous electrodes show wide variations in results. In general, $I_{lim} \propto P_{O_2}^{1/2}$. Adsorption-dissociation of O_2, surface diffusion, charge-transfer, and migration of electronic defects in the electrolyte have all been adduced as rate-limiting steps. Well defined studies of rigorously characterized systems are required to resolve these discrepancies.

In mixed-conduction cathodes, roughly equal transport numbers for ions and electrons through the overall electrode are desirable. In the absence of a suitable intercalation compound, use of an embedded current collector seems necessary to achieve this goal. No basic research on these systems exists in the open literature.

The anode (fuel electrode) presents fewer problems. For

sufficiently porous Pt or Ni anodes, no overpotential is observed in H_2-H_2O (10) or O_2-Ar (3) mixtures. Polarization does appear in CO-CO_2 mixtures (3), but is reduced when H_2O is added to the fuel gas (11). Apparently a combined surface reaction-charge transfer step is rate-controlling. Results of Grabke (12) indicate that O transfer from H_2O to metal and oxide surfaces is generally much faster than from CO_2, in agreement with the proposed anodic polarization mechanism.

References

1. M. Guillou, J. Millet, S. Palous, Electrochim. Acta, 13, 1411-1423 (1968).

2. C. S. Tedmon, Jr., H. S. Spacil, S. P. Mitoff, J. Electrochem. Soc., 116, 1170-1175 (1969).

3. T. H. Etsell, S. N. Flengas, J. Electrochem. Soc., 118, 1890-1900 (1971).

4. P. Fabry, M. Kleitz, Electroanal. Chem. and Interfacial Electrochem, 57, 165-177 (1974).

5. K. Schwerdtfeger, E. T. Turkdogan, in Physicochemical Methods in Metals Research, Part 1, R. A. Rapp, ed. (Wiley-Interscience, New York, 1970), pp. 321-408.

6. J. E. Bauerle, J. Phys. Chem. Solids, 30, 2657-2670 (1969).

7. H. Yanagida, R. J. Brook, F. A. Kröger, J. Electrochem. Soc., 117, 593-602 (1970).

8. R. J. Brook, W. L. Pelzmann, F. A. Kröger, J. Electrochem. Soc., 118, 185-192 (1971).

9. S. Pizzini, M. Bianchi, P. Colombo, S. Torchio, J. Appl. Electrochem., 3, 153-159 (1973).

10. J. Weissbart, R. Ruka, J. Electrochem. Soc., 109, 723-726 (1962).

11. D. H. Archer, L. Elikan, R. L. Zahradnik, in Hydrocarbon Fuel Cell Technology, B. S. Baker, ed.(Academic Press, New York, 1965), pp. 51-75.

12. H. J. Grabke, Ann. N. Y. Acad. Scis., 213, 110-136 (1973).

II. EXTENDED ABSTRACTS OF PRESENTATIONS

THIS PAGE

WAS INTENTIONALLY

LEFT BLANK

A. APPLICATION OF FUEL CELLS

1. A DOE Overview of Solid Electrolyte Fuel Cell Technology
   I. L. Harry, U.S. Department of Energy

2. Discussion of Potential of High Temperature Solid Oxide Fuel Cell Powerplant Systems
   M. Warshay, NASA-Lewis Research Center

A DOE OVERVIEW OF SOLID OXIDE ELECTROLYTE FUEL CELL TECHNOLOGY

Ian Leslie Harry, Program Manager
Division of Power Systems
U.S. Department of Energy

On behalf of ERDA, I would like to welcome you to the First Solid Oxide Electrolyte Fuel Cell Workshop. It is gratifying to see such a good turnout of the leading experts in this field. Before we get on with the agenda, I would like to say just a few words about the ERDA Fuel Cell Program, about workshops, and about the background of solid oxide electrolyte fuel cell technology.

As most of you probably know, the ERDA Fuel Cell Program is almost two years old. Clean, quiet, highly efficient power generation from a variety of fuels at a lower cost is our major objective. With this in mind, and in order to accelerate the implementation of fuel cell technology, our program has been divided into six major project areas. These are: Utility Demonstrations, Systems Development, First Generation Technology, Second Generation Technology, Fuels Utilization, and Applied Research.

The solid oxide electrolyte fuel cell program is an integral component of the Applied Research Project Area. This project area supports emerging fuel cell systems by developing a technology base to ensure continuing improvements and the development of future advanced technology options. The solid oxide fuel cell, with its potential for high system efficiency and reject heat utilization, and with its limited technology base is an appropriate project for the Applied Research area. Workshops, like this, help determine the present state-of-the-technology and provide inputs to determine the direction in which future research and development should be directed.

Initial efforts on the development of solid oxide electrolyte fuel cells for electric power generation from coal began in the early 1960's at Westinghouse under the sponsorship of the Department of Interior, Office of Coal Research (OCR). This early work resulted in the initial development of a technology base, the design of a 100 kw coal reacting fuel cell power plant, a practical fuel cell configuration -- the thin-film battery, and construction and testing of a 100 watt fuel cell battery. Unfortunately, this early thin-film battery experienced severe materials problems resulting in a useful life of less than 100 hours.

Thus, the present solid oxide electrolyte fuel cell program is building on this technology base. Although technical feasibility has been previously achieved, the short-lived demonstration and its accompanying failure require a rethinking from a technology

development prospective. It is the intent of ERDA's efforts in solid oxide electrolyte fuel cells to develop this coal utilizing option to the point where the Nation may share in the benefits derived from successful application of this technology to our energy problem.

DISCUSSION OF POTENTIAL OF HIGH TEMPERATURE SOLID OXIDE FUEL CELL POWERPLANT SYSTEMS

Marvin Warshay
NASA, Lewis Research Center
Cleveland, Ohio

Fuel cell powerplants were one of ten classes of advanced energy conversion systems studied in the Energy Conversion Alternatives Study (ECAS) undertaken by NASA(1) for ERDA and NSF. The powerplant systems were to operate on coal or coal-derived fuels and were primarily for central-station base load power generation. The objective of ECAS was to provide an evaluation of advanced fossil-fired central-station powerplants under common ground rules and constraints and to a comparable level of detail.

The ECAS Study consisted of two phases: 1- a parametric analysis and 2- conceptual designs of selected powerplant systems together with implementation assessment plans for each system. The prime contractors for the ECAS Phase 1 parametric analyses were General Electric (2) and Westinghouse (3) who conducted essentially parallel studies. The major results included performance and cost (e.g., efficiency, capital cost, and cost of electricity (COE)). In the study, emission and natural resource requirements were considered. Based upon Phase 1 and other considerations, 11 powerplant system cases were selected by the ECAS Steering Committee for more detailed study in the Phase 2 conceptual designs.

The high temperature zirconia solid oxide fuel cell (SE) was one of the systems studied as part of the fuel cell study in Phase 1. Based upon the conclusions of ECAS, the present report discusses very briefly the potential of the SE fuel cell powerplant for base load electric power generation from coal.

The ECAS results support the expectation that efficiency increases with fuel cell temperature. In particular, the results indicate that high temperature fuel cells (both SE systems which operate at approximately 1832°F and the molten carbonate (MC) system studied by Westinghouse which operates at approximately 1200°F) fit well into the ECAS Study framework. In fact, their high quality waste heat is best utilized in large powerplant systems such as the "coal-fired" base load powerplants upon which the ECAS Study is based. The fuel cell waste heat can be used either by a bottoming cycle or by a coal gasifier or in some cases by both. Further, close integration can effectively improve the energy efficiency of the coal conversion process. Finally, temperature helps the fuel

cell to approach its high efficiency potential by reducing cell polarization losses.

While the results of both contractors generally support this conclusion, the overall SE powerplant system efficiencies by Westinghouse are significantly higher than those of GE. General Electric considered four SE cases all with steam bottoming cycles. Westinghouse looked at twenty SE cases, three of which were integrated powerplant systems. The primary difference between the GE and the Westinghouse SE concepts is related to the thinner SE cells envisaged by Westinghouse which deliver higher performance than the more conservative GE SE concept. This results in a maximum of 34.3 percent efficiency for the GE integrated SE systems compared to a 53.0 percent maximum for the Westinghouse SE integrated cases.

The most important question, that of cost of electricity (COE), for the SE system can be discussed relative to the COE of a 3500 psi/1000°F/1000°F steam system with a conventional furnace. ECAS characterized this system as having 37 percent efficiency and a 32 mills/kW-hr COE (based on 1974 as the reference year for cost estimates). The COE results for all integrated SE system cases exceeded the 32 mills/kW-hr. For GE the COE range was 42 to 45 mills/kW-hr. The Westinghouse COE values ranged from 40 to 52 mills/kW-hr. In general, estimates of fuel cell efficiencies are more reliable than estimates of fuel cell powerplant costs. However, a number of important generalizations relating to cost can be drawn from the ECAS Study.

The first is that since the fuel cell systems in ECAS Phase 1 had not been optimized lower cost systems are possible. For the SE high temperature powerplant system, this is especially likely via a more thorough system integration than had been possible in the scope of Phase 1. This fact was made evident from the results of Phase 2 which consisted of 11 conceptual design cases, including a molten carbonate fuel cell powerplant system. These Phase 2 results will be covered briefly in the presentation to illustrate the impact of more detailed treatments including partial optimization.

One of the most important cost considerations for the SE system is life. For all the fuel cell systems studied in ECAS, both low temperature and high temperature, the effect of fuel cell useful life upon COE is pronounced until at least 30,000 hours. For the Westinghouse SE systems which were based upon 10,000-hour life, increasing life to beyond 30,000 hours could lower COE to the lower 30's mills/kW-hr. However, for the SE fuel cells which have been operated, less than 1000 hours life has been demonstrated. This represents a major materials hurdle.

Performance affects COE in a number of ways. Efficiency directly affects the fuel component in the COE. In addition, fuel cell power density affects the capital and the O&M components of COE. Higher power density reduces required cell area and, therefore, cost (assuming all unit costs remain the same). Thus, even though the GE SE cases were based upon a 40,000-hour life, the COE's were as high as those of the Westinghouse 10,000-hour cases because of lower power density and efficiency.

In conclusion, the SE fuel cell has the potential to be the heart of a very fuel-efficient integrated powerplant system for base load generation of electricity from coal. The ability of this system to achieve an attractive COE is directly related to achieving a SE technology capable of maintaining high power density for $30,000^{+}$ hours and achieving optimum integration of the balance of plant through design, subsystems technology, and trade-off analyses within the total system.

REFERENCES

1. Comparative Evaluation of Phase 1 Results from the Energy Conversion Alternatives Study (ECAS). NASA TM X-71855, 1976.

2. Energy Conversion Alternatives Study (ECAS), General Electric Phase 1 Final Report. NASA CR-134948, 1976.

3. Energy Conversion Alternatives Study (ECAS), Westinghouse Phase 1 Final Report. NASA CR-134941, 1976.

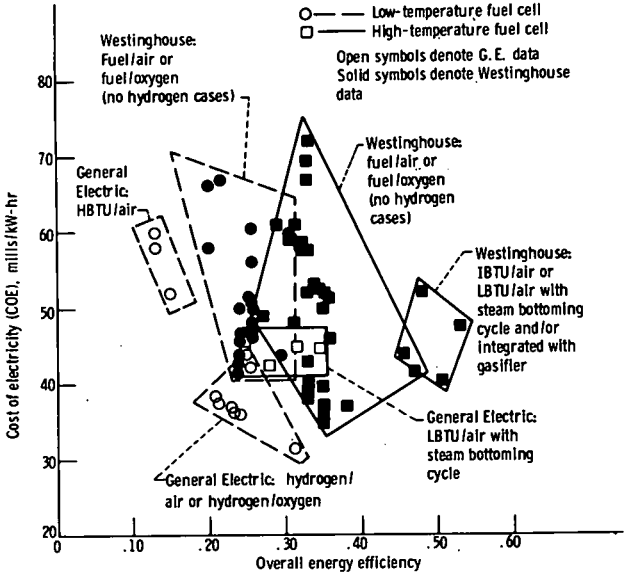

Figure 5.11-5. Energy efficiency - cost of electricity map for various types of fuel-cell powerplants.

SHORT SUMMARY OF RESULTS
"INTEGRATED" SE CASES

A. GE

4 SE POWERPLANTS WITH STEAM BOTTOMING CYCLE

PARAMETER	(1)	(2)	(3)	(4)
FUEL/OXIDANT	LBTU/AIR	→	→	→
TEMP., °F	1832	→	→	→
ELECTROLYTE THICKNESS, cm	0.051	→	→	0.013
CURRENT DENSITY, ASF	200	200	700	700
CELL VOLTAGE, V	0.59	0.59	0.18	0.42
POWER OUTPUT, MW	1112	1111	632	824
FUEL CELL LIFE, HR	90,000	→	→	→
RESULTS				
OVERALL EFF., %	32	34	25	28
COE, MILLS/KW/HR	45	44	45	42

B. WESTINGHOUSE

- (5) WESTINGHOUSE SE POWERPLANT WITH STEAM BOTTOMING CYCLE
- (6) WESTINGHOUSE SE POWERPLANT INTEGRATED WITH GASIFIER
- (7) WESTINGHOUSE SE POWERPLANT INTEGRATED WITH GASIFIER AND WITH STEAM BOTTOMING CYCLE

PARAMETER	(5)	(6)	(7)
FUEL/OXIDANT	LBTU/AIR	LBTU/AIR	LBTU/AIR
TEMP., °F	1832	1832	1832
ELECTROLYTE THICKNESS, cm	0.004	0.002	0.004
CURRENT DENSITY, ASF	400	800	400
CELL VOLTAGE, V	0.66	0.68	0.56
POWER OUTPUT, MW	1164	219	1064
FUEL CELL LIFE, HR	10,000	10,000	10,000
RESULTS			
OVERALL EFF., %	51	53	48
COE, MILLS/KW-HR	40	48	52

B. INTERCONNECTION MATERIALS

1. Studies on Glass Composites and Doped Rutile Interconnection Materials

P. G. Russell, H. S. Isaacs, S. Srinivasan, Brookhaven National Laboratory; A.C.C. Tseung, The City University (London)

STUDIES ON GLASS COMPOSITES AND DOPED RUTILE AS INTERCONNECTION MATERIALS*

P. G. Russell, H. S. Isaacs, A. C. C. Tseung†,
and S. Srinivasan
Department of Applied Science
Brookhaven National Laboratory
Upton, New York 11973

The main problem hindering the successful development of a solid oxide electrolyte fuel cell is the cracking observed in fuel cell stacks, caused by the difference in the coefficient of thermal expansion of the chromium sesquioxide, Cr_2O_3, interconnection material, and the stabilized zirconia support tube and electrolyte(1). Recently, a mechanically stronger nickel-zirconia cermet structure was obtained by carrying out the reduction of the nickel oxide component at 1350°C, i.e., closer to the sintering temperature(2). This development which gives a stronger anode bond both to the porous support tube and to the Cr_2O_3 interconnection layer, may overcome the cracking problem. Nevertheless, alternative oxide systems with improved coefficients of thermal expansion offer a more reliable long-term solution.

Any interconnection material that gives an adequate performance at the proposed operating stack temperature of 1000°C must meet the following criteria(1): (a) "chemical stability in air and fuel gas; (b) resistivity in the working environment of less than 50 ohm cm; (c) thermal expansion characteristics compatible with other fuel cell components; (d) nonreactivity toward other components; (e) fabricability as a gas-impervious layer, 40 μm or less in thickness;" (f) no phase changes or recrystallization after extended periods of time; and (g) no significant mass transfer effects under the chemical gradient which, for example, may lead to the formation of voids and/or high resistance contacts. Furthermore, additional thermal stresses will be present due to temperature differences in the system. A number of mixed oxide systems are being considered, which may satisfy these requirements.

A different approach is to use an interconnection material which is plastic and has a low modulus of elasticity at the temperature of operation. In this case, differences in the coefficient of thermal expansion between the interconnector

*This work was done under the auspices of the U.S. Department of Energy.

†Visiting Scientist from the Department of Chemistry, The City University, London, England.

and the solid oxide electrolyte and/or differences in the temperature would give low stresses and the chances of cracking would be greatly reduced. Work at The City University of London(3) has shown that Fe_2O_3 doped with TiO_2 and mixed with soda-lime glass forms a conducting and impervious coating on mild steel. This method depends on using a semiconducting oxide that is partially soluble in the glass at the sintering temperature. Partial precipitation of the dissolved oxide following the sintering process should result in a composite material consisting of a conducting oxide phase within the glassy component. When a tinuous oxide phase forms, the conductivity of the composite l be strongly dependent upon the conductive properties of semiconducting oxide. In the absence of extensive recrystallization, the conductivity of a glassy phase containing the transition metal oxide, which may be electronic(5) would be an important factor. The advantages of this approach are: (a) the coefficient of thermal expansion of this material can be adjusted within wide limits by selecting different glasses and/or oxides; (b) there is a wider choice of semiconducting oxides since considerations of the coefficient of thermal expansion are relaxed; (c) the composite coating has a very low modulus of elasticity at 700° to 1200°C, thus greatly reducing thermal stresses in the cell; (d) it is far easier to obtain gas tightness since these materials are similar to enamels and glazes used in the ceramic industry. As an example, the electrical resistivity in a low melting silica glass containing lead ferrite crystals in close proximity has been found to be as low as ∿1 ohm cm at 500°C(4).

Chromium sesquioxide was chosen as a reference material because of its previous use in a high temperature fuel cell stack. Samples containing Cr_2O_3 and lead glass (Corning #0120) in a 1:1 ratio by volume were sintered at 1200°C. With this sintering temperature the room temperature resistivity is about 10^8 ohm cm, while the values at 1000°C are ∿10^5 ohm cm. Much lower values would have been observed if samples containing less glass had been sintered at higher temperatures (∿1700°C). Chromium sesquioxide is only slightly soluble in silica at a high temperature and is not a suitable oxide for use in an interconnection composite.

Initial measurements showed that sintered pellets of Ti-doped Fe_2O_3 have a room temperature resistivity of less than 100 ohm cm. Room temperature resistivity measurements (Figure 1) were made on a series of Ti-doped Fe_2O_3 pellets, pressed at room temperature and 12,000 psi, which were sintered for 24 hours at :h 1000° and 1200°C. Some contact resistance is included in ;se measurements. The resistivity decreases rapidly to a ....imum value upon the addition of a small amount of TiO_2 and then increases more slowly in a linear fashion with further additions. The minimum value at room temperature was observed

with a 1.5 at % (1000 ohm cm) and a 0.7 at % (35 ohm cm) Ti-doped Fe_2O_3 pellet for sintering temperatures of 1000 and 1200°C, respectively. These results are in good agreement with the previous work on glazes containing Fe_2O_3 doped with TiO_2 or SnO_2 where an ∿1 at % impurity ion content gives a minimum value in the surface resistivity(6). Titanium increases the conductivity as it enters the octahedral site of the Fe_3O_4 spinel $Fe^{3+}\left[Fe^{3+}_{1-2x}\ Fe^{2+}_{1+x}\ Ti^{4+}_{x}\right]O_4$, where $x \leq 0.2$, by increasing the number of Fe^{2+} ions present. The charge hopping conduction mechanism is due to rapid electron transfer between Fe^{2+} and Fe^{3+} cations on adjacent octahedral sites which are closer together than the tetrahedral sites(7). The small number of Fe^{2+} ions, obtained under the sintering conditions, accounts for the high resistivity in the absence of Ti^{4+} ions.

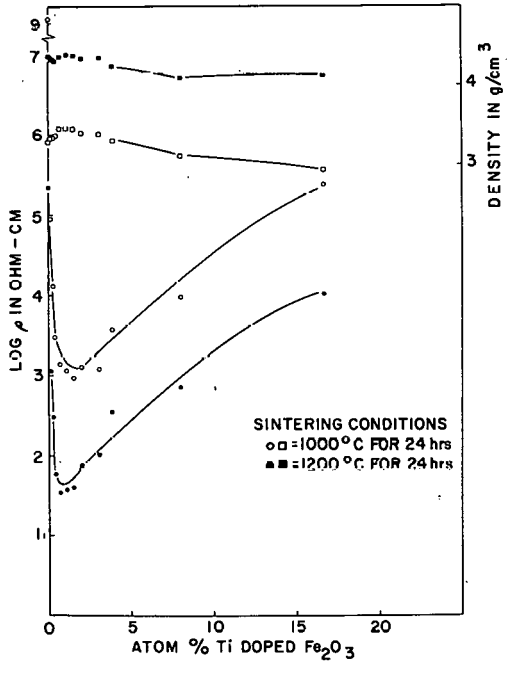

Figure 1. Log ρ versus at % Ti-doped Fe_2O_3.

Room temperature resistivity measurements were made on two series of Ti-doped Fe_2O_3-glass composite materials sintered for 24 hours at 1200°C (Figure 2). In the series containing soda-lime glass, the logarithm of the resistivity increases in a linear fashion with the wt % glass (Δ log ρ/Δ wt % $\approx$ 0.04 ohm cm/wt %), while in the series containing borosilicate glass the resistivity remains approximately constant as the amount of glass is increased to 16.7 wt %.

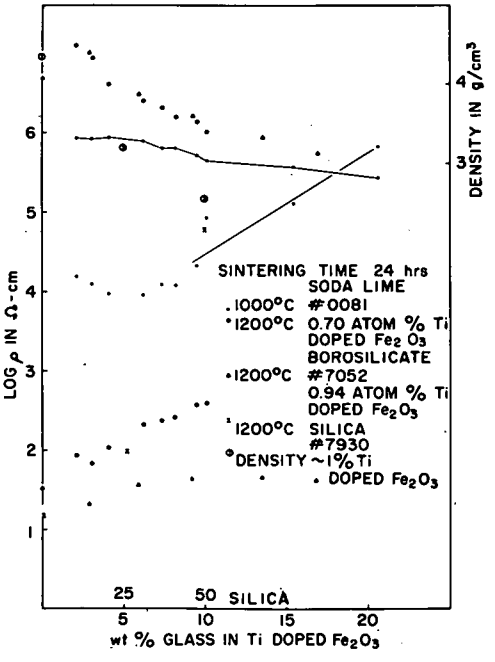

Figure 2. Log ρ versus Ti-doped Fe_2O_3 - wt % glass composites.

In each case, the minimum value of the resistivity occurs close to the maximum relative density. A maximum densification of ∿88% was obtained with a sample containing 2.14 wt % soda-lime glass sintered at 1200°C. A densification of over 95% has been reported previously with a Ti-doped Fe_2O_3 sample containing 10 wt % soda-lime glass sintered at 1250°C(3). With a 25 wt % silica glass having a densification of ∿83%, the resistivity is

still relatively low (~100 ohm cm). Although the resistivity at 1000°C in air would be 2 to 3 orders of magnitude less than at room temperature, these composites must be chemically stable in a H_2 environment.

The chemical stability of these materials was examined in a H_2 environment at 1000°C. A number of samples containing 1 at% Ti-doped Fe_2O_3 and borosilicate glass were kept at 1000°C for 96 hours in an argon + 8.5% H_2 mixture. In each case, the iron oxide component was reduced to metallic iron, the weight loss corresponding closely to the oxygen content of the Fe_2O_3 present in the glass. Additional samples containing up to 75 wt % glass behaved in the same manner. These results rule out Fe_2O_3-glass composites for use as an interconnection material since the glass does not prevent reduction by hydrogen. In contrast, composites of Cr_2O_3 and soda-lime glass suffer a smaller weight loss (~3.5%) under the same conditions due to the formation of a volatile product that condenses downstream. High temperature glasses containing a chromite system were not considered for further study.

Doped rutile and alkaline earth titanates have been examined for use as interconnection materials. In previous work at Harwell(8), the examination of a large number of mixed oxides revealed that rutile (TiO_2) was potentially useful as an interconnection material in the YSZ solid oxide electrolyte fuel cell. The best results were obtained with TiO_2 + 5 m/o Nb_2O_5, where the resistivity at 1000°C was found to be 0.7 and 0.03 ohm cm in air and H_2, respectively. The rutile structure was retained after extended annealing at this temperature.

Measurements were made in both air and H_2 on a Nb-doped TiO_2 sample sintered at 1700°C (Figure 3). High resistivities were observed at low temperatures when the sample was tested in air. The results obtained in air with decreasing temperature before and after treatment in H_2 are in good agreement. The resistivity is lower in the reducing environment, and it increases with the temperature. Here the hydrogen atoms in rutile act as electron donors(9) along with the interstitial Ti atoms. The electronic mobility, which decreases with an increase in temperature due to scattering effects, accounts for the increased resistivity observed here at higher temperature.

The densification of TiO_2 sintered at 1700°C was found to be about 83%. Since rutile is soluble in various glass compositions, further densification could be obtained with the addition of small amounts of the proper glass. This approach should result in a gas-impervious sample having semiconducting properties close to those of doped rutile in both air and hydrogen.

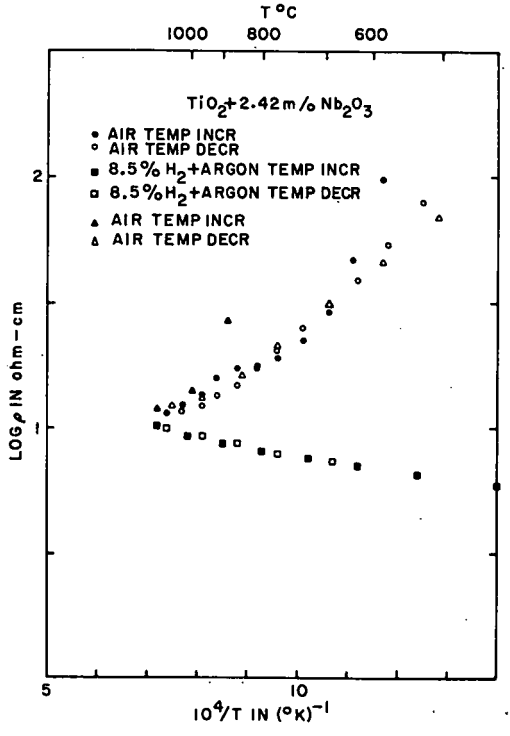

Figure 3. Log ρ versus Nb-doped TiO_2 in both air and H_2 environments.

1. Warde, C. J., Isenberg, A. O., and Brown, J. T., High Temperature Solid Electrolyte Fuel Cells -- Status and Program at Westinghouse, Westinghouse Research Laboratories, Pittsburgh, Pennsylvania.

2. Feduska, W., Isenberg, A. O., Iskoc, J. L., Ruka, R. J., and Nabpa, P., Thin Film Battery/Fuel Cell Power Generating System, Project Status Report for the Period July-September, 1976.

3. Johnson, A. S. W., and Tseung, A. C. C., Japanese Patent 50-97583, August 2, 1975.

4. Schultz, P. C., Front Glass Sci. Technol., Proc. Annu. Meet. Int. Comm. Glass 1969 (Pub. 1970), 35-40 (Eng).

5. Mazurin, O. V., Pavolva, G. A., Lev, E. Ia., and Leko, E. K., Zh. Tekh. Fiz. 27, 2702 (1957).

6. Binns, D. B., Trans. Brit. Ceram. Soc. 72, 7-17 (1973).

7. Banerjee, S. K., and O'Reilly, W., J. Phys. Chem. Solids 28, 1323-1335 (1967).

8. Markin, T. L., Bones, R. J., and Dell, R. M., High Temperature Solid Electrolyte Fuel Cells, presented at the Conference on Superionic Conductors, May 10-12, 1976, General Electric Research and Development Center, Schenectady, New York.

9. Hill, G. J., Brit, J., Appl. Phys. (J. Phys. D), Ser. 2, 1, 1151 (1968).

10. Blumenthal, R. N., Kirk, J. C., Jr., and Hirthe, W. M., J. Phys. Chem. Solids 28, 1077 (1967).

C. ELECTROLYTES

1. Optimized Electrolytic Domain Boundaries in Solid Oxide Electrolytes
   H. L. Tuller, Massachusetts Institute of Technology

2. Fundamental Factors that Might Limit the Application of ZrO_2 Solid Electrolytes in Fuel Cells: Electronic Transport, Electrolyte-Electrode Reactions, and Electrolyte Decomposition
   W. Weppner, Stanford University

OPTIMIZED ELECTROLYTIC DOMAIN BOUNDARIES IN SOLID OXIDE ELECTROLYTES

Harry L. Tuller
Massachusetts Institute of Technology
Department of Materials Science and Engineering
Cambridge, Massachusetts 02139

For many years high oxygen ion conduction has been known to exist in a number of oxides which crystallize in the fluorite structure. Enhanced conduction in these oxides is due in large part to the readiness with which the fluorite structure incorporates large numbers of lower valent ions into its cation sublattice while retaining the overall structure intact. The most successful fluorite type oxide electrolytes have been based on the oxides ZrO_2, ThO_2, CeO_2 and HfO_2 having additions of alkaline earth oxides, Sc_2O_3, Y_2O_3 or rare earth oxides (1). These substitutional lower valent cations cause the formation of anion vacancies to preserve electroneutrality. The resulting increase in oxygen ion conductivity leads to exclusively ionic conduction within certain ranges of temperature and oxygen pressure. This region in P_{O_2}, T space is often called the "electrolytic domain". It is primarily within this domain that the above oxides may be expected to function as solid oxide electrolytes in such applications as electrochemical probes, oxygen pumps and solid state fuel cells. Nevertheless, the positions of these electrolytic domain boundaries have only been mapped out precisely for a limited number of potential electrolytes (2,3). In almost no case has a systematic study been performed to identify the dopant and concentration of dopant which would lead to optimized electrolytic behavior. In this paper we will first outline the major requirements for optimized electrolytic behavior and then review recent experimental data which can be utilized in establishing the above requirements or conditions for a number of solid electrolytes based on the ceria and thoria systems.

The operation of the above electrochemical devices all depend on the ability to establish a stable emf across an electrolyte due to the imposition of an oxygen concentration gradient. This "Nernst" emf may under open circuit conditions be approximated by (1)

$$\varepsilon = t_i \, RT/4F \, \ell n \, (P'_{O_2}/P''_{O_2}); \quad t_i \sim 1 \qquad (1)$$

with R and F representing the gas and Faraday constants respectively, and t_i the ionic transport number defined as

the fraction of the total conductivity which is ionic in nature. This configuration may, for instance, be used as a thermochemical probe to determine the oxygen activity of a system when P_{O_2} is fixed at a known reference state. If an external load is connected across the oxygen ion conducting electrolyte, current will flow causing oxidation of the fuel gas at the anode and resulting in the direct conversion of chemical to electrical energy. In this mode the cell can be said to be operating as a "fuel cell".

The two major parameters which control the relative usefulness of a given solid electrolyte are

1. the magnitude of the ionic conductivity, σ_i
2. the size of the electrolytic domain.

The first parameter is particularly important in fuel cell applications since the magnitude of σ_i controls the internal resistance of the cell. The ability to pass high current densities depends, at least in part, on having sufficiently low internal cell resistances and therefore relatively high σ_i's. Adequate levels of conductivity are usually only achieved for temperatures above 800-1000°C in these oxide electrolytes. For sensor applications this requirement is not as critical, but one still needs sufficiently high σ_i's so that equilibration times do not become excessively long.

The second parameter, i.e., the extent of exclusive ionic conductivity ($t_i > 0.99$), controls the maximum emf obtainable under equilibrium conditions (see Eq. (1)). This is due to the fact that difficulties occur when the electronic conductivity becomes a significant fraction of the total conductivity. This causes a drop in the emf (due to decreasing t_i) as well as allowing mass transport within the electrolyte even under open circuit conditions. For applications such as in thermodynamic probes, problems already arise when the electronic conductivity approaches $\sim$1% (4) of the total (i.e., for $t_i \leq 0.99$). For fuel cell operation, up to $\sim$15% electronic conduction may still be tolerated (5). Electrolytes which exhibit exclusive ionic conduction over a wide range of conditions are therefore most desirable. Such properties are, for instance, exhibited by calcia stabilized zirconia (CSZ), which maintains an ionic transport number, $t_i > 0.99$ at 1000°C over a P_{O_2} range of from $10^{5} - 10^{-20}$ atm (4) - i.e., over $\sim$25 orders of magnitude!

To summarize for optimum operation of a solid oxide electrolyte, one desires

a) maximum possible magnitude of ionic conductivity
b) as wide a range of operating conditions as possible
c) minimal electronic contributions over the entire operating range.

Unfortunately these requirements do not always go hand in hand. For instance to obtain increased σ_i one would move to higher operating temperatures, but this could, at the same time, result in a shrinkage of the electrolytic domain, not to mention the general problem associated with decreased materials stability at elevated temperatures. One must therefore determine the optimum conditions for which one obtains sufficiently high σ_i (the actual magnitude depending on how thin one can fabricate the electrolyte) while still maintaining a sufficiently wide domain. In the present paper we attempt to correlate the magnitude of the ionic conduction parameters and location of the electrolytic domain boundaries to both the type and concentration of lower valent dopants used in the fabrication of ceria and thoria oxide electrolytes, and thereby determine the optimum composition and operating conditions for these electrolytes.

THEORY

Ionic Conductivity: In the oxide electrolytes considered here, the concentration of mobile ionic defects (doubly ionized oxygen vacancies, $V_O^{\cdot\cdot}$) is greatly enhanced above intrinsic levels by doping with lower valent cations, eg., Ca^{2+} and/or Y^{3+}. The concentration of these mobile ionic defects, n_i given by the electroneutrality equation as

$$n_i = [V_O^{\cdot\cdot}] = [Ca_M''] + 1/2[Y_M'] \qquad (2)$$

(where M is the appropriate quadravalent cation of the host lattice) is therefore expected to remain practically independent of temperature and P_{O_2}. The ionic conductivity σ_i however, given by

$$\sigma_i = n_i q \mu_i = n_i q \frac{\mu_{io}}{T} \exp -\Delta H_i/kT \qquad (3)$$

$$= \frac{C_i}{T} \exp -\Delta H_i/kT$$

will show the temperature activated dependence of its defect mobility μ_i. Following the above equations the ionic conductivity is expected to increase linearly with dopant concentration (Eq. 2) and exponentially with T, with an activation enthalpy ΔH_i independent of dopant. Experimental evidence to be presented later show, however, that these relationships are true only at small dopant levels.

Electrolytic Domain Boundaries and Electronic Conductivity: Under sufficiently reducing or oxidizing conditions all

solids display some degree of nonstoichiometry which is almost always accompanied by electronic defects viz., electrons or holes. By considering the appropriate mass action relations it can easily be shown (6) that the electron contribution, important under reducing conditions, takes the form

$$\sigma_e = \frac{D_e}{T} \exp(-\Delta H_e/kT)\ P_{O_2}{}^{-1/4} \qquad (4)$$

while the electron-hole contribution under oxidizing conditions takes the form

$$\sigma_h = \frac{D_h}{T} \exp(-\Delta H_h/kT)\ P_{O_2}{}^{+1/4} \qquad (5)$$

where ΔH_e and ΔH_h, the activation enthalpies for electrons and holes respectively, include contributions both for defect formation and motion (when transport is by the hopping model). One also finds (6) that D_e is proportional to $n_i^{-1/2}$ while (7) D_h is proportional to $n_i^{+1/2}$. From the above relations one expects the smallest overall electronic contributions and therefore the largest domains at low temperatures. (Note that enhanced σ_i is obtained instead at elevated temperatures.) As far as the effects of dopant levels are concerned, the above shows that high dopant levels depress electron contributions while enhancing hole contributions in these electrolytes.

One may experimentally locate the positions of the domain boundaries and thereby check the validity of the above predictions by taking advantage of the fact that the electronic contributions are strongly P_{O_2} dependent while the ionic conductivity is not. By measuring the total conductivity σ_t as a function of P_{O_2} one can identify σ_i from the "plateau" in the data and σ_e from the difference between the total conductivity and σ_i. One therefore has the means for determining the ionic transport number t_i as a function of P_{O_2} at each isotherm.

One obtains an equation defining the electrolytic domain boundaries by taking the ratio of the ionic to electronic conductivity in terms of t_i given by

$$\sigma_i/\sigma_{electronic} = \frac{t_i}{1-t_i} \qquad (6)$$

Substituting in the above definitions for σ_i and $\sigma_{electronic}$ (σ_e or σ_h) and solving for $\ln P_{O_2}$ one obtains

$$\ln P_{O_2} = 4 \ln \left(\frac{D_e}{C_i} \frac{t_i}{1-t_i} \right) - 4 \left(\frac{\Delta H_e - \Delta H_i}{kT} \right) \qquad (7)$$

under reducing conditions and

$$\ell n\ P_{O_2} = 4\ \ell n \left(\frac{C_i}{D_h} \frac{t_i}{1-t_i} \right) + 4 \left(\frac{\Delta H_h - \Delta H_i}{kT} \right) \qquad (8)$$

under oxidizing conditions. Thus one expects to find a linear dependence between $\ell n\ P_{O_2}$ and $1/T$. With the above equations, which combine the contributions of both the ionic and electronic carriers, it becomes possible to predict how the location of the domain boundaries depend, for instance, on temperature and dopant concentration. From the above relations it also becomes clear, that the electrolytic domain need not necessarily shrink at elevated temperatures. This will depend on whether ΔH_i is greater or less than ΔH_e and ΔH_h. Similarly the dependence on dopant concentration can be predicted from the ratios D_e/C_i and C_i/D_h which, according to the above relations, should be proportional to $n_i^{-3/2}$ and $n_i^{1/2}$ respectively. Since one desires $\ell n\ P_{O_2}$(reducing) to be as low as possible and $\ell n\ P_{O_2}$(oxidizing) as high as possible, one would optimally choose a high value of n_i and therefore a high dopant level.

One can use the above technique most easily for solids which exhibit a P_{O_2} dependent region of σ_t within accessible experimental conditions. This occurs for instance for CeO_2 electrolytes for P_{O_2}'s $< 10^{-4} - 10^{-10}$ atm (3) and for ThO_2 electrolytes for P_{O_2}'s $> 10^{-4} - 10^{-6}$ atm (7) at temperatures above ~700-800°C. This is not the case however for stabilized ZrO_2 which only begins to generate electrons for P_{O_2}'s $< 10^{-20}$ atm at 1000°C.

Experimental results obtained for CeO_2 and ThO_2 electrolytes doped with various types and concentrations of impurities will be analyzed in the next section and compared with the predictions obtained above. Furthermore, since both pure CeO_2 and ThO_2 crystallize in the fluorite structure (ZrO_2 must be "stabilized" into the fluorite structure by a minimum of ~10 m/o dopant) the effect of various dopants on the magnitude of σ_i, the enthalpy of motion ΔH_i and the location of the domain boundaries may be studied as a function of dopant concentration at small as well as at large dopant levels.

RESULTS AND DISCUSSION

Data for the variation of conductivity as a function of P_{O_2}, obtained recently by the author (6), for CeO_2 + 5 m/o Nd_2O_3 are presented in Fig. 1. The predicted P_{O_2} dependence of the overall conductivity is observed, i.e., a P_{O_2} independent component (σ_i) at high P_{O_2}'s and a $P_{O_2}^{-1/4}$

dependent component (electrons) at low P_{O_2}'s as indicated by the solid curves ($\sigma_e = \sigma_t - \sigma_i$). Similar curves were obtained for CeO_2 + 2 and 7 1/2 m/o Nd_2O_3 and CeO_2 + 5, 7 1/2 and 10 m/o Y_2O_3 in the same study (6). For ThO_2 + Y_2O_3 electrolytes, on the other hand, the P_{O_2} independent region has been observed by Lasker and Rapp (7) to be at low P_{O_2}'s, while at high P_{O_2}'s, a $P_{O_2}^{+1/4}$ dependence ($\sigma_h = \sigma_t - \sigma_i$) is obtained indicating instead positive-hole contributions. Plots of the electrolytic domains for CeO_2 + 5 m/o CaO, Nd_2O_3 and Y_2O_3 are presented in Fig. 2. The data points shown represent the conditions of P_{O_2} and T for which t_i = 1/2 for the various electrolytes. These were obtained (6) from σ vs. log P_{O_2} data of the type shown in Fig. 1 in the manner described above. The data points are seen to fall on a straight line (within experimental error) as predicted from Eq. (7). The slopes as well as the locations of these electrolytic boundaries can be seen to be strongly dependent on the type of dopant. At least for this dopant concentration, additions of Y_2O_3 appear to result in the largest electrolytic domain. Values for $\Delta H_e - \Delta H_i$ obtained from the slopes of these curves (Eq. 7) and other data on ceria electrolytes (3, 6 and 8) are listed in the first column of Table 1 as a function of composition. These values show a general tendency to decrease with increasing dopant concentrations. It thus appears that the earlier assumption made, i.e., that these activation energies ΔH_i

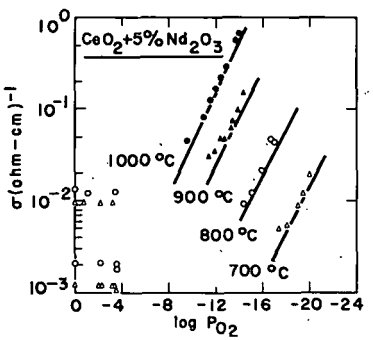

Figure 1. Electrical conductivity of CeO_2 + 5 m/o Nd_2O_3 measured isothermally as a function of oxygen partial pressure (6). The solid curves represent the electronic component, σ_e.

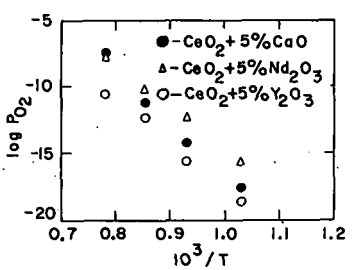

Figure 2. Comparison of data for log P_{O_2} vs. T^{-1} at t_i = 1/2 for three different ceria solid solutions with equal dopant levels (6). CeO_2 + 5 m/o Y_2O_3 is seen to exhibit the largest electrolytic domain of the three at low P_{O_2}'s.

TABLE 1

Ionic and Electronic Conduction Parameters

of Selected Ceria Electrolytes

	$\Delta H_e - \Delta H_i$ (eV)	C_i (10^5 K/Ωcm)	ΔH_i (eV)	σ_i(1000°K) (10^{-2}/Ωcm)	D_e (10^9 K atm$^{1/4}$/Ωcm)	ΔH_e (eV)
CaO						
1 m/o	1.96	0.11	0.72	0.26	45.1	2.68
5	1.77	1.76	0.78	2.08	10.4	2.55
12	1.70	3.02	0.77	4.01	9.2	2.47
Nd_2O_3						
2	1.72	0.64	0.79	0.67	5.0	2.51
5	1.55	0.76	0.74	1.43	1.0	2.29
7 1/2	1.70	0.88	0.74	1.65	1.9	2.44
Y_2O_3						
5	1.61	5.65	0.87	2.35	4.3	2.48
7 1/2		61.6	1.21	0.50		
10		114	1.25	0.58		
Gd_2O_3 (+ MgO)						
5(8)		1.00	0.68	3.77		
10(13)		2.65	0.73	5.59		
15(18)		18.4	0.92	4.29		
20(23)		372.	1.31	0.94		
25(28)		155	1.41	1.23		

and ΔH_e remain independent of dopant level, appears to be contradicted.

Even more dramatic effects of composition on the position and slopes of the domain boundaries can be observed in Fig. 3 for the thoria-yttria system where the yttria content varies from < 0.42 - 12.5 m/o Y_2O_3. Not only do the slopes of the curves vary dramatically from low to high dopant levels but the size or extent of the domain is seen to pass through a maxima at high dopant levels in contradiction to our earlier predictions. An interesting observation to be made is that in the thoria system the domain at high

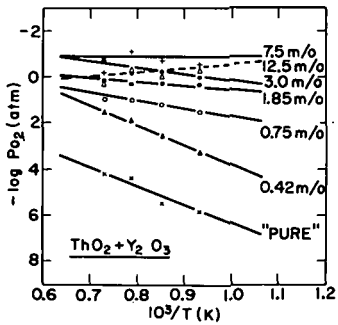

Figure 3. Comparison of data for log P_{O_2} vs. T^{-1} at $t_i = 1/2$ for a series of $ThO_2 + Y_2O_3$ solid solutions. Data points were derived from data of Lasker and Rapp (7). In almost all cases, the electrolytic domain (at high P_{O_2}'s) increases with increasing temperature.

P_{O_2}'s actually increases with increasing temperature, particularly for the lower dopant levels, thus indicating that $\Delta H_i > \Delta H_h$ in these solids.

To understand the above results more clearly, it is useful to separate out the ionic and electronic contributions in Eqs. (7) and (8). For ceria electrolytes, for instance, we know the conductivity to be entirely ionic at high P_{O_2}'s. Thus by measuring the conductivity in pure oxygen as a function of temperature, one may obtain experimental values for C_i and ΔH_i for the various solid solutions. Values for these parameters so obtained experimentally as well as σ_i (1000°K) are presented in Table 1. For dopant levels up to 5-10 m/o, all the systems seem to show a consistent value for $\Delta H_i \sim 0.7 - 0.8$eV in agreement with predictions. Similarly, in this dopant range, σ_i (1000°K) is, as expected, roughly linear with concentration of a given dopant but does show a sensitivity to the type of dopant added

$$\left(\text{e.g., } \frac{\sigma_i\,[CeO_2 + 5\ \text{m/o}\ Gd_2O_3]}{\sigma_i\,[CeO_2 + 5\ \text{m/o}\ Nd_2O_3]} \simeq 2.6\right).$$

At larger dopant levels ΔH_i increases rapidly with further increases of dopant while σ_i is observed to pass through a maxima. Similar maxima in σ_i have previously been observed for ZrO_2 (1) and ThO_2 (4) electrolytes, the cause of which has generally been attributed to vacancy ordering. Given this information one may, with the aid of Eq. (7), determine the values of D_e and ΔH_e from the experimental data. Values for D_e and ΔH_e so obtained are also listed in Table 1. One finds that ΔH_e, which is primarily associated with the formation energy of electrons or the ease with which the solid deviates from stoichiometry, generally decreases with

increasing dopant levels (6). This effect plus the maxima exhibited by σ_i at high dopant levels explains why the domain size itself goes through a maxima at some concentration of dopant. What appears to be occurring at these high dopant levels is that σ_i is decreasing due to ordering effects while, at the same time, σ_e is increasing due to increased deviations from stoichiometry (6).

It therefore becomes clear at this point that certain types of dopants not only give higher ionic conductivities than others (for a given electrolyte host) but also more extensive domains. Similarly for a given dopant, there exist optimum concentrations with respect to the magnitude of σ_i and to the size of the electrolytic domain - the two not being necessarily identical. The exact choice of type and concentration of dopant will depend on the specific application. For fuel cells, for example, one would likely choose a higher σ_i at the expense of a somewhat smaller domain. The reverse would be true for sensor applications.

In conclusion, it has been shown that the two most important parameters controlling electrolytic behavior, σ_i and domain size, are very sensitive to both dopant type and concentration. It was further shown experimentally that both these parameters can be optimized separately by choosing the appropriate solid solutions, while the final choice of composition depends on the specific requirements imposed upon the electrolyte.

REFERENCES

1. T. H. Etsell and S. N. Flengas, "The Electrical Properties of Solid Oxide Electrolytes", Chem. Rev., Vol. 70, No. 3., pp. 339-376, March, 1970.

2. J. B. Hardaway III, S. W. Patterson, D. R. Wilder and J. D. Schieltz, "Ionic Domain for Y_2O_3-Doped ThO_2 at Low Oxygen Activities", J. Am. Ceram. Soc., Vol. 54, No. 2, pp. 94-98, Feb., 1971.

3. H. L. Tuller and A. S. Nowick, "Doped Ceria as a Solid Oxide Electrolyte", J. Electrochem. Soc., Vol. 122, No. 2, pp. 255-259, Feb., 1975.

4. W. L. Worrell, "Electrochemistry of Ceramic Electrolytes", Cer. Bull., Vol. 53, No. 5, pp. 425-533, May, 1974.

5. T. Takahashi, Physics of Electrolytes - Vol. 2, (J. Hladik, ed.), pp. 989-1049, Academic Press, London, 1972.

6. H. L. Tuller and D. S. Tannhauser, "Influence of Dopant and Dopant Concentrations on Ionic Conduction and Stoichiometry in Solid Ceria Electrolytes", to be published.

7. M. F. Lasker and R. A. Rapp, "Mixed Conduction in ThO_2 and ThO_2-Y_2O_3 Solutions", Z. Phys. Chem. N. F., Vol. 49, No. 3/5, pp. 198-221, March-May, 1966.

8. R. N. Blumenthal, F. S. Brugner and J. E. Garnier, "The Electrical Conductivity of CaO-Doped Nonstoichiometric Cerium Dioxide from 700° to 1500°C", J. Electrochem. Soc., Vol. 120, No. 9, pp. 1230-1237, Sept., 1973.

FUNDAMENTAL FACTORS THAT MIGHT LIMIT THE APPLICATION OF ZrO_2 SOLID ELECTROLYTES IN FUEL CELLS: ELECTRONIC TRANSPORT, ELECTROLYTE-ELECTRODE REACTIONS, AND ELECTROLYTE DECOMPOSITION

Werner Weppner
Department of Materials Science and Engineering
Stanford University, Stanford, California 94305

I. Introduction

This paper will discuss several factors which can provide fundamental limitations to the application of solid electrolytes in high temperature fuel cells. Although specific experiments are discussed which have been performed on ZrO_2 the principles that are involved can be applied to any solid electrolyte. Topics to be discussed include electronic conductivity and an experimental technique for the separation of the concentrations and mobilities of electrons and holes, reactions between the solid electrolyte and the electrode material, especially at low oxygen partial pressures, and a method for the experimental determination of the decomposition potential of solid electrolytes that have some electronic conduction.

II. Concentrations and Mobilities of Electrons and Holes in Doped ZrO_2

Zirconia, which is stabilized in the cubic CaF_2 structure by the incorporation of several mole % of yttria or some other lower valent oxide, has a high and predominantly ionic conductivity at elevated temperatures. It has been considered for use in various technological applications such as fuel cells and oxygen sensors. Such uses may be limited, however, if either electrons or holes make appreciable contributions to the total conductivity. Such electronic transport acts as a partial internal electrical short circuit, thus reducing the cell voltage and the efficiency of the system.

Several previous studies have been concerned with the partial electronic conductivities of several doped zirconia compositions (e.g., 1-4). Little information exists, however, on the separate contributions of the concentrations and mobilities of the two electronic charge carriers. Instead attention has been given only to the influence of oxygen partial pressure and temperature upon the total electronic conductivity. Separation of the concentration and mobility contributions may provide guidance concerning the effectiveness of doping and the relative importance of various types of impurities in the design of new solid electrolytes or improvements upon existing ones.

Experiments will be described in which the diffusion coefficients (related to the mobilities) of electrons and holes have been separately measured in samples of 10 mole % yttria-doped zirconia ($Zr_9Y_2O_{21}$) as a function of the temperature. By use of data on the electron and hole conductivities, the concentrations of electrons and holes have been calcu-

lated as a function of the oxygen partial pressure and temperature.

The technique which was used to determine the diffusion coefficients of the electronic species involved measurements of the time dependence of the voltage relaxation of the following galvanic cell.

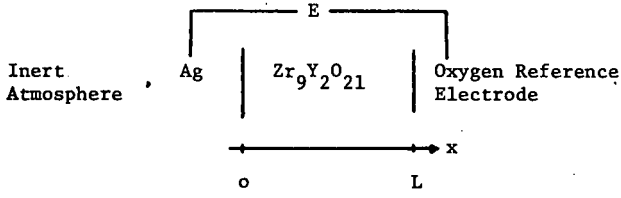

At one side the electrolyte is exposed to a defined reference oxygen partial pressure, either a mixture of Fe and "FeO" or air, using a porous platinum electrode as a current collector. An inert atmosphere, either nitrogen or argon, of very small volume, is present at the other side. Electrical contacts were made using sputtered silver layers. Platinum, and a number of other metals, may not be used in contact with the inert atmosphere because of the possibility of the formation of zirconium - metal compounds at low oxygen partial pressures (5-7), as discussed later.

If a positive voltage less than that which would decompose the electrolyte is applied to the galvanic cell, no ionic current can exist under steady state conditions, since the inert electrode is not able to supply oxygen ions. Thus any current which passes through the cell must be due to the transport of electronic species. The partial conductivities of the electrons and holes can be determined by use of the Hebb-Wagner method (8,9). The results for $Zr_9Y_2O_{21}$ are shown in Fig. 1.

The chemical potential of the oxygen ions can be regarded as uniform throughout the solid electrolyte because of the presence of a high concentration of oxygen vacancies (10), which is essentially independent of the oxygen partial pressure. Likewise, the electrochemical potential of the oxygen ions is approximately constant because of the very high ionic conductivity of the solid. Therefore, the electric field which exists within the solid electrolyte must be negligible. As a result the transport of electrons and holes is due only to diffusion related to concentration gradients, which we can assume obeys Fick's laws.

If a constant voltage is applied across the galvanic cell, a linear concentration gradient of the prevailing conductive electronic species (holes at p_{O_2} greater than 10^{-10} atm and electrons at p_{O_2} less than 10^{-10} at 900°C) is obtained after steady state is reached. If, subsequently, this externally applied voltage is switched off, the electron and/or hole concentration profiles will tend to flatten out as a result of transport under the influence of their concentration gradients

according to normal diffusion laws. The concentrations at the interfaces determine the cell voltage and their time dependence can be measured and compared with expectations related to theoretical solutions of the diffusion equations.

Additional factors which must be taken into account include the existence of an internal p-n junction, recombination and formation of electron-hole pairs, and the equilibrium between the electron and hole concentrations.

The details of this technique and the data analysis have been presented elsewhere (4, 11, 12).

The values obtained for the electron diffusion coefficient as well as those for the diffusion coefficient of the holes are presented in Fig. 2, as a function of the temperature. It is seen that the diffusion coefficient of the electrons is about 2 orders of magnitude greater than that for the holes, and also has a lower activation enthalpy (0.56 eV versus 1.4 eV). For this reason the stoichiometric point at which the electron and hole concentrations are equal occurs at an oxygen partial pressure about 8 orders of magnitude lower than that at which the conductivities are equal.

The concentrations of electrons and holes have been calculated from the conductivity and diffusion coefficient data and the results are given in Fig. 3, as a function of the oxygen partial pressure for temperatures from 700 to 900°C.

From the temperature dependence of the product of the electron and hole concentrations the electronic band gap is estimated to be about 4.1 eV.

III. Reaction Between ZrO_2 and Electrode Material

Another matter that may be life-limiting or may influence the kinetics or voltage range over which a solid electrolyte fuel cell can be operated involves possible reactions between the electrolyte and the electrode or interconnection materials. A new dynamic method that might be utilized to quantitatively investigate electrolyte-electrode reactions has been developed and applied to the case of ZrO_2-Pt interactions at low oxygen partial pressure.

It was found that voltage relaxation experiments using the configuration mentioned earlier were characterized by voltage plateaus which remained essentially constant over long periods of time, when platinum was used instead of silver at the polarized low oxygen partial pressure electrode. The temperature dependence of the values of these voltage plateaus in the ZrO_2-Pt case is shown in Fig. 4. These data can be related to the free energy of the reaction between the ZrO_2 electrolyte and platinum compounds. By comparison with thermodynamic data available in the literature (6) it is possible to identify which specific compounds are formed, assuming that the free energy of formation of the electrolyte itself is already known.

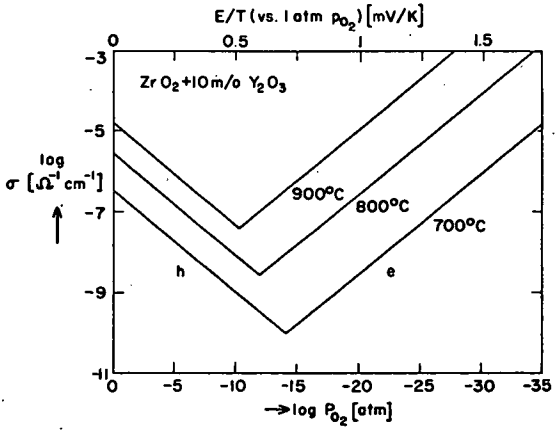

Figure 1. Partial electron and hole conductivities in $Zr_9Y_2O_{21}$ as a function of the oxygen partial pressure.

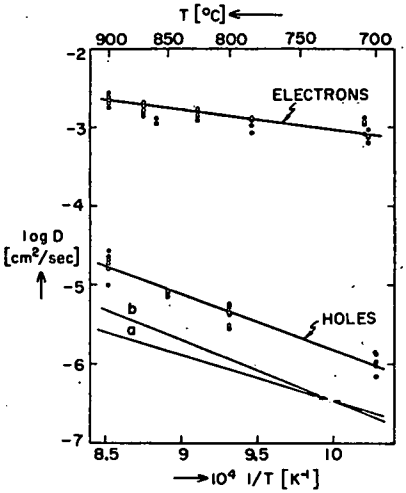

Figure 2. The electron and hole diffusion coefficients as a function of the temperature.

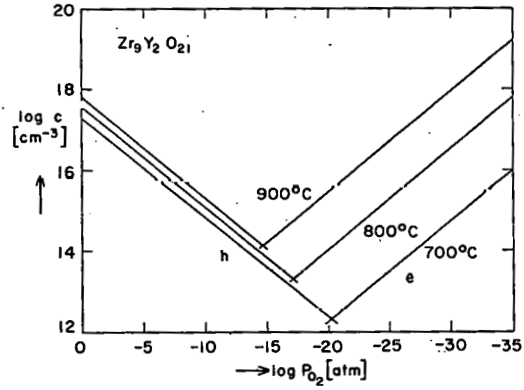

Figure 3. Concentrations of electrons and holes in $Zr_9Y_2O_{21}$ as a function of the oxygen partial pressure.

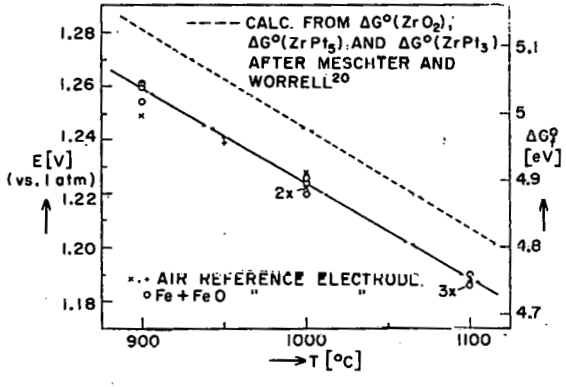

Figure 4. Temperature dependence of the plateau voltage due to the formation of Pt-Zr compounds.

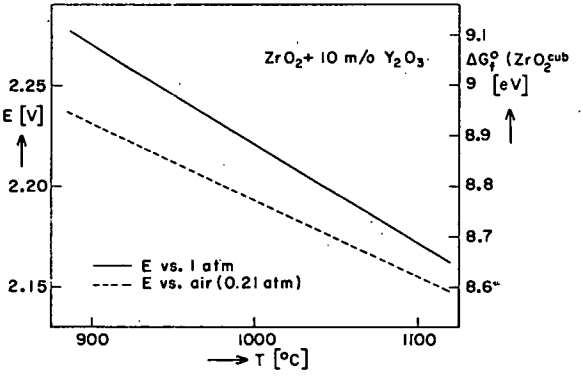

Figure 5. Decomposition voltage of yttria-doped zirconia.

IV. Stability Range of Solid Electrolyte

Direct measurements of the range of stability of solid electrolytes are sometimes difficult to make because of the screening effect of electronic conduction before the voltage necessary for decomposition is reached. An alternate method that might be applicable in such cases involves the use of electrochemical cells in which electrolyte-electrode reactions are deliberately caused to occur. If thermodynamic data related to these reaction products are available or readily measured, this method can give information about the free energy of formation of the electrolyte without complications due to electronic conduction.

This method has been used to measure for the first time the free energy of formation of doped cubic ZrO_2, using its interaction with a platinum electrode at low oxygen partial pressure. The decomposition voltage of ZrO_2 doped with 10 mole % Y_2O_3 as well as its free energy of formation are shown versus temperature in Fig. 5. These data indicate that the doped zirconia is slightly less stable at low oxygen partial pressures than is the case for the undoped monoclinic ZrO_2.

Acknowledgement

The author is gratefully indebted to Professor R. A. Huggins for helpful discussions and aid in the preparation of this contribution.

References

(1) J. W. Patterson, E. C. Bogren and R. A. Rapp, J. Electrochem. Soc. 114, 752 (1967).

(2) L. Heyne and N. M. Beekmans, Proc. Brit. Ceram. Soc. 19, 229 (1970).

(3) L. D. Burke, H. Rickert and R. Steiner, Z. phys. Chem. N.F. 74, 146 (1971).

(4) W. Weppner, J. Solid State Chem. 20, No. 3 (March, 1977).

(5) W. Weppner, to be published in J. Electroanal. Interfacial Chem.

(6) P. J. Meschter and W. L. Worrell, Metall. Trans. 8A, 503 (1977).

(7) L. Brewer and P. R. Wengert, Metall. Trans. 4A, 83 (1973).

(8) M. Hebb, J. Chem. Phys. 20, 185 (1958).

(9) C. Wagner, in: Proc. Int. Comm. Electrochem. Thermodyn. and Kinetics (CITCE), 7th Meeting, Lindau 1955, p. 361, Butterworths, London (1957).

(10) F. Hund, Z. phys. Chem. 199, 142 (1952).

(11) W. Weppner, Z. Naturforsch. 31a, 1336 (1976).

(12) W. Weppner, to be published in Electrochim. Acta.

D. FUEL CELL DESIGN

1. High Temperature Solid Oxide Fuel Cells: Present State and Problems of Development
   F. J. Rohr, Brown, Boveri & Cie AG (Heidelberg)

2. A Thin Solid Film Fuel Cell Approach
   M. Croset, J. P. Schnell, G. Velasco, Thompson-CSF; J. Siejka, Universite Paris

HIGH TEMPERATURE SOLID OXIDE FUEL CELLS: PRESENT STATE AND PROBLEMS OF DEVELOPMENT

F. J. Rohr
Brown, Boveri & Cie AG
Heidelberg, W.-Germany

The technical realizability and economic use of high-temperature fuel cells are dependent on whether it will be possible to solve all problems in view of technology and material, arising from the high operating temperature, and to attain the expected power density and efficiency data for a sufficiently long lifetime. Extensive research work has been done in some laboratories to solve these problems. Above all, efforts have been concentrated on the development of the solid electrolyte, the fuel- and air-electrode, as well as on the lifetime testing of these components in single cells. Furthermore, studies have been made concerning the basic problem of connecting cells in series by means of an interconnection material, and also on the development of module concepts for the construction of batteries.

I. Development of Cell Components

1. Solid electrolyte

The solid electrolyte to be used for the construction of high-temperature fuel cells has to meet the following requirements for operating temperatures up to 1000 ^{0}C: high oxygen ion conductivity at neglectable electron conductivity, phase stability, mechanical strength, gas tightness, thermoshock stability, chemical resistance to the reaction gases, as well as compatibility with the electrode- and interconnection materials. These requirements are sufficiently satisfied by ceramic solid electrolytes of doped zirconia. Inspite of numerous tests, it has not been possible until now to find better oxygen ion conductors, e.g. by replacing the ZrO_2 with CeO_2. Solid electrolytes on CeO_2-basis suffer from the disadvantage that due to the high electronic conductivity in reducing atmospheres cell voltage and thus efficiency are reduced.

For the construction of high-temperature fuel cells ZrO_2-solid electrolytes are preferably used, which are doped with 15 mole percent calcium oxide or 10 mole percent yttrium oxide (1) or 4 mole percent yttrium oxide and ytterbium oxide each (2). Doping zirconia with low valued metal oxides results in a high oxygen ion conduction and stabilization of the cubic crystal structure over a very broad temperature range. Fig. 1 shows the influence of doping material and temperature on ion conductivity. The specific electrical resistivities ρ_E which result at 800 and 1000 °C are shown in Table I. Moreover, the table gives the allowed maximum wall-thickness d_E of the solid electrolyte for power densities up to 0.25 W/cm^2.

TABLE I

SPECIFIC RESISTIVITY OF ZIRCONIA SOLID ELECTROLYTES AT 800 °C AND 1000 °C AND CORRESPONDING MAXIMUM WALL THICKNESS d_E FOR POWER DENSITIES p = 0.25 W/cm^2

Solid Electrolyte	800 °C		1000 °C	
	ρ_E [Ωcm]	d_E [mm]	ρ_E [Ωcm]	d_E [mm]
$(ZrO_2)_{0.85}(CaO)_{0.15}$	250	0.04	50	0.2
$(ZrO_2)_{0.9}(Y_2O_3)_{0.1}$	45	0.22	10	1
$(ZrO_2)_{0.92}(Y_2O_3)_{0.04}$ $(Yb_2O_3)_{0.04}$	20	0.5	5	2

Production of thin-walled, gas tight ZrO_2-ceramics presented a lot of difficulties for quite a long time. By using special pressing and sintering techniques and pressing aids, as for instance NH_4HCO_3, it is now possible to make gas tight solid electrolytes in form of tubes and discs with wall thicknesses $d_E \geq 0.3$ mm (3). Even thinner gas tight ZrO_2-solid electrolyte films, having a thickness $d_E \geq 30$ µm were coated on a porous ceramic substrate by means of special thin film procedures (4). By using thin film techniques it will be possible to reduce the operating temperature to 900 °C, when doping zirconia electrolyte with CaO, to 800 °C with Y_2O_3, and to 700 °C with Y_2O_3/Yb_2O_3. In this latter case, material costs are cut considerably. Whereas until recently cell concepts with self-supporting solid electrolytes (d_E > 0.3 mm) predominated, the development of thin film concepts will henceforth be emphasized.

Long-term behaviour under working conditions as well as thermoshock resistance of ZrO_2-solid electrolytes have been sufficiently tested. Life tests of cells with Y_2O_3/Yb_2O_3-doped electrolytes at 1000 °C showed that during a working period of 4 years the required properties of the electrolyte, i.e. the oxygen ion conductivity, phase stability, gas thightness, mechanical strength, and chemical compatibility with the electrode materials and the reaction gases will not be affected (5).

2. Electrodes

The voltage-current characteristics and the long time behaviour of a high-temperature fuel cell are not only influenced by the quality of the solid electrolyte but also by the properties of the air and fuel electrode. These are dependent on both the appropriate electrode materials and the structure of the electrode (porosity), as well as on the phase transition electrolyte - electrode (adherence). The electrical properties of the electrodes are usually evaluated by the resistivity to thickness ratio ρ_e/d_e, resulting from the specific resistivity ρ_e and the thickness d_e of the electrode, and by the polarization voltage losses V_p. The latter arises if the charge transition at the electrolyte - electrode interface is inhibited (charge transfer polarization) and if the mass transfer of the reacting gases or reaction products within the porous electrodes is hampered (concentration polarization).

a) Fuel electrode (anode)

Due to the reducing atmosphere of the fuel gas, normal metals can be used as electrode material for the anodes. In long time tests at 1000 °C nickel and cobalt proved to be the most suitable. The porous electrode films of 30 to 100 µm thickness are prepared either by plasmaspraying the fine metallic powder (6), (2) or by sintering fine grained cobalt-zirconia or nickel-zirconia-cermets (7). Both processes produce porous electrode films of good adherence. Roughening the surface of the solid electrolyte favourably affects adherence and polarization behaviour of the electrodes. The polarization losses which occur at the nickel and cobalt electrodes at 1000 °C are shown in Table II. Tests with laboratory cells over a period of 34.000 hours at 1000 °C have shown that plasmasprayed nickel electrodes exhibit long time stability and that they are compatible with the solid electrolyte (5).

TABLE II

PROPERTIES OF DIFFERENT ANODES AND OXIDE CATHODES AT 1000 °C

Electrode material	ρ_e/d_e [Ω]	I·R [mV] 0,5 A/cm²	V_p [mV] 0,5 A/cm²
Anode:			
Nickel, PS (PS=plasmasprayed)	< 0.04	< 20	< 80
Ni- or Co/ZrO_2-cermet	< 0.2	< 100	< 70
Oxide cathode:			
In_2O_3 (SnO_3), CVD	< 0.3	< 150	50 - 100
$LaNiO_3$ (Bi), PS	< 0.3	< 150	50 - 100
$LaMnO_3$ (Sr), PS	< 0.2	< 100	50 - 100

b) Air electrode (oxide cathode)

Due to the high corrosion effect of oxygen at working temperatures of 800 to 1000 °C, only noble metals or electron conducting metal oxides can be used as air electrode material. Noble metals such as platinum are completely out of question because of prohibitive costs and insufficient long term stability. The search for suitable oxide cathodes to replace the platinum and silver electrodes which were originally used, turned out to be a difficult task. With operating temperatures up to 1000 °C in air or oxygen atmosphere, the electrode material has to meet the following requirements: high electron conductivity, thermal and chemical stability, compatibility with the solid electrolyte, sufficient porosity and good adherence at the surface of the electrolyte. From the many oxide compounds which were tested, only a few proved to be satisfactory with regard to long term operation and thermal cycling. For example, cathodes made from praseodym cobaltite ($PrCoO_3$) show a high electronic conductivity, yet the

electrodes processed by sintering scaled off the surface of the electrolyte during cooling to room temperature (8). No such scaling off will take place with oxide cathodes made from indium oxide doped with tin (In_2O_3/SnO_2), which are applied to the rough or porous surface of the solid electrolyte by means of chemical vapor deposition (CVD) (9). Plasmasprayed oxide cathodes of doped lanthanum nickel oxide ($LaNiO_3$) (10) and lanthanum manganese oxide ($LaMnO_3$) (5), showing a perowskite-structure like that of $PrCoO_3$, also satisfied the requirements at operating temperatures of 1000 °C, with regard to electron conductivity, thermal and chemical stability, compatibility with the solid electrolyte and adherence during thermal cycling. Oxide cathode made from doped $LaNiO_3$ have been tested in laboratory cells at 1000 °C for 4 years without affecting the properties of the electrodes (5).

The characteristic data of some well tested oxide electrodes are shown in Table II. The ohmic losses $I \cdot R_C$ of these cathodes at 0.5 A/cm^2 caused by the electrode resistivity ρ_e/d_e range between 70 to 150 mV. The polarization losses V_p are of similar size. With increasing thickness of the electrode d_e the ohmic loss is reduced, but polarization losses are increased, due to retarded transport of the reactants within the porous electrodes. For this reason, the thickness of the cathode should amount to $d_e \leq 0.01$ cm. For oxide cathodes with very good electron conductivity ($\rho_e \leq 10^{-3}$ Ω·cm at 1000 °C) a resistivity to thickness ratio $\rho_e/d_e \leq 0.1$ Ω might be reached. Hence it follows that due to the low cell voltage of approx. 1 V only those cell and battery concepts are suitable, in which the current path in the air electrode is not more than 1 cm. This is of special significance for the construction of batteries.

II. Single Cell

1. Design and voltage-current characteristics of the high-temperature fuel cell

The voltage-current characteristics of a high-temperature fuel cell are dependent on the cell parameters and working conditions, in particular on the electrical properties and the dimension of the electrolyte and the electrodes as well as on the operating temperature and the partial pressure of the reacting gases. For the investigation of the voltage-current - and the long term behaviour, tubular cells as shown in Fig. 2 were used. The cylindrical solid electrolytes have a diameter of $D_E \leq 25$ mm, a height of $h_E \leq 12$ mm and a wall thickness of $\bar{d}_E \geq 0.4$ mm. The height of the cells is limited by the electrical resistivity

ρ_e/d_e of the oxide cathode. According to the composition and thickness of the solid electrolyte, the operating temperature ranges between 800 and 1000 °C. The reactants for cell operation may be oxygen or air at the cathode and hydrogen or gas mixtures of hydrogen, carbon monoxide, water and carbon dioxide at the anode. The latter can be generated from natural gas or coal in a reactor connected with the cell.

Typical voltage-current characteristics of a HT-fuel cell when operated with H_2 and O_2 or H_2/CO-mixture and air are shown in Fig. 3. At 1000 °C and a thickness of the electrolyte d_E = 0.5 mm, maximum power densities of 0.3 W/cm² (H_2/O_2) or 0.2 W/cm² (3 H_2 + CO/air) are achieved. By reducing the thickness of the electrolyte ($d_E \leq 0.3$ mm) and shortening the length of the cathode in current direction to less than 5 mm, the power density can be improved to 0.4 - 0.5 W/cm². Depending on the composition of the fuel mixture, the experimental open cell voltage E_o amounts to 0.9 - 1.1 V and corresponds well with the theoretical values. The voltage losses under load, particulary the ohmic loss IR of the solid electrolyte and the electrodes as well as the polarization losses V_p are shown in Fig. 6.

2. Operation as HT-electrolysis cell

HT-fuel cells may also be used as electrolysis cells for the generation of hydrogen from water. In this case, water vapor, electrical energy and heat are led to the cell. Due to the high operating temperature of 800 - 1000 °C the applied DC-voltage at the electrodes ranges between 1.2 and 1.5 V. Fig. 3 (curve 3) shows the current density as a function of the applied voltage at 1000 °C. With an electrolysis voltage of about 1.3 V, a thickness of the electrolyte of d_E = 0.5 mm and a hydrogen/water ratio H_2/H_2O = 1, current densities of 0.5 A/cm are obtained. In this case, additional heat is needed for the decomposition of water, since the formation enthalpy ΔH of water corresponds to a voltage of nearly 1.5 V.

ZrO_2-solid electrolysis cells can be alternately used for the generation of hydrogen and electricity, thus being very suitable for energy storage and peak power levelling.

3. Long term behaviour of HT-fuel cells

In addition to the voltage-current characteristics, the lifetime is of crucial importance for the evaluation of the high-temperature fuel cell. Life tests with single cells at 1000 °C have shown that open cell voltage and power density remain practically constant over a period

of 4 years (34.000 operation hours). Even repeated switching off due to power breaks, and cooling down of the cell to room temperature followed by reheating, did not affect lifetime (5). The test cell still in operation that achieved the longest lifetime up to now, consists of a tubular solid electrolyte of 1.2 mm thickness having plasmasprayed electrodes of nickel (anode) and of doped lanthanum-nickel oxide (cathode). With a constant load of 120 mA/cm^2 over a period of 34.000 hours, practically constant values of open cell voltage (approx. 1 V) and power density (approx. 80 mW/cm^2) were obtained after some start-up effects during the first 1.000 operation hours. On the basis of these results it can be expected that with the tested solid electrolytes and electrodes a lifetime of 5 and more years might be reached.

III. Batteries

1. Series connection (interconnection material)

Except for the limited electronic conductivity of the oxide cathode, the main problems in developing HT-fuel cells arise not so much from the single cell and its components but from the difficulties in combining the cells to multi-cell modules. For series connection, it is necessary to fit the tubelike cells together in a way that gas tightness and electronic conductivity are achieved by means of a suitable interconnection material, as shown in Fig. 2. This interconnection material (ICM) has to meet the following requirements at operating temperatures up to 1000 ^{0}C:

- high electronic conductivity and neglectable low ion conductivity in oxydizing and reducing atmospheres ($\rho_{ICM} \leq 20$ Ωcm)
- chemical stability and phase stability
- gas tightness and mechanical strength
- good adherence and compatibility with the ZrO_2-electrolyte and the electrodes

Some oxide materials have been developed which fulfil these qualifications to quite a great extent, as for instance:

- cobalt chromite: $CoCr_2O_4$ (11)
- lanthanum chromite, doped with Sr and Ni (12), (13)
- lanthanum manganite, doped with Sr (5)

With cobalt chromite, gas tight and stable connections are achieved, but the electronic conductivity in a reducing atmosphere is about 0.02 $\Omega^{-1}cm^{-1}$, which does not completely satisfy the requirements. Interconnection materials of doped lanthanum chromite and lanthanum manganite have the advantage of better electronic conductivity in a reducing atmosphere ($\rho_{ICM} < 5$ Ωcm), but the necessary gas tightness is not completely reached, due to sintering difficulties. Insufficient electronic conductivity or gas tightness of the interconnection material result in electrical losses, which reduce the total efficiency of the battery. Future development mainly has to aim at improving the electronic conductivity and gas tightness of the interconnection material, thus reducing the electrical losses to an acceptable degree.

2. Development of modules

For series connection of the cells in a battery several concepts have been developed. On the one hand, there are self-sustaining concepts with ZrO_2-solid electrolytes, having a minimum wall-thickness of 0.4 - 0.5 mm, thus giving the necessary strength to the battery, and on the other hand thin film concepts with a porous ceramic support, coated with the electrolyte- and electrode films of 30 to 100 µm thickness.

a) Self-sustaining module concepts

Tubular modules are obtained when cylindrical tubes are fitted together at their front faces by means of interconnection material (Fig. 2). Following this concepts, modules with 20 - 30 series connected cells have been constructed and tested in small battery units, consisting of 100 - 120 series connected cells. Fig. 4 shows a module constructed from 25 cylindrical cells and the photograph of a 100-cell-battery consisting of 4 of these modules is shown in Fig. 5.

The voltage losses under load of a 10-cell-module at 1000 °C, resulting from the ohmic resistivity of the solid electrolyte (R_E), the oxide cathode (R_C), the nickel anode (R_A), and the interconnection material (R_{ICM}), as well as from the polarization at the cathode and anode ($V_C + V_A$) are shown in Fig. 6. In order to diminish these losses and to increase the power density, improvements should be aimed for with respect to the resistivity of the solid electrolyte R_E, the resistivity to thickness ratio R_C of the cathode, and the polarization of the electrodes $V_C + V_A$.

This can be achieved by using thin film techniques for the preparation of electrolytes, by shortening the length of the oxide cathode in current direction, as well as by improving the porous electrode structure of the anode and cathode.

The power losses caused by series connection are partly due to the electrical resistivity R_{ICM} and partly to the fact that no complete sealing is obtained by the interconnection material. Thus, the quality of this interconnection material has to be improved as well.

Such module concepts suffer from the disadvantage that for the construction of huge batteries a lot of single cells have to be produced and series connected by means of a relatively expensive manufacturing process. Thus, production and investment costs would be too high.

b) Thin film module concepts

A further simplification and a reduction of battery manufacturing costs is possible by using thin film techniques as demonstrated in Fig. 7. By means of special procedures, i.e. chemical vapor deposition, plasmaspraying or a combined spraying and sintering technique, a porous electrode layer, a gas tight ZrO_2-electrolyte film, and a second porous electrode layer as well as a gas tight ICM-film are applied one after the other onto a highly porous ceramic support. The thickness of the different film amount to 30 - 100 µm. In this way, multicell modules with tubular support according to Fig. 7a (4) or plate-type support according to Fig. 7b (5) can be constructed. When using such thin film concepts, it is not only possible to cut costs by savings of material and simplification of the manufacturing process, but also to reduce the operating temperatur to 700 - 800 °C, thus reducing the technological problems which arise from high working temperatures.

References

1. Archer, D.H. and Sverdrup, E.F. (1962). Ann. Power Sourc. Conf. 16, 34.

2. Eysel, H.H. and Rohr, F.J. (1967). BBC-Nachrichten 49, 532 - 540.

3. Böhme, H.J. and Rohr, F.J. (1969). Third Int. Symp. on Fuel Cells, Bruxelles, Proc. 120 - 124.

4. Isenberg, A.O.; Pabst, W.A.; Sverdrup, E.F. and Archer, D.H. (1969). Proc. 6th Biennial Fuel Cell Symp., New York.

5. Rohr, F.J. (1975). EUCHEM-Conf., Elmau/W.-Germany.

6. Schachner, H. and Tannenberger, H. (1965). 1st Int. Symp. on Fuel Cells, Bruxelles, Proc. III, 19 - 26.

7. Isenberg, A.O. (1970). Abstr. 138th Nat. Meet. Electrochem. Soc., Nr. 13, 43.

8. White, D.W. (1968). General Electric Res. and Dev. Rep. No. 68-C-254.

9. Sverdrup, E.F.; Archer, D.H. and Glasser, A.D. (1969). Adv. in Chem. Ser. 90, Amer. Chem. Soc., Washington, 301 - 314.

10. Steiner, R.; Rohr, F.J. and Fischer, W. (1972). 4th Int. Symp. on Fuel Cells, Antwerpen, Proc. Vol. 113.

11. Sun, C.C.; Hawk, E.W. and Sverdrup, E.F. (1972). J. Electrochem. Soc., Vol. 119, 1433 - 1438.

12. Kleinschmager, H.; Reich, A. and Steiner, R. (1972). Abstr. 141st Nat. Meet. Electrochem. Soc., Vol. 72-1, 472 - 473.

13. Baukal, W.; Kuhn, W.; Kleinschmager, H. and Rohr, F.J. (1976). J. Power Sources, 1 (1976/77) 2, 203 - 213.

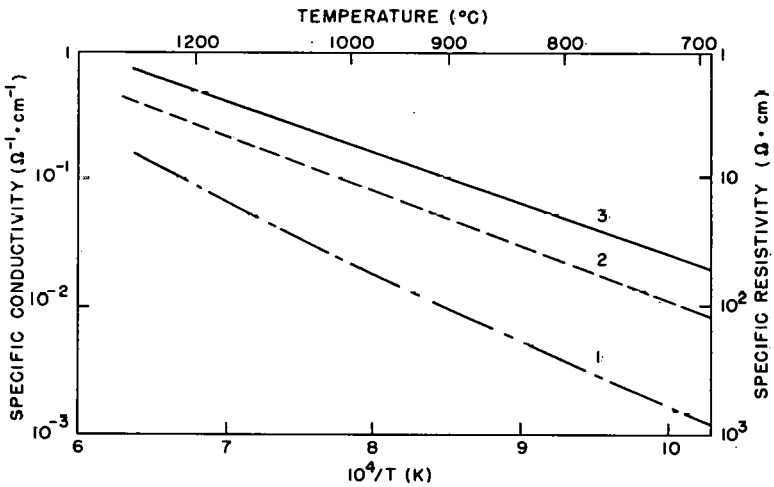

Figure 1. Oxygen ion conductivity and specific resistivity of zirconia solid electrolytes as a function of temperature and reciprocal absolute temperature.

Curve 1: $(ZrO_2)_{0.85}(CaO)_{0.15}$

Curve 2: $(ZrO_2)_{0.9}(Y_2O_3)_{0.1}$

Curve 3: $(ZrO_2)_{0.92}(Y_2O_3)_{0.04}(Yb_2O_3)_{0.04}$

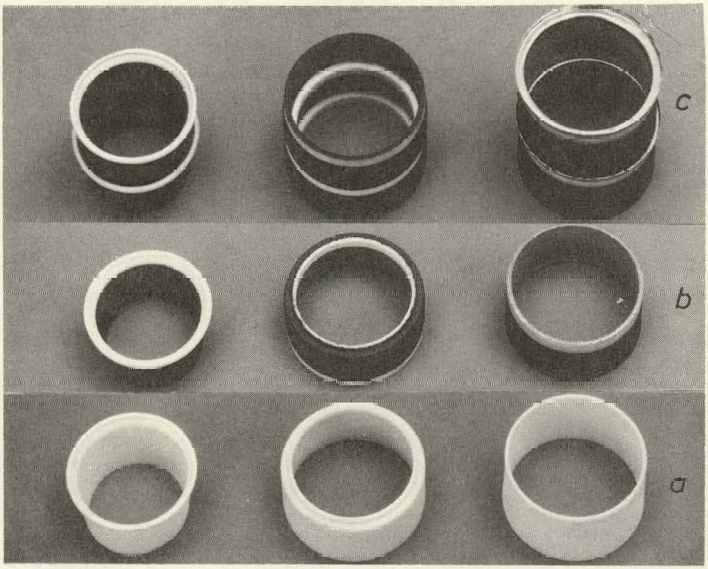

Figure 2. Conical and cylindrical tubular solid electrolytes (a) with plasmasprayed electrodes (b and c).

Electrolyte: $(ZrO_2)_{0.92}(Y_2O_3)_{0.04}(Yb_2O_3)_{0.04}$, diameter $D_E \leq 25$ mm; height $h_E \leq$ 12 mm; thickness $d_E \geq 0{,}4$ mm

Fuel electrode (inside): Ni
Air electrode (outside): $LaNiO_3$ (Bi); $LaMnO_3$ (Sr)

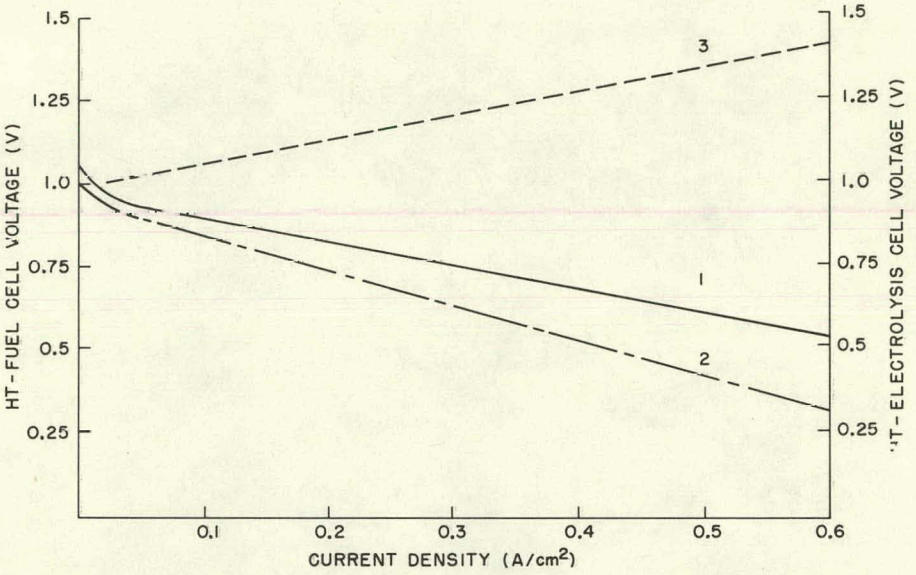

Figure 3. Voltage - current density characteristics of a HT-fuel cell (curve 1 and 2) and HT-electrolysis cell (curve 3) at 1000°C. Electrolyte and electrodes correspond to Figure 2. (D_E = 22 mm; H_E = 11 mm; d_E = 0,5 mm). Gas composition (1) H_2/O_2; (2) 3 H_2 + CO/air; (3) H_2 : H_2O = 1.

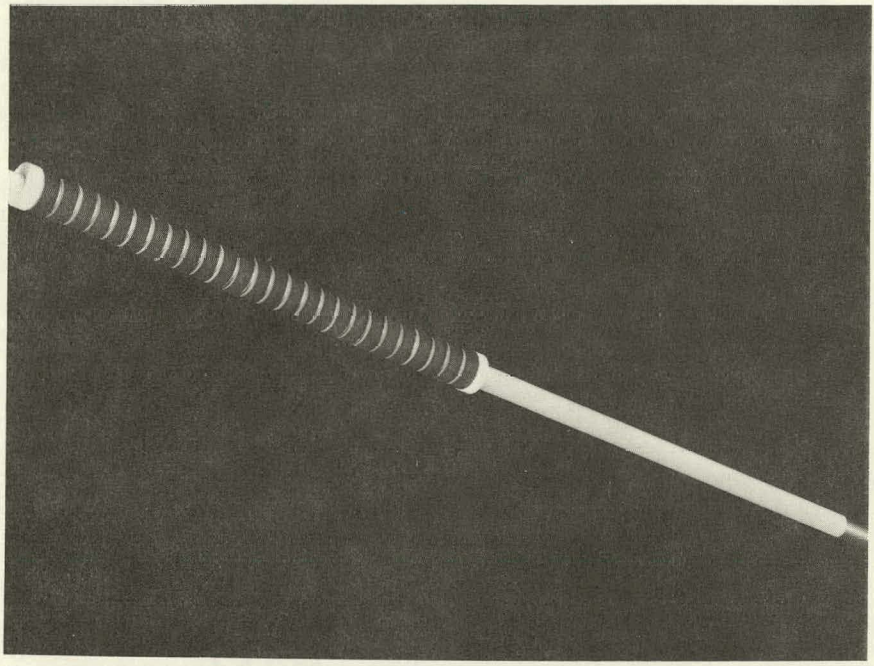

Figure 4. Battery module with 25 series connected cells. Solid electrolyte (D_E = 22 mm; h_E = 11 mm; d_E = 0.5 - 0.6 mm) and electrodes correspond to Figure 2. Interconnection material: $LaCrO_3$ (Ni, Sr) or $LaMnO_3$ (Sr).

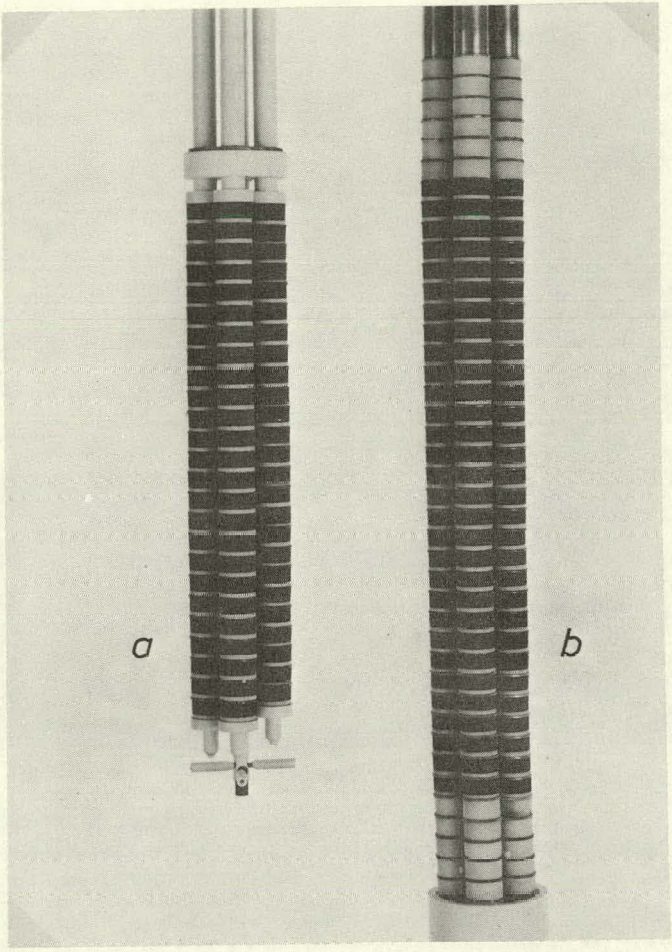

Figure 5. High temperature fuel cell batteries with 100 (a) and 120 (b) series connected cells.

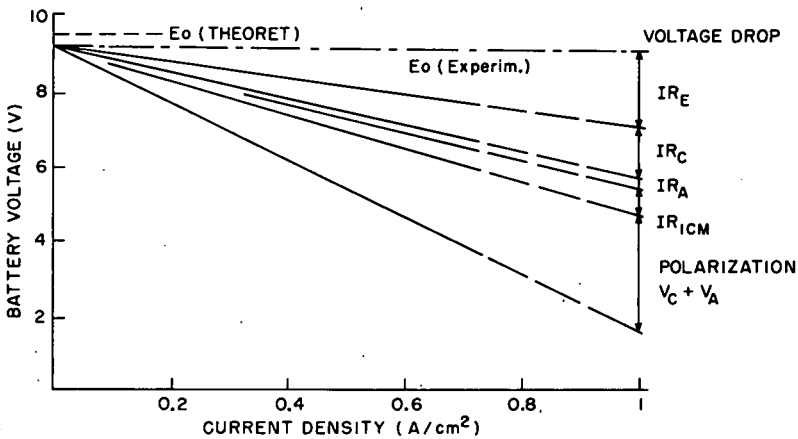

Figure 6. Resistance and polarization voltage losses of a 10-cell-battery as a function of current density at 1000°C. Module and cell components correspond to Figure 2 and 4. Fuel/oxidant: H_2 (H_2O at 70°C)/air.

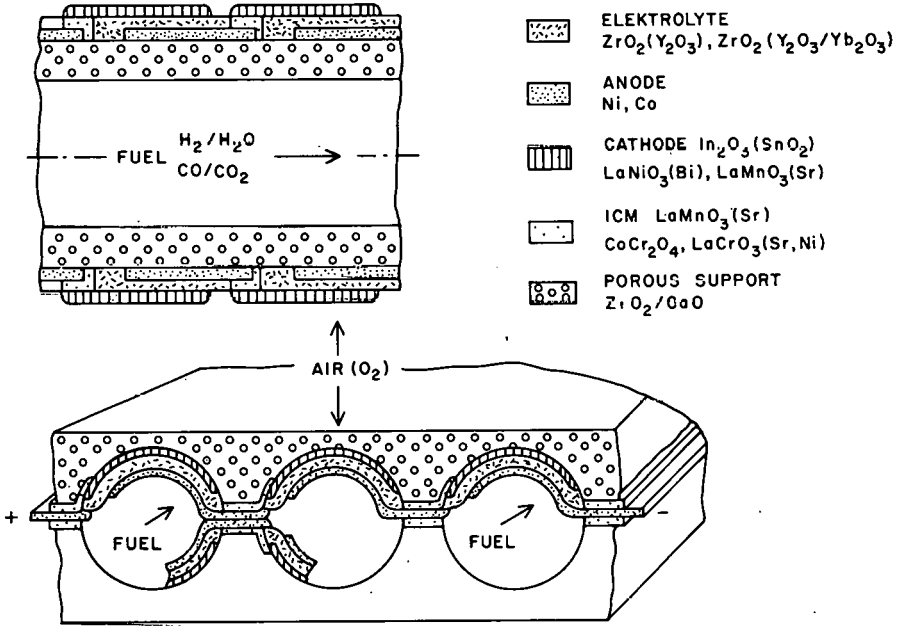

Figure 7. Cross section of thin-film fuel cell batteries with tubular (a) or plate-type (b) porous ceramic support.

A THIN SOLID FILM FUEL CELL APPROACH

M. Croset, J.P. Schnell, G. Velasco.
Thomson-CSF (L.C.R.) Domaine de
Corbeville - 91401 ORSAY, France

J. Siejka
Groupe de Physique des Solides de l'Ecole Normale Supérieure
Université Paris VII, Tour 23
2, Place Jussieu 75005 Paris, France

INTRODUCTION

Thin films (< 1 µm) have widely proved their usefulness in micro-electronics industry. Vacuum deposition techniques such as cathodic sputtering allows one to obtain thin films of metals, semiconductors and isolators having simple or multilayered structures of well-defined geometry. Advantages of these techniques in the solid electrolyte fuel cells domain have been recognized by some authors (1, 2, 3, 4). In 1966. N.J. Maskalick proposed a thin film solid electrolyte fuel cell using a thin film ZrO_2-Y_2O_3 as a solid electrolyte. The film was obtained by anodization or sputtering method. It was concluded that the stabilized zirconia phase (fluorite type structure) could not be obtained by anodization or sputtering techniques. Greene et al. in two recent papers (1976, 1977) reported on results on Y_2O_3 stabilized zirconia thin films obtained by RF sputtering ; polycrystalline films were obtained ; their structure and electrical properties (transport number t_i, activation energy of conduction E_c) seemed to be largely dependent of sputtering conditions. The t_i (0 - 0.14) and E_c (0.2 eV) values reported in the first paper evinced a predominant electronic conductivity, whereas in the second paper the measured conductivity was attributed to ionic transport ($t_i \sim 1$ for T > 200°C and $E_c \sim 1$ eV). In 1975 we reported preliminary results (4) which showed that dense and stoichiometric films of CaO doped ZrO_2 having the fluorite crystallographic structure can be obtained by RF sputtering in oxygen atmosphere ; the activation energy of conduction in such films was near that found for oxygen in bulk materials. A detailed study of these layers and their use for sensor applications have been presented and published recently (5, 6, 7).

The aim of this paper is to discuss from a research point of view various advantages that may be associated with the use of thin films ; the device and system approach is a subject open to discussion. We shall try to cover the field of thin solid electrolytes and electrodes for fuel cell application (note that sensors applications have already been discussed in (7)).

Thin solid oxide films as electrolytes

Up to now, work on thin electrolyte films was essentially done on zirconia based oxides. The experimental techniques used for their preparation are anodic oxidation, RF sputtering and electron gun evaporation. Results obtained are scattered and seem to depend not only on the technique chosen but also on its practice. Numerous parameters are concerned (vacuum cleanliness, partial pressure of reactive gases, nature of the source - cathode or evaporant - temperature, nature of the substrate). It appears that precise control of these parameters is needed for the adjustment of composition and structure of the deposits. Such a control can only be achieved by using well-adapted characterization techniques used in closed loops. Sophisticated characterization tools, developped for surface science studies, such as SIMS, RBS, ISS, Auger, X ray, SEM are of valuable assistance. As an example, Fig. 1 shows the RBS spectra obtained on ZrO_2-CaO layers deposited respectively by RF sputtering of a ZrO_2-CaO cathode (Fig. 1a) and by electron gun evaporation of a ZrO_2-CaO source of the same composition (Fig. 1b). It appears that RF sputtering gives layers having uniform Ca distribution ; by comparing pure and doped ZrO_2 deposits one may conclude that doped layers are stoichiometric. The Ca distribution in the evaporated films is not reproducible (1b), this being probably due to variation with time of the surface composition of the source. This example evinces clearly that deposit techniques may be rapidly compared and optimized leading to the realization of thin films of well defined and uniform composition. Note that adjustments of the technological parameters during deposition would permit the realization of films having graded composition with depth. The extension of such techniques to the deposit of other electrolytes has been announced (3) In fact we have found that thin stoichiometric doped CeO_2 films are easily obtained in the same way as doped ZrO_2 films.

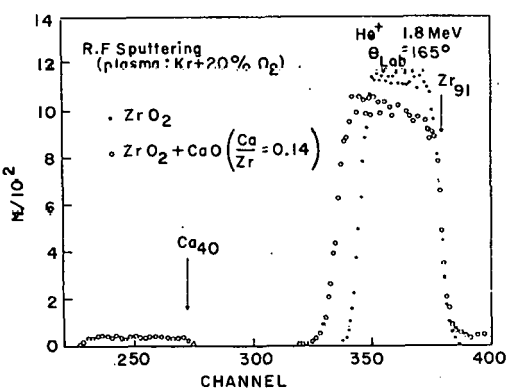

Figure 1a. Rutherford backscattering spectra of a pure zirconia film (•) and a CaO doped zirconia film (o) (each having about 1500 Å thick).

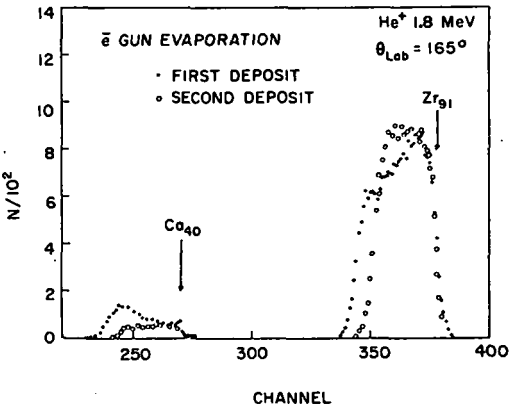

Figure 1b. Rutherford backscattering spectra of gun evaporation CaO doped zirconia films (about 1000 Å thick).

The ion implantation technique is an interesting tool largely used in microelectronics technology. Its use for modifying the composition of thin films of electrolytes has been tempted in our laboratory. Preliminary experiments have been done on $CaO-ZrO_2$ films obtained by implantation of Ca in a thin thermal oxide of Zr and by direct implantation in Zr followed by thermal oxidation in air at 600°C. It appeared that uniform Ca distribution may be achieved by using the first technique ; the second one seems to induce CaO precipitates.

The electrical conductivity of thin films can be easily measured by a.c. techniques down to very low temperatures (∿ 150°C). Note that the time constant of dielectric relaxation τ decreases linearly with the electrolyte thickness (for 1000 Å thick CaO doped ZrO_2, τ is in the 10^{-3}s range at 350°C). Fig. 2 shows the total electrical conductivity of ZrO_2-CaO films of various compositions between 11% and 19% ; all these layers were obtained by RF sputtering, the composition of the layer depending directly on that of the cathode used (for details, see (6)). One may deduce form Fig. 2 that, for thin films, the activation energy of the conduction is not very dependent on composition in the range studied ; this result seems to be in contradiction with that found on bulk material. The results obtained for 11% composition coincide with those of bulk materials ; prelimnary results obtained on implanted layers seem to indicate that activation energy of conduction near that of sputtered films may be obtained, whereas lower values of preexponential factor may be attributed to the existence of defects due to implantation technique.

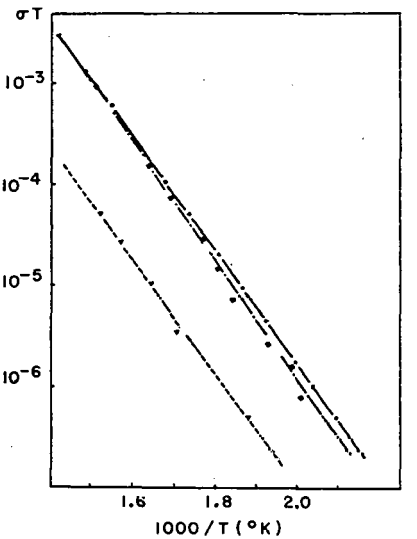

Figure 2. Arrhesius plot of conductivity-temperature product $(\Omega.cm)^{-1}(°K)$ measured on $CaO-ZrO_2$ deposits of about 1500 Å thick.

(●) 11.5 ± 0.5 atomic %
(■) 15.5 ± 0.5 atomic %
(▲) 19 ± 0.5 atomic %

The explored temperature (150°C - 450°C) with the thin film demonstrates the usability of such films at relatively low temperatures, the low conductivity being compensated by the thinness of the layer ; in fact 1000 Å thick CaO doped ZrO_2 has a specific resistance of 12 $\Omega.cm^2$ at 350°C ; the same value on 1 cm thick electrolyte is obtained at about 1000°C.

Thin solid films as electrodes

Kinetics of the whole electrochemical reaction taking place in solid galvanic cells based on oxygen conducting electrolytes is limited in practice (in known systems) by electrode reactions. For example, the resistance of Pt/CSZ interface (8) is equal to 10^5 $\Omega.cm^2$ at 600°C (pO_2 = 1 atm) i.e. many orders of magnitude higher than electrolyte resistance of 1000 Å thick electrolyte. Many other electrode materials have been examined. The doped SnO_2, $PrCoO_3$ and Ag were found to be the most satisfactory. Ag is very attractive because of its high diffusion coefficient for oxygen ; its rapid evaporation is a serious problem in thick classical electrolyte cells which need high temperature conditions.

It is well established (8) that the catalytic activity of the electrodes depends strongly on their techniques of preparation, texture

(porosity) and surface state of the electrolyte. The influence of all these parameters on electrodes properties can be easily studied on layers obtained by vacuum deposition techniques. Some preliminary results evinced the relationship between the Pt electrode porosity and its catalytic activity (7). Such catalytic activity is strongly related to the surface disorder. ISS technique is now in progress in our laboratory to study this effect by monitoring the oxygen adsorption-desorption equilibrium on Pt as a function of temperature and pO_2. First results seem to indicate that ion bombardment of the Pt deposits increase its adsorption capacity. Following our results and literature data, one can conclude that the oxygen catalytic activity of electrodes is at present time the limiting factor governing the use of thin film fuel cells.

Technological aspects of thin oxide fuel cell preparation

When thin films are concerned, baking problems are of great importance and have to be taken into account, wholly self supported thin films seem to be of no practical use. The substrate has to provide electronic current, gas and eventually permit the elimination of reactive products. When using the $1/2\ O_2 + H_2 \rightarrow H_2O$ reaction with an O^{-2} thin film conductor, it is better to provide the oxygen via the substrate and create water in the external medium. Maskalick developped a porous substrate made by sintering Y_2O_3 powders and Zr in order to provide electronic conductivity and hydrogen permeability supply ; some difficulties may arise such as adhesion and continuity of the deposited film ; a compromise has to be found between porosity of the substrate and thickness of the layer. On dense substrates (metals : C, Al, Fe, Ni, Cu, Zr, Mo, Pd, Ag, Ta, W, Pt, Au ; semiconductors or insulators such as SiO_2 and Al_2O_3) we have found that 1000 Å thick layers deposited by RF sputtering are dense, pore free and adhesive with no crack formation at temperatures as high as 600°C. The density of defects in such layers is essentially dependent on surface cleanliness and substrate handling prior to film deposition. On porous nickel (with a developped surface 20 times higher than geometrical surface), thicker deposits (up to 3000 Å) are needed to provide continuous films.
The $1/2\ O_2 + H_2 \rightarrow H_2O$ reaction used with an H^+ thin film conductor if it was available, would surely limit the substrate problems. Dense electronic conductors saturated with hydrogen, such as $FeTiH_x$ could probably be easily used. Known pure H^+ conductors are bad conductors ; the use of a thin film technology, by limiting the series resistance of the electrolytic layer, might be in this case a particularly interesting approach.

In order to provide higher voltages, a series interconnections of a multi cell assembly has been described in the past (9). The proposed structure which was based upon the use of rather thick electrolytic films (∿30 µ) is completely compatible to thinner electrolytes.

DISCUSSION

The consequence of the general thin film technology concept applied to fuel cell fabrication is the possible decrease by several orders of magnitude of the specific resistance of the electrolyte. This fact may be exploited in two different ways : first, the use of good electrolytes at lower temperatures than classically, and second the possibility of using poor ionic conductors having no practical interest as bulk material. Two important cases can be distinguished, depending of the material used as electrolyte, which may be an O^{-2} conductor or an H^+ conductor, the technological problems associated with each type are very different. In the first case, two difficulties may arise : to find substrates having a high gas permeability and eventually, to find electrodes working at low temperatures. In the second case (the use of H^+ electrolytes) the electrode problems may be less crucial. In fact, electrodes such as platinum or Ni seem to have much lower resistance to the H_2 ionisation than the O_2 one (if one extrapolates the data obtained in liquid systems). The second advantage is the possibility of using substrates such as metallic hybrides which could be used as hydrogen storage systems or permeable membranes connected with H_2 containers.
Very little work has been published on anhydrous H^+ conductors. The possibility of H^+ β-alumina preparation, pointed out by Kummer (10) and Bettman (11), has been reconsidered recently by Farrington (12). The conduction mechanism in this material is not clear, but the electrical carrier seems to be H_3O^+. The use of new techniques such as ion implantation in thin films has been considered in our laboratory as a possible tool for preparing, in anhydrous conditions, new protonic conductors.

REFERENCES

(1) M.S. Whittingham - Electrochim. Acta Vol. 20, p. 575 (1975)

(2) J.E. Greene, C.E. Wickersham, Z.L. Zilko, L.B. Welsh and F.R. Szofram - J. Vac. Sci. Technol. Vol. 13, p. 72 (1976)

(3) J.E. Greene, R.E. Klinger, L.B. Welsh and F.R. Szofram - J. Vac. Sci. Technol. Vol. 14 n° 1, pp. 177-180 (Jan/Feb. 1977)

(4) M. Croset, G. Velasco and J. Siejka - Electrode Processes in Solid Ionics (NATO Advanced Study Institute) Ajaccio, Corsica 1975 (Extended abstract)

(5) M. Croset, G. Velasco, and J. Siejka - "Composition and electrical properties of RF sputtered stabilized zirconia thin films" Int. Conf. on Superionic Conductors, Chemistry, Physics and Applications- Schenectady 10/12 May 1976

(6) M. Croset, J.P. Schnell, G. Velasco and J. Siejka - J.A.P. Vol. 48 n° 2 (Feb. 1977) p. 775

(7) M. Croset, J.P. Schnell, G. Velasco and J. Siejka - "A study of calcia stabilized zirconia thin film sensors" in press in J. Vac. Sci. Technol. May/ June 1977

(8) E. Schouler, M. Kleitz and C. Deportes - J. de Chimie Physique, Vol. 70 pp. 923-935 (1973)

(9) H.F. White - I.E.E.E. Trans. Power Apparatus System, Vol. PAS-87, p. 1956 (1968)

(10) J.T. Kummer - Prog. Solid State Chem. Vol. 7, p. 141 (1972)

(11) M. Bettman - Private communication.

(12) G.C. Farrington - J. Electrochem. Soc. Vol. 123, pp. 833-834, June 1976

THIS PAGE

WAS INTENTIONALLY

LEFT BLANK

E. ELECTRODE CHARACTERISTICS

1. Transport Considerations in Oxygen Electrodes of the Triphase Boundary Type for Zirconia Cells
   E. Bergmann, Battelle Memorial Institute (Geneva); H. Tannenberger, Alusuisse Research Center

2. An AC Technique for Characterizing Solid Oxide Fuel Cells
   H. S. Isaacs, L. J. Olmer, Brookhaven National Laboratory

3. Electrocatalysis of Coal Gas Compounds on Solid Oxide Electrolytes
   D. M. Mason, C. J. Wen, Stanford University

4. Cathodic and Anodic Polarization Phenomena at Platinum Electrodes with Doped Cerica as Electrolyte
   D-Y Wang, A. S. Nowick, Columbia University

5. Complex Impedance Measurements of Y^{3+} Doped CeO_2
   K. F. Young, A. D. Franklin, National Bureau of Standards

TRANSPORT CONSIDERATIONS IN OXYGEN ELECTRODES OF THE TRIPHASE BOUNDARY TYPE FOR ZIRCONIA CELLS

E. Bergmann and H. Tannenberger [1]
Battelle Memorial Institute, Geneva Research Centre
1227 Carouge-Geneva (Switzerland)

In principle three types of gas electrodes can be built on solid electrolytes [2] :

- electronic conductors with high gas diffusion capacity,
- triphase boundary structures : gas / metal / solid electrolyte,
- intercalation compounds with simultaneous high electronic and ionic conductivity.

Cathodes used in high temperature zirconia solid electrolyte fuel cells are usually made from porous layers of silver, platinum or indium oxide and combine, to a different degree, features of the first two types. In the case of silver, it is known [3] that oxygen sorption takes place at the triphase boundary as well as on the metal surface. Oxygen ions are injected into the solid electrolyte at the metal/solid electrolyte interface and at the triphase boundary. With platinum contacts, electronic conduction in the solid electrolyte seems to be the rate limiting process [4].

Since true intercalation compounds with sufficient electronic conductivity are not yet available for zirconia cells, the development of a special type of contact has been pursued and could be called a pseudotriphase boundary. An oxide layer with good ionic conductivity and appreciable electronic conductivity is intercalated between a metal or indium oxide structure and the solid electrolyte. Materials used are ceria [5] or doped zirconia [6] [7]. These intercalation layers are supposed to considerably decrease the polarization losses per unit triphase boundary. When combined with a well elaborated porous superstrate, these cathodes permit current densities of several hundred milliamperes without significant polarization losses.

To verify the envisaged mechanism of a pseudotriphase boundary contact we have compared the experimental and calculated current density / polarization relations of an idealized structure.

The experiment was made on a line contact as shown in the first two figures.

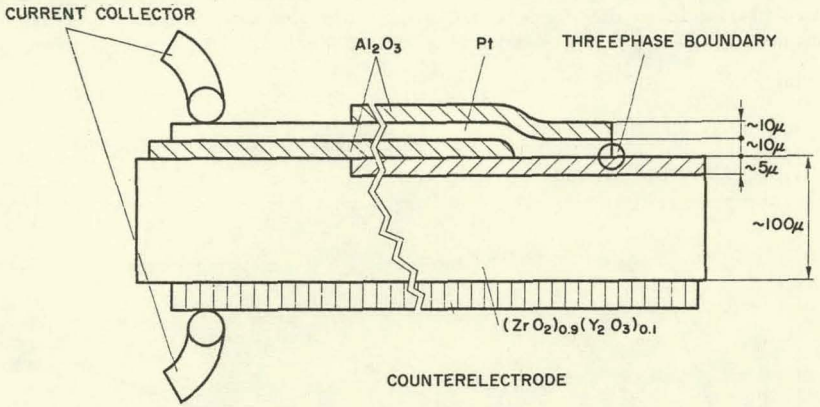

Figure 1. Cross-section through element with linear threephase boundary electrode (schematic).

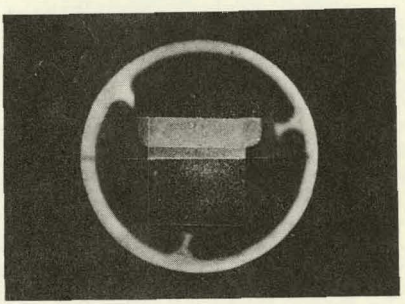

Figure 2. View of the linear threephase boundary from above (without current collector).

The alumina layer ensures complete oxygen impermeability. The intercalation layer has a slightly higher total conductivity than the electrolyte. At 800°C transport numbers for ions and electrons are approximately 1/2. The electronic transport shows a higher activation energy. These elements were placed in an air furnace and stationary characteristics measured between 700°C and 900°C. They are shown in Fig. 3.

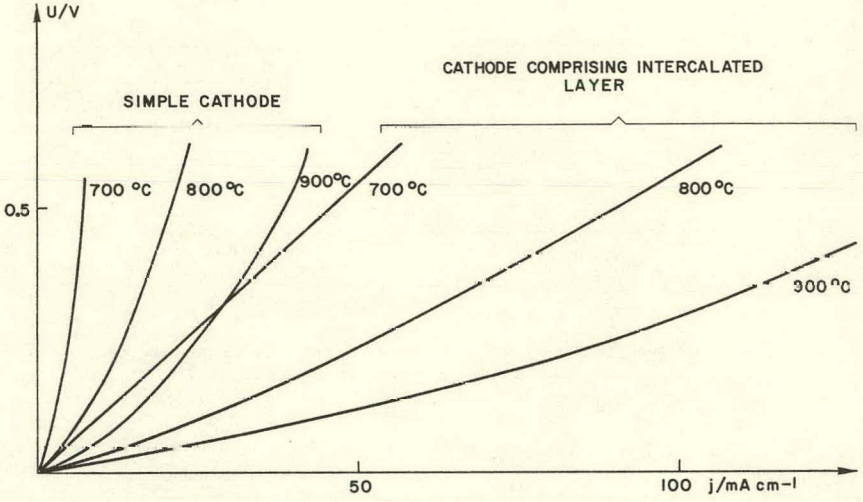

Figure 3. The counterelectrode used has very low polarization under anodic load, comparable to the ohmic conductivity of the electrolyte.

For the model calculations we made two assumptions:

- the oxygen sorption at the solid electrolyte surface shows a linear response,
- the metal / solid electrolyte interface has negligible electronic polarizability.

The first of these two assumptions implies that we do not assume that oxygen sorption requires an activation energy (8). We then remain with a mixed diffusion/migration problem for holes between the surface and the metal contact described by the following set of equations for the variables:

The first of these two assumptions implies that we do not assume that oxygen sorption requires an activation energy (8). We then remain with a mixed diffusion/migration problem for holes between the surface and the metal contact described by the following set of equations for the variables :

$J\ (O^{2-})$: current carried by oxygen ions

ϕ : electrostatic potential

μ_e : electron chemical potential

$J\ (\oplus)$: hole current

$$\text{div}\ J\ (O^{2-}) = \text{div}\ J\ (\oplus) = 0 \qquad (1)$$

$$J\ (O^{2-}) = \frac{\sigma\ (O^{2-})}{2\ F}\ \text{grad}\ \phi \qquad (2)$$

$$J\ (\oplus) = \sigma\ (\oplus)\ \{\ \frac{1}{F}\ \text{grad}\ \mu_e - \text{grad}\ \phi\ \} \qquad (3)$$

with the boundary conditions :

$\mu_e = -FV$ at the metal/solid electrolyte interface

$J = \frac{K}{F^2}\ \mu_e$ at the electrolyte / air interface

K : oxygen sorption rate.
The current density which is a linear function of the distance from the line contact has been calculated for different values of hole conductivity and sorption rate taking into account the dependence of the conductivity on the oxygen activity. The results show good qualitative agreement with the experiments.

(1) Present address : ALUSUISSE Research Centre 8212 Neuhausen (Switzerland)

(2) E. Bergmann and H. Tannenberger, Interfacial phenomena, to be published.

(3) H. Tannenberger and H. Siegert, The behaviour of silver cathodes in solid electrolyte fuel cells, Adv. Chem. 90 (ACS 1969) 281.

(4) E. Schouler, M. Kleitz and Ch. Déportes, Application selon Bauerle du tracé des diagrammes d'admittance complexe en électrochimie des solides I. étude de quelques réactions d'électrode sur $(ZrO_2)_{0.91}(Y_2O_3)_{0.09}$, J. Chim. Phys. 70 (1973) 923.

(5) H.H. Möbius, B. Rohland, Entwicklung von Elektroden für Festelektrolytbrennstoffzellen, Abh. Sächs. Akad. Wiss., Math. Naturwiss. Kl. 49 (1968) 343.

(6) Morganite R & D Ltd., Method of securing electrical connections to a solid electrolyte, Brit. Patent 1, 118, 655.

(7) H. Tannenberger, H. Siegert and P. Kovacs, Electrode pour pile à combustible à électrolyte solide, Swiss patent 478.463.

(8) E. Bergmann and J.F. Antonini, Application of response theory to adsorption / desorption kinetics, J. Phys. Chem. 79 (1975) 123.

AN AC TECHNIQUE FOR CHARACTERIZING SOLID OXIDE FUEL CELLS[+]

H. S. Isaacs, L. J. Olmer
Brookhaven National Laboratory
Upton, N. Y. 11973

High temperature solid ZrO_2-Y_2O_3 electrolyte fuel cells offer a high efficiency route for the conversion of coal to electricity(1). The optimization of the electrochemical cells depends on minimizing voltage losses due to the resistance of the cell components and the characteristics of the interfaces. The voltage losses at the electrodes, for example, will depend on the rate-controlling steps in the reaction sequence and a knowledge of these mechanisms will indicate where improvements in design or manufacture of the cell can be made. A wide range of techniques are available for the study of the electrical and electrochemical characteristics of the fuel cells. The technique employed in this work incorporated a square current wave which was passed across the system being studied and observing and interpreting the voltage response(2,3). There are advantages in using a square current wave. The method is rapid, it allows separation of any series resistance, and it essentially incorporates a wide range of frequencies. There are various methods for analyzing the voltage response. An interpretation, in terms of an electrical analogue, was chosen as it was simple and rapid. The voltage response was approximated by a capacitance and resistance, Cp and Rp, in parallel, and a series resistance, R_s. The R_s values were not, however, true resistive responses but rather the resistive contribution of one or more short time constants. The largest time constant of the voltage response at a given square wave frequency was measured, being equal to the product of Cp and Rp (which was usually 1000 Hz). Details of the apparatus have been discussed elsewhere (2,3).

There were three types of ZrO_2-Y_2O_3 oxides studied. The thinest oxide was about 30μ thick and was grown by an electrochemical vapor-depositor technique(4). This electrolyte is planned for use in solid oxide fuel cells(5) being developed by Westinghouse. The other oxides were prepared via green-sheet* and slip-cast** routes. The slip-cast oxide contained 8 m/o Y_2O_3, the other oxides about 12 m/o Y_2O_3. Electrochemical cells were constructed from these oxides with platinum

[+]This work was performed under the auspices of the U.S. Energy Research and Development Administration.
*Obtained from T. B. Reed, MIT.
**Obtained from Zircoa Corp.

electrodes and studied in air. Leads were attached to the oxide with a Pt powder paste and the electrodes painted around them. Platinum pastes and Pt-organic solutions were used for the electrodes. Electrodes were applied on each side of the electrolyte adjacent to similar electrodes on the opposite side of the oxide. Two, three and four electrode configurations were used. Two electrode measurements included two opposite electrodes and the electrolyte between them. Three electrode measurements were used to study the interfacial characteristics of a single electrode/electrolyte contact. The four electrode measurements, on the other hand, eliminated any electrode contributions to the observed electrolyte resistances.

When the vapor-grown oxide was studied, the electrodes dominated the overall characteristics of a two electrode cell. When the impedance of a cell with annealed electrodes was measured, the R_s and R_p values varied rapidly with temperature as shown by the largest values in Figure 1. Electrodes were annealed by heating at 1000°C or higher for over an hour. The curves as plotted in Figure 1 were not linear, indicating more than one process dominated the temperature dependence; the temperature dependence approximated an activation energy of 25 to 30 Kcal/g mole. This temperature dependence was also observed for the resistance at higher frequencies of 50,000 Hz as shown by the broken line in Figure 1.

The magnitude of the impedances of the two electrode cell was markedly reduced when the electrodes were recoated with the Pt-organic paint. The curves shown for R_s' and R_p', in Figure 1, were obtained during the first heating after recoating. Holding or annealing the cell at 1000°C for one hour increased the resistances which on cooling were the same as those observed prior to recoating the electrodes. These marked changes in resistances were the result of changes in the electrode characteristics alone and as recoating the electrodes would not influence the electrolyte behavior.

The resistance of the electrolyte expected in the two electrode cell configuration with the vapor-grown oxide was calculated from four electrode measurements of the electrolyte resistivity. The calculated resistance (R_{calc}) was markedly lower than the observed resistances although the highly active nonannealed recoated electrode cell did approach the calculated electrolyte resistance, at the lower temperatures as shown in Figure 1. In addition, the electrolyte resistivity showed a single activation energy of 20 ± 1 Kcal/g mole. This analysis and the results clearly demonstrated that with this electrolyte, the impedance of the electrodes dominate the cell and the contribution of the electrolyte was negligible. Four electrode a-c resistance measurements on the vapor-grown and slip-cast oxides showed no discernible time dependence, whereas the green-sheet oxide did. This indicated a probable grain boundary impurity for this oxide(6,7).

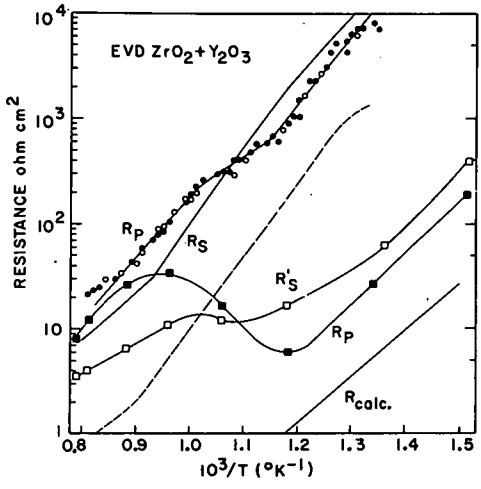

Figure 1. The dependence of resistance on temperature for the vapor-grown ZrO_2-12 m/o Y_2O_3 oxide cell with two electrodes

□ ■ R_s' R_p measured at 1000 Hz on annealed electrodes
R_s' R_p measured at 1000 Hz on Pt-organic recoated electrodes during heating
--- Total resistance measured at 50k Hz
R_{calc} resistance calculated from measured electrolyte resistivity.

The influence of d-c potentials on a single electrode was studied using a three electrode cell where the third electrode acted as a reference and carried no current.

The variation of the analogue R_s, R_p, and C_p components of the interface are shown in Figure 2 for the vapor-grown oxide. The capacitance of an interface may be related to its electrical double layer, space changes or the electrochemical reactions taking place. If the capacitance was a function of the electrical double layer or space change, it would be expected that the measured resistance would be independent of the capacitance(8). This is not the case in Figure 2, as they were inversely related. At positive potentials, the capacitance was high (up to 500 $\mu F/cm^2$ at 0.5 volts) and the parallel resistance is low. At negative potentials, the reverse was true and a minimum in capacitance was also reflected by a maximum in resistance.

The d-c current was also not symmetrical about the zero potential. At positive potentials, the anodic currents were

higher than the cathodic currents at negative potentials. This reflects a higher resistance or impedance at negative potentials than at positive potentials, as was observed from impedance measurements. These curves were interpreted in terms of a resistance or differential resistance, R_{DC}, as can be seen from Figure 2. The differential resistance was obtained by graphical differentiation of the dc current/voltage curve and is plotted in Figure 2. All the resistance R_{DC}, R_p and R_s were higher at negative potentials and had a maximum at negative potentials. These similarities indicate that both the a-c and d-c behavior of the electrode are determined by the same factors.

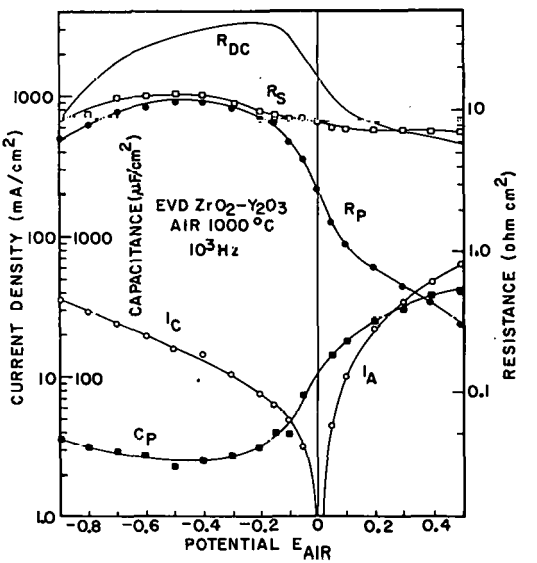

Figure 2. The potential dependence of (a) the anodic I_A and cathodic I_C currents; (b) the a-c capacitance C_p, resistance R_p and series resistance R_s measured at 1000 Hz; (c) the differential resistance R_{DC}. The results were for a single electrode on vapor-grown oxide at 1000°C.

The polarization current for the electrode is shown again in Figure 3, plotted on a linear axis. It is interesting to note that both the anodic and cathodic curves are approximately linear but have distinctly different slopes. If the electrolyte resistance had controlled the polarization characteristics the anodic and cathodic curves would be linear and have the same slope. The slopes were determined by the potential dependence of the reaction kinetics at the electrodes.

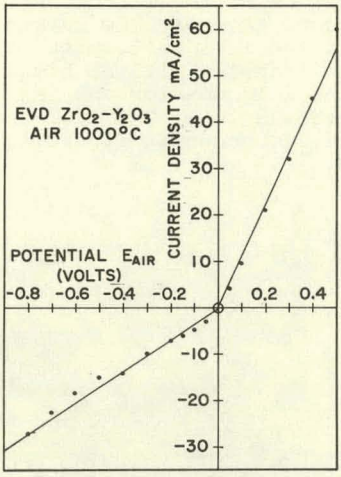

Figure 3. The variation of the anodic and cathodic currents plotted from Figure 2 as a linear function of potential.

The electrode kinetic characteristics are significantly different from those observed in aqueous systems(3). The approximately linear current behavior over a range of potential of 800 mV as observed cathodically is not observed in aqueous electrochemistry even taking into account the influence of increasing the absolute temperature from 300 to 1270°K. At the reversible potential of the solid oxide electrodes in air, the electrode kinetics may be controlled by the heterogeneous reaction kinetics or concentration polarization. Concentration polarization would control the reaction rates when the reaction kinetics were rapid. Under these conditions, the capacitance should show a distinct maximum and the parallel resistance a minimum at the reversible potential (i.e., the Warburg impedance)(8). This was not observed which indicates that reaction kinetics and not concentration polarization determined the reaction rates. In aqueous systems, reaction kinetics control is referred to as activation polarization. Activation polarization is essentially the same as a high field conduction process and the current increases logarithmically with potential. This current was also not observed with the solid oxide and attempts to increase the currents above 60 mA/cm^2 with the vapor-grown oxide was unsuccessful because of heating effects. The

heating was a consequence of the methods used in this investigation and would not occur at these low current densities in a fuel cell system. In the fuel cell system, the mass of the cell is large and the heat transfer will be high. In these experiments, the mass of the film was low and the heat transfer coefficient to the air was low. The cell heated to extremely high temperatures and, as shown in Figure 4, both the platinum and the oxide melted.

Figure 4. Part of a vapor-grown oxide cell after passing high polarization currents. The rounded edges of the oxide and beads of platinum indicate melting had occurred.

These measurements have led to the following conclusions:

1. The electrolyte resistance in fuel cells will be negligible in comparison to the effective resistances of the electrodes. The electrolyte composition can therefore be changed to maximize the electrochemical reaction rates even though the oxide resistivity would be lower. For example, the Y_2O_3 concentration could be increased to increase the oxygen vacancy concentration which may increase the rate of oxygen reduction.

2. The resistance, as shown by recoating the electrodes, can be decreased by over an order of magnitude and the polarization currents would be expected to increase markedly. However, the improved electrodes in this investigation were unstable and lost their activity at higher temperatures.

3. The mechanisms of electrode reactions on oxide electrolytes at present appear to be significantly more complex than those in aqueous electrolytes. These effects are possibly a result of the electronic conduction in the oxide which even though <1%, could markedly change potential distributions at the electrolyte/electrode interfaces.

4. The a-c techniques employed encompass a wide range of variables relevant to solid oxide electrochemical cells and could be applied to monitoring cells, quality control, and understanding the reaction mechanisms which could lead to improvements in fuel cell performance.

REFERENCES

(1) C. J. Warde, R. J. Ruka, and A. O. Isenberg, ECAS Final Report, Vol. XII - Fuel Cell Report No. CR-134941, February 1976.

(2) H. S. Isaacs and J. S. LL. Leach, J. Electrochem. Soc. 110, 680 (1963).

(3) H. S. Isaacs and J. S. LL. Leach, J. Electrochem. Soc. 115, 238 (1968).

(4) A. O. Isenberg, Extended Abstract, Electrochemical Society Meeting, Philadelphia, Pa., May 1977, Vol. 77-1, Abstract No. 380, p. 363.

(5) A. O. Isenberg, Abstract, ibid, No. 394, p. 1000.

(6) J. E. Bauerle, J. Phys. Chem. Solids 30, 2657 (1969).

(7) N. M. Beekmans and L. Heyne, Electrochemica Acta 21, 303 (1976).

(8) D. C. Grahame, J. Electrochem. Soc. 99, 370C (1952).

ELECTROCATALYSIS OF COAL GAS COMPOUNDS ON SOLID OXIDE ELECTROLYTES

David M. Mason and C. John Wen
Department of Chemical Engineering
Stanford University
Stanford, CA 94305

Abstract

It is generally accepted that the nature of the metal electrode is very critical in determining the rate of electrochemical reactions in cells employing solid oxides as electrolytes. On the other hand, the role of the oxide electrolyte in catalyzing cathodic electrochemical reactions involving gases containing oxygen has not been given much attention. In the investigation of NO decomposition on scandia or calcia stabilized zirconia by electrolytic removal of oxygen, there is a remarkable enhancement of reactivity by several orders of magnitude on the zirconia electrolyte surface itself over that on platinum or gold. The purpose of this paper is to discuss some aspects of the electrocatalytic nature of the solid electrolyte electrodes including enhancement of the rate of the oxygen cathodic reaction by presence of protons on the electrolyte surface. Also, data on the anodic electrocatalysis H_2 and CO are discussed.

Experimental

The experimental set-up is schematically shown in Figure 1. The essential part of the cell comprised an 8 mole% scandia stabilized zirconia disc pressed between two alumina tubes with two gold rings as seals which also served as current collectors. Gold wires 0.3 mm in diameter were welded on the gold seals by a spot-welder to provide the electrical leads. Generally, the gas samples were passed through a water saturator or a liquid nitrogen cold trap depending upon the purpose of experiment. Purified He gas was maintained in the chamber of the furnace. All electrical measurements were made on a Fluke 8200A digital voltmeter with an input impedance of 10^{14} ohm.

The experimental observations consisted of measuring the current-potential characteristics. The cell overpotential, η, at given current, I was calculated from the following relationship of:

$$E = E_o \pm I R_{ac} \pm \eta \qquad (1)$$

where E is the measured cell potential, E_o is the open circuit potential and R_{ac} is the cell internal resistance obtained by A.C. method at 1kHz. The positive and negative signs in Equation (1) represent the situations for self-generating (fuel cells) and driven cells, respectively. Temperature was measured with a chromel-alumel thermocouple.

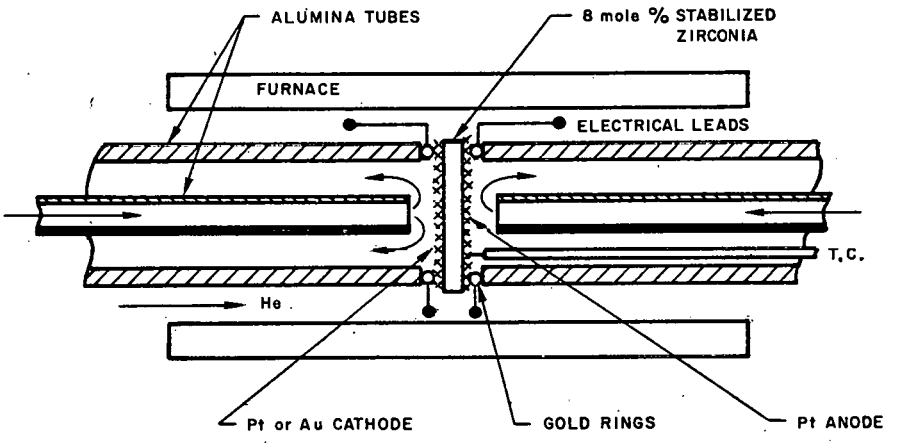

Figure 1. Schematic of experimental solid-electrolyte cell.

Results and Discussions

Oxygen Reduction at the Cathode

Until recently metal electrodes were thought to play the predominant role in catalyzing the reduction of gaseous oxygen compounds in solid-oxide electrolyte systems. However, Fabry and Kleitz [1] have noted that the catalytic activity of these electrode-electrolyte systems can be accounted for by both the metal electrode and electrolyte. Also in some recent work of Pancharatnam et al. [2], it was observed that the rate of NO decomposition electrochemically on stabilized zirconia with platinum as the electrode was several orders of magnitude greater on the zirconia electrolyte than on the platinum electrode. It was hypothesized that F-centers on the surface of the zirconia created by the presence of the electric potential were active sites for the NO decomposition, though this hypothesis has to be further carefully tested. Also the electrochemical system gave decomposition rates at 800°C 10^8 times that observed by Amirnazmi et al. [3] on zirconia in the absence of an electric field.

Figure 2 shows the influence of water vapor on the cathodic reduction of oxygen on a porous Au electrode. As it can be seen the total current at a given overpotential η is substantially increased by adding a small amount (3% by volume) of water vapor to the oxygen-feed stream at the cathode. The same behavior has been reported in the study by Yuan et al. [4] of oxygen pumps using stabilized zirconia. Similarly, the electrode resistance of an electrochemical cell using calcia-stabilized zirconia with porous Pt paste electrodes has been observed by Yanagida et al. [5], to increase significantly in the absence of water vapor. In fact, this catalytic effect of water vapor on the current overpotential characteristics has been observed not only in the reduction of oxygen in Pt but also in the decomposition of CO_2 as demonstrated by Weisbart et al. [6]. For those runs in which the feed gas ($CO + CO_2$) is mixed with a small amount of water vapor, the cathode current efficiency was much higher than for runs using dry gaseous mixture.

In order to interpret this behavior, it is important to examine the overall cathodic reduction of oxygen via the following defect reaction

$$O_2(g) + 2V_o^{\infty}\ (ZrO_2) + 4e'\ (Au) \rightarrow 2O_o^{\times}\ (ZrO_2) \qquad (2)$$

where V_o^{∞} denotes the doubly ionized oxygen-ion vacancies and $O_o^{\times}$ represents the oxygen ions occupying the normal sites. It is clear that the three-phase contact zone where electrode, electrolyte and gas are in mutual contact is the most reasonable location for the prepondernace of electrochemical active sites. In fact, the necessity of maintaining as much three-phase contact as possible has been shown by Karapachev [7]. Furthermore, it has been emphasized that the charge transfer overpotential for cathodic-oxygen reduction is not negligible by Casselton [8]. As a consequence, the rate of formation of oxygen ions depends upon the electron transfer steps and the cathodic overpotential arising partially as a result of the irreversibilities of electrochemical reactions.

In the presence of the water vapor, the oxygen ions, however, can be

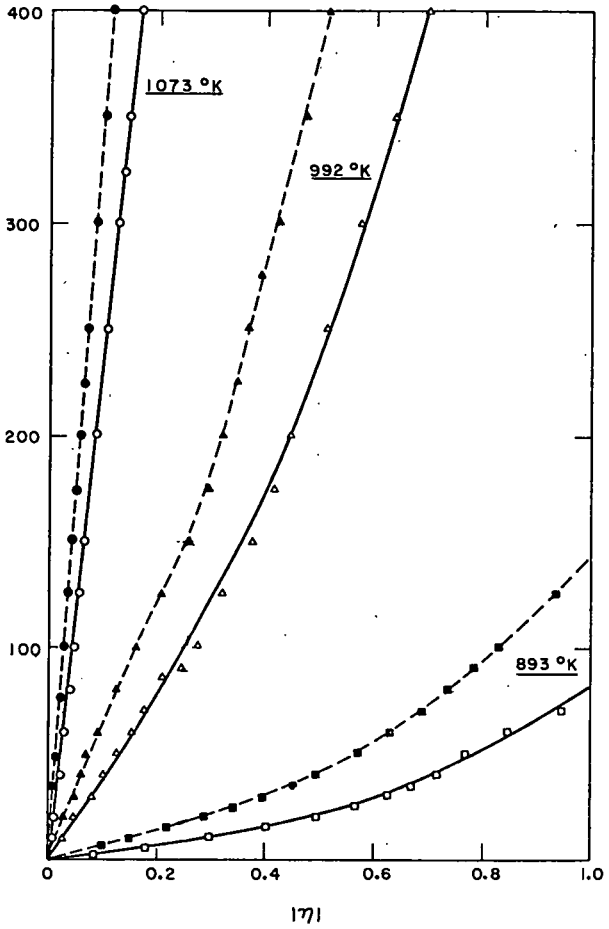

Figure 2. Influence of water vapor on the cathodic overpotential in the reduction of oxygen on a gold electrode.

(+) Air, $Pt/ZrO_2 \cdot Sc_2O_3/Au$, $O_2+H_2O(-)$

	O_2	H_2O
——	100%	0%
---	969%	3.1%

produced directly according to the reaction

$$H_2O(g) + V_o^{\infty}(ZrO_2) \rightleftarrows O_o^{\times}(ZrO_2) + 2H_i^{\circ}(ZrO_2) \qquad (3)$$

As a matter of fact, Wagner [9] has reported that the solubility of hydrogen in the $ZrO_2 + Y_2O_3$ solid solution as interstitial protons is proportional to square root of the partial pressure of the ambient water vapor as expressed by the equation:

$$[H_i^{\circ}] = (K_S P_{H_2O}[V_o^{\infty}]/[O_o^{\times}])^{1/2} \qquad (4)$$

The mole fraction of H_i was estimated to about 2×10^{-4} at 1000°C and 1 atm H_2O. The temperature dependence was small. Moreover, the diffusion coefficient of H_i° is of the order of 10^{-6} cm^2/sec at 900-1000°C. This value is at least two orders of magnitude higher than that of oxygen ions by a vacancy mechanism by Kingery et al. [10]. Therefore, the catalytic effect of water vapor on oxygen reduction can be attributed to its solubility in the oxide electrolyte.

Effect of Anode Reactions on Cell Total Overpotential

It has been suggested by Weisbart et al. [11] that the anode reactions can occur in one of two ways, either (i) the oxygen ion ($O_o^{\times}$) forming oxygen (1/2 O_2) at the electrode surface and the latter then reacting with the fuel or (ii) the oxygen ion ($O_o^{\times}$) directly with the fuel at the electrode-electrolyte interface.

The experimental results of current versus overpotential shown in Figure 3 were obtained by passing various gases through the anode compartment. Although the datum points denoted by different symbols are quite scattered, they (except for H_2 at the anode) generally fall into a single curve, thus suggesting that for these species the behavior of the processes occurring at the cathode determines the current versus overpotential curves, oxygen being released without reaction at the anode except for H_2--the overpotential at a given current for H_2 being considerably less than those for other gases. It is interesting to note that unlike H_2, CO is not appreciably reactive at the anode.

The electrode reaction involving hydrogen may take a completely different route than that suggested above, possibly that suggested by Wagner [9]:

$$H_2(g) \rightleftarrows 2e'(Pt) + H_i^{\circ}(ZrO_2) \qquad (5)$$

$$2H_i^{\circ}(ZrO_2) + O_o^{\times}(ZrO_2) \rightleftarrows H_2O(g) + V_o^{\infty}(ZrO_2) \qquad (6)$$

In Figure 4 can be seen the excellent reproducibility of current versus overpotential at 707°C. It is interesting to note that there is no significant difference in overpotential characteristic between a fuel cell and a driven cell. This behavior leads to the conclusion that the electrode potential appears not to affect the overall anodic oxidation of hydrogen appreciably. A more detailed study of the solid electrolyte systems may be found in the work of Wen [12].

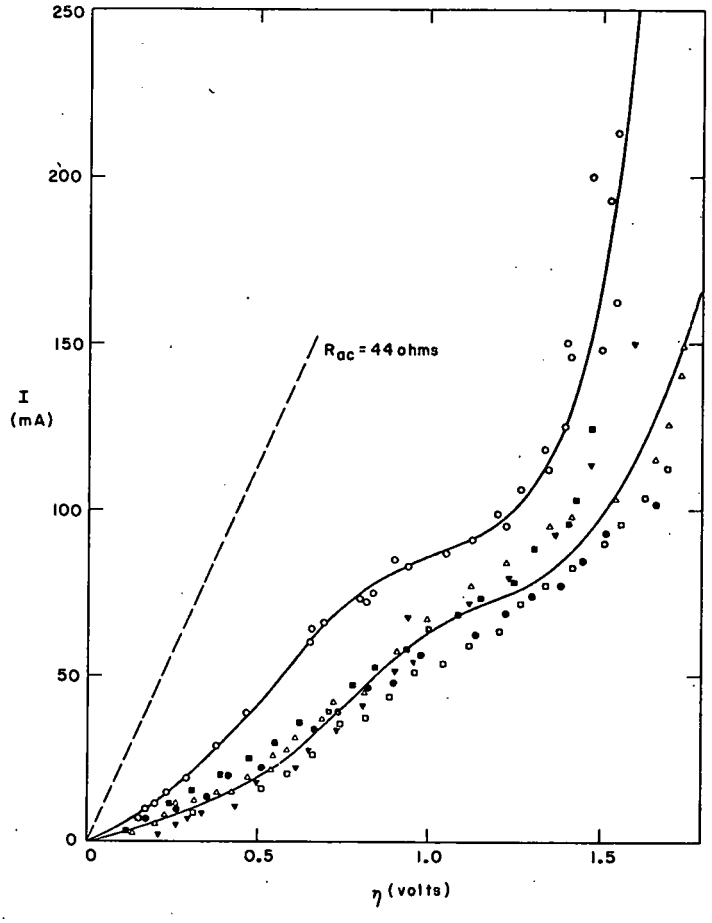

Figure 3. Influence of anodic gases on over-potential behavior.

(-) Air, $Pt/ZrO_2 \cdot Sc_2O_3/Pt$, X(+)

T = 980°K, Flow Rate of Gases = 50 ml/min

- ○ H_2
- △ CO
- ▼ CO_2
- □ He
- ■ O_2
- ● Air

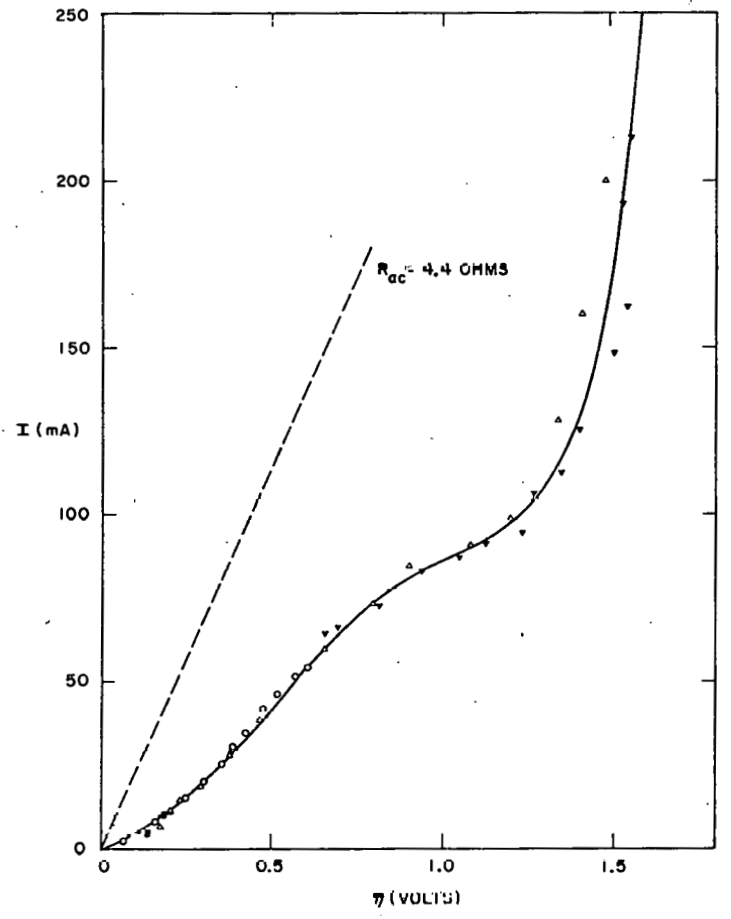

Figure 4. Reproducibility of current-overpotential behavior at 980°K and gas flow rates of 50 ml/min.

○ (+)Air, Pt/ZrO_2 · Sc_2O_3/Pt, H_2(-) Fuel Cell

▼ (-)Air, Pt/ZrO_2 · Sc_2O_3/Pt, H_2(+) Driven Cell

△ (-)Air, Pt/ZrO_2 · Sc_2O_3/Pt, H_2(+) Driven Cell

Conclusion

Based on the preceding discussion, it is tentatively concluded that the solid-oxide electrolyte cell acts as an oxygen concentration cell and the presence of point defects such as interstitial protons on the oxide surface enhances the rate of reduction of O_2 at the cathode and may be responsible for catalyzing the oxidation of H_2 at the anode. In order to obtain a much better understanding of the electrode processes involving interstitial protons and F-centers, it is necessary to obtain more extensive results by performing experiments using different electrode metals than just gold and platinum and vary the metal-oxide surface morphology. Also different solid-oxide electrolytes besides the zirconia family (e.g., ceria, gadolinia, etc.) are being studied with a focus on cathodic decomposition of NO and anodic oxidation of coal gas compounds such as H_2, CO, CH_4 and their derivatives such as CH_3OH.

Acknowledgment

The authors wish to express their appreciation to the National Science Foundation who partially supported this research on Grants No. Eng 75-02397 and 75-05462 and also to the Gould Foundation via a grant to the Stanford Energy Institute.

References

1. P. Fabry and M. Kleitz, "J. Electroanal. Chem. and Interf. Chem.", 57, 165, 1974.

2. S. Pancharatnam, R. A. Huggins and D. M. Mason, "J. Electrochem. Soc.", 122, 869, 1975.

3. A. Amirnazmi, J. E. Benson and M. Boudart, "J. Catalysis", 30, 55 1973.

4. D. Yuan and F. A. Kröger, "J. Electrochem. Soc.", 116, 594, 1969.

5. H. Yanagida, R. J. Brook and F. A. Kröger, "J. Electrochem. Soc.", 117, 593 1970.

6. J. Weisbart, W. H. Smart and T. Wydeven, "Aerospace Med.", 40, 136, 1969.

7. S. V. Karpachev and A. T. Filayev, "Soc. Electrochem.", 2, 1215, 1966.

8. R.E.W. Casselton, "J. Sppl. Electrochem.", 4, 25, 1974.

9. C. Wagner, "Ber Bunsengesellschaft Phys. Chem.", 72, 778, 1968.

10. W. D. Kingery, J. Pappis, M. E. Pappis and D. C. Hill, "J. Am. Cer. Soc.", 42, 393, 1959.

11. J. Weisbart and R. Ruka, Chap. 4, in "Fuel Cells", Vol. 2, ed. by G. J. Young, p. 45, Reinhold, New York, 1963.

12. C. John Wen, "Electrochemical Kinetics of Oxygen Electrode Reactions in Solid Oxide Electrolyte Fuel Cells Operating on Coal Gas", Engineer's Thesis, Stanford University, January 1977.

CATHODIC AND ANODIC POLARIZATION PHENOMENA AT PLATINUM ELECTRODES WITH DOPED CERIA AS THE ELECTROLYTE

Da-Yu Wang and A.S. Nowick
Henry Krumb School of Mines
Columbia University
New York, New York 10027

Our understanding of electrode processes which give rise to polarization is very limited due to the conflicting results of past studies (1), most of which have been carried out using Pt electrodes and stabilized zirconia as the electrolyte. In the present study, the current interruption method, is selected. This method is advantageous because (a) it allows separate study of the anodic and cathodic polarization effects, and (b) it can effectively separate the ohmic polarization (IR drop) from the other effects. Porous platinum electrodes are selected because these have been so widely studied, while doped ceria is chosen for the electrolyte because of its promise for fuel cells (2,3).

All of the samples are calcia doped ceria with CaO content from 6 to 15 mole %. The mechanically mixed powders with the right composition are first calcined at 1000°C, then ground and pressed into pellets and sintered at 1600°C for 24 hours. Before applying electrodes, all of the samples are polished with 6μ and 1μ diamond paste for several hours.

The electrodes are applied by firing platinum paste (Englehard #6082) at 800°C in open air. Semi-circular electrodes are put on both sides of the sample as cathode and anode. The reference is on one side of the sample separated by at least 0.5 cm from the nearest electrode; its area is kept as small as possible.

A schematic diagram of the current interruption method is given in Fig. 1. The anodic or cathodic overpotentials, η, (relative to the reference electrode) are measured with a storage type oscilloscope which records the residual voltage after switching off the applied current. The voltage drop which occurs immediately upon switching is attributed to the ohmic polarization. In general, the IR drop from anode to cathode or from either electrode to the reference shows a linear relation with the applied current. The resistance thus obtained (after correction for the electrode resistances which had been measured directly by using a platinum foil to

replace the sample) agrees well with the value of electrolyte resistance which is obtained from independent 4-probe dc conductivity measurement. Therefore the residual voltage is believed to come purely from anodic or cathodic overpotentials.

Thus far we have studied several calcia doped samples with the compositions of 6%, 8%, 10% and 15% CaO, over the temperature range from 600°C to 900°C, and with the partial pressure of oxygen from 1 atm to 10^{-5} atm (obtained with argon-oxygen gas mixtures).

For the anodic polarization, we have found that when the overpotentials η_a are small ($\eta_a << kT/e$) the relation between η_a and the applied current I is linear. At higher overpotentials, the linear relation is no longer obtained. For large overpotentials ($\eta_a >> kT/e$), the characteristic Tafel behavior is observed (i.e. linear plot of logarithm of applied current I, vs. η_a) with a slope equal to $e/2.3\ kT$. The entire curve can be fitted well with the Butler-Volmer equation (4)

$$I = I_o \left[\exp\left(-\frac{en\beta\eta_a}{kT}\right) - \exp\left(\frac{en(1-\beta)\eta_a}{kT}\right) \right]$$

with $n = 2$ and $\beta = 0.5$. Here I_o is the "exchange current". This equation gives a linear I-η_a relation at low η_a and Tafel behavior at high η_a. Figure 2 shows some typical examples of the fit of the above equation to the data for anode polarization. In this way, we have been able to obtain the dependence of I_o on temperature and oxygen partial pressure. In several cases, however, it was found that by using the values of I_o obtained from small overpotentials we could not fit the data for the range of large overpotentials unless the values of β were increased from 0.5. In these cases, it was also found that there was a step-wise change in the curve of IR drop vs. applied current. This irregularity is believed to be due to changes in the effective electrode area, often due to the deterioration of the electrode surface caused by a heavy current.

The Butler-Volmer equation with $n = 2$, $\beta = 0.5$, implies that at this electrode, the rate limiting process is the exchange charge process, which can be represented by

$$O^{=} \rightleftarrows O + 2e$$

The plot of cathodic overpotential η_a vs. logarithm of applied current I at pure oxygen or dry air atmosphere, also

can be fitted with the Butler-Volmer equation with $\beta = 0.5$, $n = 2$. It is thus also consistent with the idea of an exchange charge process. When the partial pressure of oxygen is decreased further, however, the data deviate from the Tafel plot and, depending on the partial pressure, a limiting current is reached at different cathodic overpotential ranges. Using the idea that the transport of oxygen from the gas atmosphere through the cathode is slow, and combining the diffusion and exchange charge processes, the equation

$$I = \frac{\exp(-\frac{ne\beta\eta_c}{kT}) - \exp(\frac{ne(1-\beta)\eta_c}{kT})}{I_o^{-1} + (I_c^{\ell})^{-1} \exp(-\frac{ne\beta\eta_c}{kT})}$$

is derived (5), where I_c^{ℓ} is the cathodic limiting current.

By choosing an appropriate value of I_c^{ℓ}, it was found that the data could be fitted to this equation, again with $n = 2$ and $\beta = 0.5$. In this way the temperature and oxygen partial pressure dependence of I_c^{ℓ} could be obtained. When the cathodic overpotential was increased beyond the limiting current range, it was found that the current rises again. This effect is illustrated in Fig. 3, which shows typical cathodic overpotential curves. This last region gives a slope of 2.3 kT/e in the plot of η_c vs. log I. At the same time, the electrolyte resistance, obtained from the plot of the IR drop vs. I, decreases as the current increases. This suggests the onset of electronic conduction through reduction of the electrolyte. Furthermore, we found that the range of cathodic overpotential at which the current starts to turn up depends strikingly on the thickness of the electrolyte, in support of this hypothesis (6). Finally, the electronic transference number deduced from the plot of η_c vs. log I falls into the same range of values as obtained from independent sources (3,7). See Fig. 4.

In conclusion, we have found that, in contrast to the confusion in the literature pertaining to previous polarization studies (mainly on stabilized zirconias), the present work using doped ceria and the current interruption method shows that the polarization phenomena can be interpreted in a relatively simple and straightforward way. In particular, the present data provide perhaps the clearest demonstration to date of the charge transfer process both in the anodic polarization and in the cathodic case for high p_{O_2}.

Acknowledgment: This work is being supported by the National Science Foundation under grants NSF-DMR74-23877 and DMR76-80157.

REFERENCES

1. D.O. Raleigh, Adv. Electroanal. Chem., Vol. 6, (Ed., A. Bard), Dekker, New York 1973.

2. T. Kudo and H. Obayashi, J. Electrochem. Soc., Vol. 122, No. 1, p. 142, 1975.

3. H.L. Tuller and A.S. Nowick, J. Electrochem. Soc., Vol. 122, No. 2, p. 255, 1975.

4. J.O.M. Bockris and A.K.N. Reddy, Modern Electrochemistry, Vol. II, Chapter 9, Plenum Press, New York 1970.

5. T.N. Anderson and H. Eyring, in Physical Chemistry: An Advanced Treatise, Vol. IXA, (Ed. H. Eyring), Academic Press, New York 1970, Chapter 3.

6. R.J. Brook, W.L. Pelzmann and F.A. Kröger, J. Electrochem. Soc., Vol. 118, No. 2, p. 185, 1971.

7. R.N. Blumenthal, F.S. Brugner and J.E. Garnier, J. Electrochem. Soc., Vol. 120, No. 9, p. 1230, 1973.

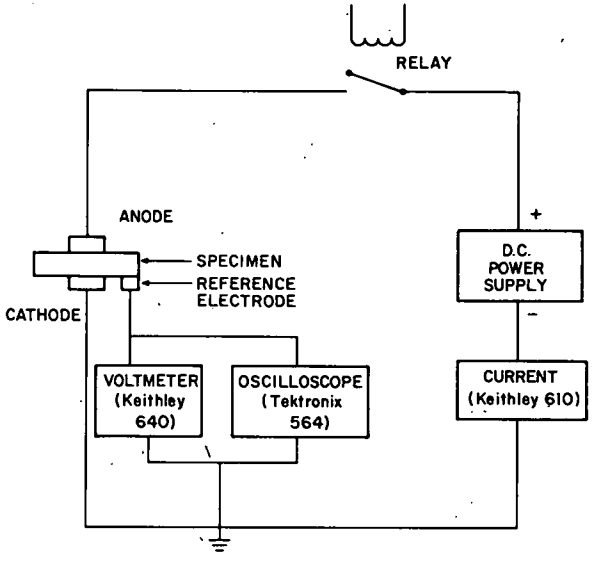

Figure 1. Schematic diagram of current interruption apparatus, arranged to measure cathodic polarization.

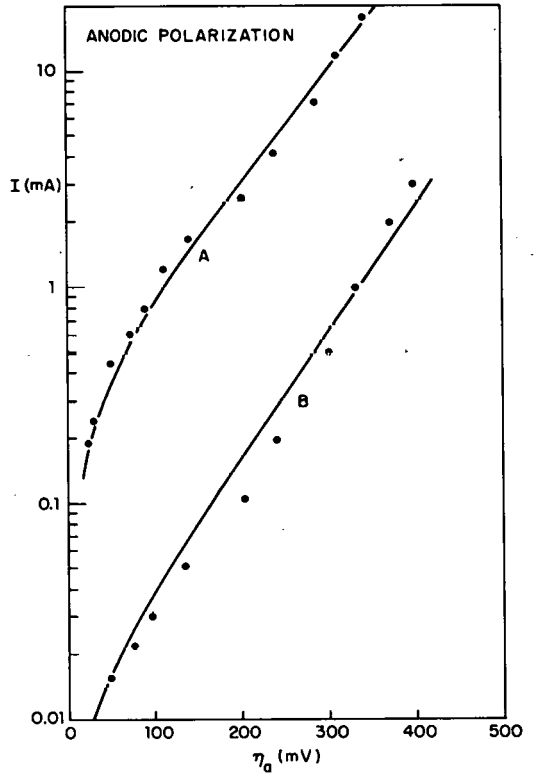

Figure 2. Typical anodic polarization curves. Curve A is for a CeO_2 + 8% CaO electrolyte, run at 700°C and in an 0.012% O_2-argon mixture; curve B is for CeO_2 + 6% CaO, at 600°C and an 0.92% O_2-Ar mixture.

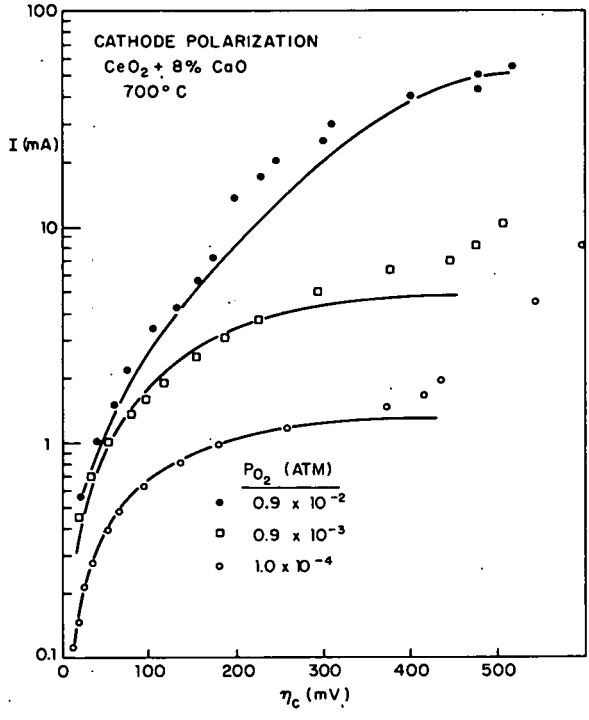

Figure 3. Typical cathodic polarization curves at three different oxygen partial pressures.

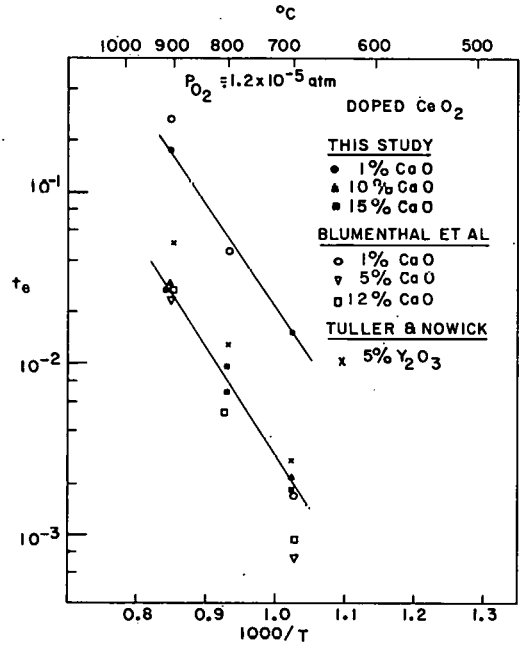

Figure 4. Comparison of data for electronic transference number, t_e, as obtained from analysis of cathodic polarization curves for three different CeO_2:CaO compositions, with values determined by direct methods by previous workers.

COMPLEX IMPEDANCE MEASUREMENTS OF Y^{3+} DOPED CeO_2

K. F. Young and A. D. Franklin
National Bureau of Standards
Washington, D. C. 20234

We are developing electrical measuring techniques to determine the long-term stability of oxygen-transporting solid electrolyte-electrode systems at high temperatures. This should make it possible to elucidate the mechanism producing whatever degradation occurs in bulk transport properties and in electrode-electrolyte interfaces. The complex impedance can be used, as shown by Bauerle [1], to obtain information about the intrinsic conductivity of the electrolyte, the influence of impurities on the grain boundaries and the rate of electron ion transfer at the electrodes. We are using a network analyzer system to make these kinds of measurements on Y^{3+} doped CeO_2.

Using a network analyzer system provides an extended frequency range and rapid measurement as compared to the time honored technique of using an a.c. impedance bridge. A network analyzer sacrifices some resolution in the mid range of frequencies (1 kHz to 20 kHz), however, the extension of the low frequency limit to 10 Hz and the high frequency limit to 13 MHz plus its faster operation make it far more useful in sorting out multiple relaxation processes and other related phenomena. We presently operate a network analyzer system in a semiautomatic mode and data collection is about 5 to 10 times faster than using an a.c. bridge. We have developed computer programs using least squares fitting techniques for our data analysis.

When a network analyzer is operated in an insertion loss mode, as we use it, then its operation bears some resemblance to an a.c. bridge measurement technique. Fig. (1) shows schematically the circuit we use to measure an unknown complex impedance Z*. It was drawn in such a way as to show its resemblance to an a.c. bridge. The most fundamental difference is that a bridge is adjusted to a null output for each desired frequency and a network analyzer just compares V_A* with V_B* and gives the result directly. From the circuit shown in Fig (1) Z^*_B can be written as:

$$Z^* = 100 \left[\frac{V_A^*}{V_B^*} - i \right]$$

where V_A* and V_B* are complex voltages. Since the voltages vary sinusoidally then they can be expressed as:

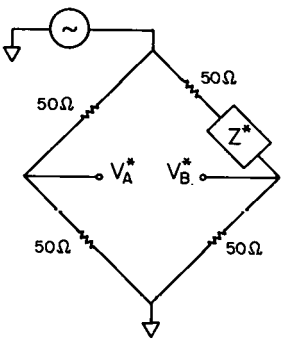

Figure 1. Schematic diagram of measuring circuit for a network analyzer.

$$V_A^* = V_A e^{j\omega t}$$

$$V_B^* = V_B e^{j(\omega t - \phi)}$$

where ω = frequency, t = time and ϕ = phase shift between V_A^* and V_B^*. The unknown Z^* then becomes

$$Z^* = 100 \left[\frac{V_A}{V_B} e^{j\phi} - 1 \right]$$

The output of the network analyzer operating over a frequency range of 10 Hz to 13 MHz is the voltage ratio V_A/V_B and the phase shift ϕ. For our purposes, V_A/V_B can be considered as the amount of attenuation by the unknown loss which has been inserted, and ϕ is the amount of capacitive phase shift introduced by the unknown.

Impedance measurements have been made for several sputtered Pt electroded specimens of yttria doped ceria up to 800°C in both O_2 and N_2 atmospheres. Figure 2 illustrates reasonably typical data, the main features of which can be summarized as follows:

High Temperature-Low Frequency

At high temperature and low frequency a well-defined relaxation occurs, visible on the right side of the plots in Fig. 2. This relaxation is rather sensitive to the atmosphere, and is at least tentatively ascribed to reactions at the electrodes. Our high temperature low frequency data appears to require two parallel conducting paths. On the right hand side of Fig. 3 is presented an equivalent circuit capable of representing the data, in which R_d represents a simple charge carrier exchange with an infinite reservoir, such as oxygen ions with the atmosphere or electrons with the Fermi sea of the Pt electrodes. -W- is a Warburg impedance, representing perhaps the diffusion of reaction products into and out of a reservoir, as for instance atomic or molecular oxygen in Pt.

The Warburg impedance can be written

$$Z_w^* = \sigma(1-j)\omega^{-\frac{1}{2}}$$

where σ is an intensity constant, $j = \sqrt{-1}$, and ω is the circular frequency. The impedance at low frequencies of the equivalent circuit shown in Fig. 3 is given by:

$$Z_{el}^* = \frac{R_d}{1+ (j\omega\tau_e)^{\frac{1}{2}}}$$

where

$$\tau_e = 1/2 \left(\frac{Rd}{\sigma}\right)^2$$

This equation is of the form given by Cole and Cole (2) and describes a semi-circular arc with its center depressed below the real axis, such that the angle subtended by the real axis and a line connecting the center of the arc with its left intercept on the real axis is $(\pi/4)$. R_d is the distance between the intercepts along the real axis, and τ_e is the time

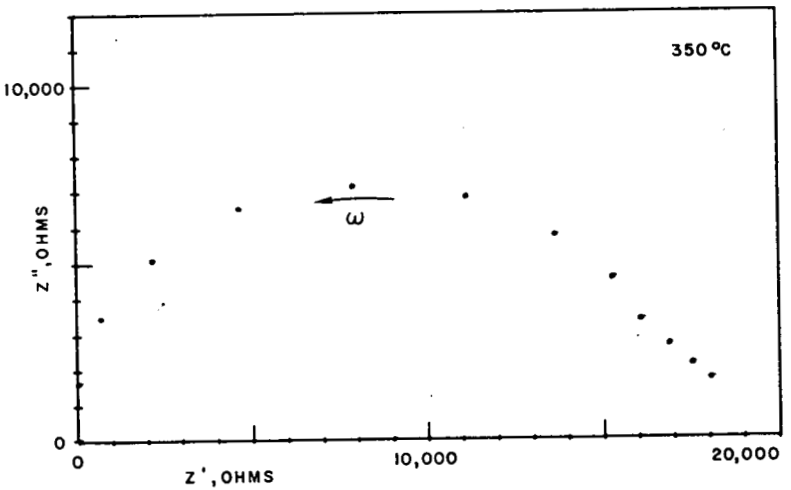

Figure 2a.

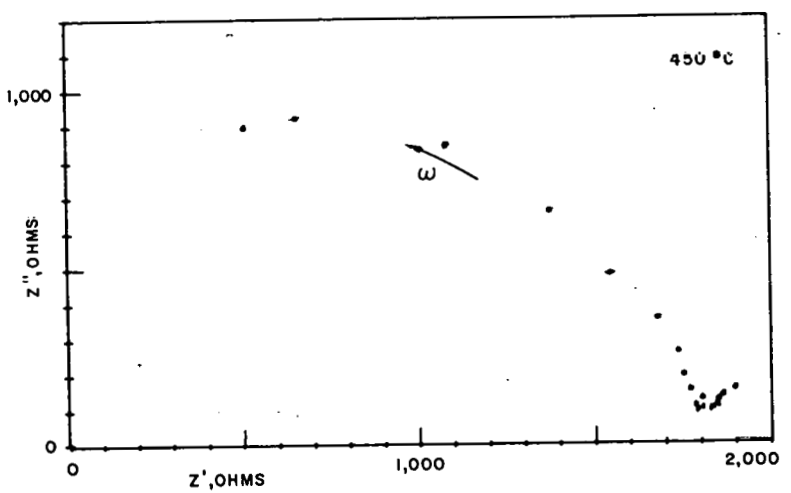

Figure 2b.

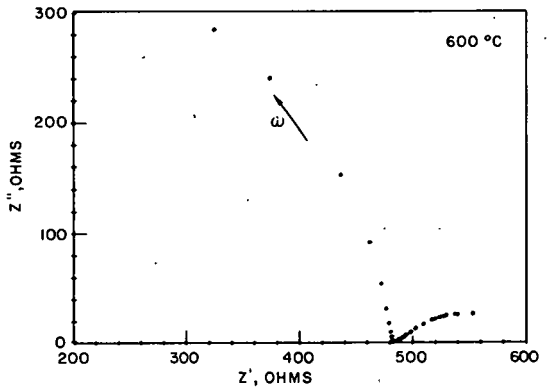

Figure 2c.

Figure 2. Complex impedance of Y^{3+} doped CeO_2 specimen measured over the same frequency range, 10 Hz to 13 MHz, at three different temperatures, a) 350°C, b) 450°C, c) 600°C.

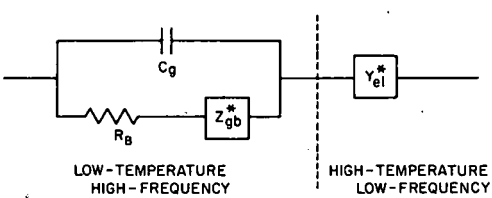

Figure 3. Equivalent circuit capable of representing our complex impedance measurements. C_g = geometric capacitance of the specimen, R_B = bulk resistance, Z^*_{gb} = complex impedance of the distribution of grain boundaries, Z^*_{el} = complex impedance of the electrode processes.

constant for this process. In Fig. 4 the partially sketched arc has been obtained by fitting eqn. (1) to the appropriate data by a least squares technique. The agreement between data and eqns are excellent, thus providing a mathematical framework for more intensive study of the electrode processes.

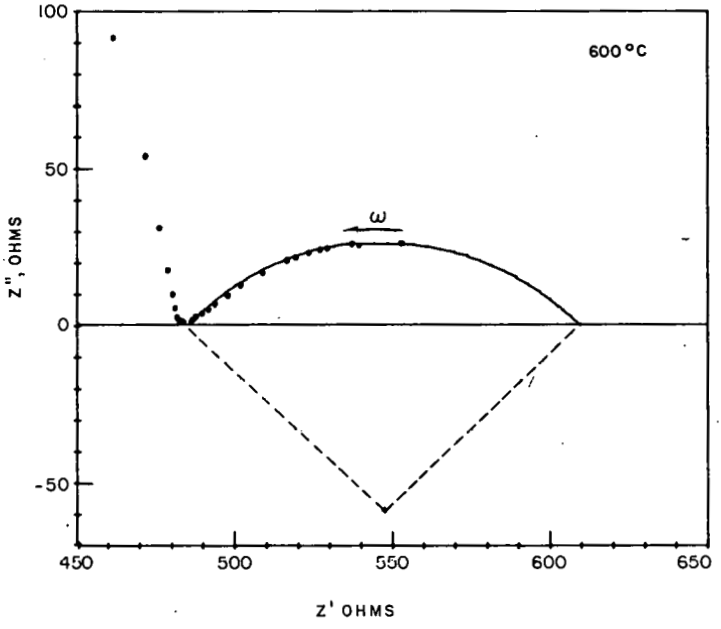

Figure 4. Complex impedance of yttria doped CeO_2 specimen measured from 10 Hz to 12 MHz at 600°C (enlargement of Figure 2C). The arc shown is calculated using eqn.(2) of text and least-squares fit.

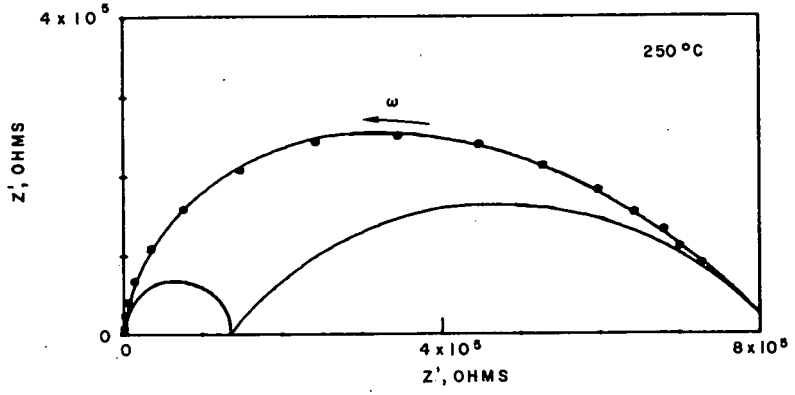

Figure 5. Complex impedance of Y^{3+} doped CeO_2 measured at 250°C. The right hand arc was least-squares fitted using eqn.(2) and the left hand arc is due to R_B and C_g. These two arcs are summed according to the equivalent circuit (Figure 3) and the result is the third curve which passes through the data points.

Low Temperature - High Frequency

In our available frequency range (10 Hz - 13 MHz) and at temperatures below about 450°C a response is seen which appears to be compounded of several relaxations. The equivalent circuit of the left side of Fig. 3 can be made to fit the experimental data if the grain boundary impedance, Z^*_{gb}, is given by

$$Z^*_{gb} = \frac{\Delta Z}{1 + (j\omega\tau)^n}$$

This equation corresponds to a distribution of relaxation times given by Cole and Cole (2) where ΔZ is the separation between intercepts along the real axis and n is a measure of how far the arc is depressed below the real axis ($\frac{1}{2} < n < 1$). Figure 5 shows the complex impedance of yttria doped ceria measured at 250°C. The arcs drawn represent eqn (2) on the right hand (low-frequency) side, and therefore the "grain-boundary" effect, and the simple parallel R_B-C_g network on the left, at high frequencies.

The "grain-boundary" effect appears large ($\Delta Z > R_B$) probably because the specimen is quite porous and it is really the pores that control the effect here. The internal resistance of the grains is represented by R_B. Estimation of its value depends heavily on the goodness of fit to the "grain-boundary" effect. A 4-probe measurement would produce a value for $(R_B + \Delta Z)$, which in this case would be useless as an estimate of the resistance to be assigned to the material itself.

Here again, a mathematical framework for separating and studying the responses of various parts of the electrolyte-electrode system appears now to be available. We are carrying out further experiments to confirm the assignment of the various parameters in Fig. 3 to physical processes. Then, using this complex impedance measuring technique we will begin long-term stability experiments on high temperature solid electrolyte-electrode systems.

References

1. J. E. Bauerle, J. Phys. Chem. Solids, 30, 2657 (1969).

2. K. S. Cole and R. H. Cole, J. Chem. Phys. 10, 98 (1942).

APPENDICES

1. Workshop Agenda

2. List of Participants

3. Letter of Invitation

4. Information Letter of June 10, 1977 with attachment - "Thermal Efficiency of Solid Electrolyte Fuel Cells with Mixed Conduction,"* P. N. Ross and T. J. Benjamin, United Technologies Corporation

---

*Paper distributed to participants after Workshop.

WORKSHOP ON "HIGH TEMPERATURE SOLID OXIDE FUEL CELLS"*

May 5-6, 1977

Hamilton Seminar Room, Chemistry Building
Brookhaven National Laboratory
Upton, N. Y. 11973

Thursday, May 5, 1977

a.m.

Chairman - H. S. Isaacs

9:00 Welcoming Remarks - F. J. Salzano, BNL

9:10 DOE Overview of Solid State Fuel Cell Technology - I. L. Harry, DOE

Chairman - I. L. Harry

9:30 Discussion of Potential of High Temperature Solid Oxide Fuel Cell Powerplant Systems - M. Warshay, NASA-Lewis

9:50 Interconnection Materials for the Thin Layer Zirconia Electrolyte Fuel Cell - R. J. Ruka, Westinghouse

10:10 Compositional Dependence of Thermal Expansion, Lattice Parameters, Volatilization Rate and Electrical Conductivity of $LaCrO_3$ Based Oxides - H. U. Anderson R. Murphy, A. K. Fox, University of Missouri, B. Rossing, Westinghouse, A. Aldred, ANL

10:30 Intermission

10:45 Studies on Glass Composites and Doped Rutile as Interconnection Materials - P. G. Russell, H. S. Isaacs, S. Srinivasan, BNL, A. C. C. Tseung, The City University (London)

11:05 Highly Conducting Oxide Materials - P. E. D. Morgan, University of Pittsburgh

11:25 Optimized Electrolytic Domain Boundaries in Solid Electrolytes - H. L. Tuller, MIT

*Sponsored by the U.S. Department of Energy and Brookhaven National Laboratory

Thursday, May 5, 1977
(Cont'd)

p.m.

12:05	Fundamental Factors that Might Limit the Application of ZrO_2 Solid Electrolytes in Fuel Cells: Electronic Transport, Electrolyte-Electrode Reactions, and Electrolyte Decomposition - W. Weppner, Stanford University
12:25	Phase Relationships and Ordering in ZrO_2-CaO and ZrO_2-Y_2O_3 Systems - S. P. Ray, V. S. Stubican, Pennsylvania State University
12:45	Lunch
	Chairman - S. Srinivasan
2:00	High Temperature Solid Oxide Fuel Cells Present State and Problems of Development - F. J. Rohr, Brown, Boveri & Cie AG (Heidelberg)
2:20	A Thin Solid Film Fuel Cell Approach - M. Croset, P. Schnell, G. Valasco, Thomson-CSF, J. Siejka, Université Paris
2:40	Transport Considerations in Oxygen Electrodes of the Triphase Boundary Type for Zirconia Cells - E. Bergmann, Battelle Memorial Institute (Geneva)
3:00	An AC Technique for Characterizing Solid Oxide Fuel Cells - H. S. Isaacs, L. J. Olmer, BNL
3:20	Intermission
3:35	Electrocatalysis of Coal Gas Compounds on Solid Oxide Electrolytes - D. M. Mason, C. J. Wen, Stanford University
3:55	Cathodic and Anodic Polarization Phenomena at Platinum Electrodes Using Doped Cerica as Electrolyte - D. Y. Wang, A. S. Nowick, Columbia University
4:15	Complex Impedance Measurements of Y^{3+} Doped CeO_2 - K. F. Young, A. D. Franklin, NBS
4:35	Session Ends
6:00	Cocktail Hour at Brookhaven Center
7:00	Dinner at Brookhaven Center

Friday, May 6, 1977

a.m.

8:30 Panel Discussion on "ELECTROLYTES"

Panel: A. S. Nowick - Columbia University (Chairman)
M. Anderson - Columbia University
J. W. Patterson - Iowa State University
R. A. Rapp - Ohio State University
S. P. Ray - Pennsylvania State University

10:45 Intermission

11:00 Panel Discussion on "INTERCONNECTION MATERIALS"

Panel: G. P. Wirtz - University of Illinois (Chairman)
H. U. Anderson - University of Missouri
P. E. D. Morgan - University of Pittsburgh
R. J. Ruka - Westinghouse

p.m.

12:30 Lunch

1:30 Panel Discussion on "ELECTRODES"

Panel: T. S. Etsell - University of Alberta (Chairman)
W. L. Worrell - University of Pennsylvania
P. J. Meschter - University of Tennessee

2:15 Summaries and Recommendations by Panel Chairmen

3:30 Concluding Remarks - I. L. Harry, DOE

3:45 Workshop Ends

WORKSHOP ON "HIGH TEMPERATURE SOLID OXIDE FUEL CELLS"

May 5-6, 1977

LIST OF PARTICIPANTS

Prof. H. U. Anderson
Dept. of Ceramic Engineering
Univ. of Missouri-Rolla
107 Fulton Hall
Rolla, Missouri 65401

Mr. M. Anderson
Columbia University
1144 Seeley W. Mudd Bldg.
New York, New York 10027

Dr. J. Appleby
Laboratories de Marcoussis
C.G.E.
91, Marcoussis
France

Dr. J. Bauerle
Westinghouse R&D Center
Beulah Road
Pittsburgh, Pennsylvania 15235

Dr. E. Bergmann
Battelle Memorial Institute
Geneva Research Center
1227 Carouge-Geneva
Switzerland

Mr. K. Blurton
Institute of Gas Technology
3424 South State Street
ITT Center
Chicago, Illinois 60616

Dr. G. M. Brown
Dept. of Chemistry
Brookhaven National Laboratory
Upton, New York 11973

Dr. W. D. Clark
Dept. of Chemistry
Brookhaven National Laboratory
Upton, New York 11973

Dr. D. E. Cox
Dept. of Physics
Brookhaven National Laboratory
Upton, New York 11973

Dr. M. Croset
Thomson-CSF
Domaine de Corbeville
91401 Orsay
France

Mr. C. Davidson
Dept. of Materials Science
Univ. of Virginia
Charlottsville, Virginia 22901

Dr. G. J. Dienes
Dept. of Physics
Brookhaven National Laboratory
Upton, New York 11973

Dr. A. Dragoo
National Bureau of Standards
Washington, D.C. 20234

List of Participants (Cont'd)

Prof. T. Etsell
Dept. of Mineral Engineering
Univ. of Alberta
Edmonton, Alberta
Canada T6G 2G6

Dr. W. Feduska
Westinghouse R&D Center
Beulah Road
Pittsburgh, Pennsylvania 15235

Mr. A. Fickett
Electric Power Research Inst.
3412 Hillview Avenue
P. O. Box 10412
Palo Alto, California 94304

Mr. J. Griffith
Columbia University
1144 Seeley W. Mudd Bldg.
New York, New York 10027

Mr. I. L. Harry
Division of Power Systems
U.S. Department of Energy
Washington, D.C. 20545

Dr. H. S. Isaacs
Dept. of Energy and Environment
Brookhaven National Laboratory
Upton, New York 11973

Dr. A. Isenberg
Westinghouse R&D Center
Beulah Road
Pittsburgh, Pennsylvania 15235

Dr. M. W. Kendig
Dept. of Energy and Environment
Brookhaven National Laboratory
Upton, New York 11973

Dr. H. Kunz
Power Systems Division
United Technologies
P. O. Box 109
So. Windsor, Connecticut 06074

Ms. J. Lannen
Columbia University
1144 Seeley W. Mudd Bldg.
New York, New York 10027

Dr. L. R. Lawrence, Jr.
Gas Research Institute
3424 So. State Street
Chicago, Illinois 60616

Dr. H. Maru
Institute of Gas Technology
3424 So. State Street
ITT Center
Chicago, Illinois 60616

Prof. D. Mason
Dept. of Chemical Engineering
Stanford University
Stanford, California 94305

Dr. P. Meschter
Dept. of Chem. & Met. Eng.
Univ. of Tennessee
Knoxville, Tennessee 37916

Dr. P. Morgan
Dept. of Met. & Mat. Science
Univ. of Pittsburgh
Pittsburgh, Pennsylvania 15261

Prof. A. Nowick
Columbia University
1144 Seeley W. Mudd Bldg.
New York, New York 10027

Mr. L. J. Olmer
Dept. of Energy and Environment
Brookhaven National Laboratory
Upton, New York 11973

Dr. D. Park
General Electric Company
Research & Development Center
Schenectady, New York 12308

List of Participants (Cont'd)

Prof. J. Patterson
Mat. Sci. & Eng. Department
Iowa State University
110 Engineering Annex
Ames, Iowa 50011

Prof. R. Rapp
Dept. of Met. Engineering
Ohio State University
Columbus, Ohio 43210

Prof. S. Ray
Dept. of Materials Sciences
Pennsylvania State University
201 Mineral Industries Bldg.
University Park, Pennsylvania 16802

Dr. F. J. Rohr
Brown, Boveri & Cie AG
Heidelberg, W. Germany

Dr. R. Ruka
Westinghouse R&D Center
Beulah Road
Pittsburgh, Pennsylvania 15235

Dr. P. G. Russell
Dept. of Energy and Environment
Brookhaven National Laboratory
Upton, New York 11973

Mr. F. J. Salzano
Dept. of Energy and Environment
Brookhaven National Laboratory
Upton, New York 11973

Dr. R. Schmidberger
Dornier System GmbH
799 Friedrichshafen
Postfach 1360
West Germany

Prof. L. Seigle
Dept. of Materials Science
State Univ. of New York at Stony Brook
Stony Brook, New York 11794

Dr. J. Siejka
Group de Physique des Solides
Universite Paris VII, Tour 23
2, Place Jussieu 75005
Paris, France

Dr. S. Srinivasan
Dept. of Energy and Environment
Brookhaven National Laboratory
Upton, New York 11973

Prof. S. Stubican
Dept. of Material Sciences
Pennsylvania State University
201 Mineral Industries Bldg.
University Park, Pennsylvania 16802

Dr. A. Tseung
Dept. of Chemistry
The City University
St. John Street, E.C.I.
London, England

Prof. H. Tuller
Dept. of Mat. Sci. & Eng.
Massachusetts Institute of Technology
Cambridge, Massachusetts 02139

Dr. G. Velasco
Thomson-CSF
Domaine de Corbeville
91401 Orsay
France

List of Participants (Cont'd)

Dr. B. Vyas
Dept. of Energy and Environment
Brookhaven National Laboratory
Upton, New York 11973

Mr. D. Wang
Columbia University
1144 Seeley W. Mudd Bldg.
New York, New York 10027

Prof. F. Wang
Dept. of Materials Science
State University of New York at
Stony Brook
Stony Brook, New York 11794

Dr. M. Warshay
Electrochemical Systems Section
NASA-Lewis Research Center
Cleveland, Ohio 44135

Dr. D. O. Welch
Dept. of Energy and Environment
Brookhaven National Laboratory
Upton, New York 11973

Prof. W. Weppner
Dept. of Mat. Sci. & Eng.
Stanford University
Stanford, California 94305

Dr. G. Wirtz
Dept. of Ceramic Engineering
Univ. of Illinois
204 Ceramics Bldg.
Urbana, Illinois 61801

Dr. L. Yannopoulos
Westinghouse R&D Center
Beulah Road
Pittsburgh, Pennsylvania 15235

Dr. R. S. Yeo
Dept. of Energy and Environment
Brookhaven National Laboratory
Upton, New York 11973

Dr. K. Young
National Bureau of Standards
Washington, D.C. 20234

Dr. G. Youngblood
Montana Energy & MHD R&D
Institute, Inc.
P. O. Box 3809
Butte, Montana 59701

BROOKHAVEN NATIONAL LABORATORY
ASSOCIATED UNIVERSITIES, INC., UPTON, L.I., N.Y. 11973

DEPARTMENT OF APPLIED SCIENCE

TELEPHONE: (516) 345-4078

Dear

A Workshop on High Temperature Solid Oxide Fuel Cells has been planned for May 5 and 6, 1977, at Brookhaven National Laboratory at the request of the Division of Conservation Research and Technology, Energy Research and Development Administration. Please consider this letter as an invitation to you or your organization to attend this Workshop.

The purpose of the Workshop will be: (i) determine the present knowledge of factors limiting materials and processes taking place in this energy conversion system and (ii) the direction in which future R&D should be directed.

Contributions for presentations are requested and should be related to areas considered relevant to the development of solid oxide fuel cells. In order to maximize the opportunity for discussion, participants who wish to contribute to the discussion should submit an extended abstract or summary (less than 2000 words) of their presentation for distribution prior to the meeting. In addition, copies of visual aids presented during the Workshop should also be made available either prior to or during the meeting.

The tentative plans are to have presentations on the first day. This will be followed by panels on the second day, which will be headed by a chairman, to assess the areas of:

a. Electrolytes
b. Electrodes
c. Interconnector materials

The objectives of the panels will be to: (i) summarize present status of
lerstanding and problem areas; (ii) develop recommendations for future research
l development; (iii) establish any need for future activities or meetings;
...d (iv) provide a written summary of their conclusions. It is also intended to publish the proceedings of the Workshop. This report will include all relevant material presented and developed at the Workshop including extended abstracts, visual aids, and the conclusions of each panel.

INFORMATION OPERATOR (516) 345-2123

The following schedule has been set up:

a. We would like to be informed, as early as possible and preferably before March 6, if you will be attending the Workshop and whether you wish to contribute any formal presentation.

b. The extended abstracts of these presentations should be received by April 6 to allow sufficient time for their distribution prior to the meeting.

c. A final agenda, along with travel and accommodation details, will be sent out in mid-April at the same time as the extended abstracts.

If there are any suggestions or questions you may have regarding the Workshop, please contact me or Dr. S. Srinivasan.

Sincerely yours,

Hugh S. Isaacs

dva
Phone Numbers:

H. S. Isaacs -- (516) 345-4078
S. Srinivasan -- (516) 345-4494

BROOKHAVEN NATIONAL LABORATORY
ASSOCIATED UNIVERSITIES, INC.
Upton, New York 11973

Department of Applied Science (516) 345- 4078

June 10, 1977

Dear Participant:

At the request of Mr. I. Leslie Harry, we are sending you herewith a paper entitled "Thermal Efficiency of Solid Electrolyte Fuel Cells with Mixed Conduction", by P. Ross, Jr. and T. J. Benjamin of United Technologies Corporation. This paper will be published in the Journal of Power Sources. You may remember that Mr. Arnold P. Fickett referred to this paper during a discussion session at the Workshop on "High Temperature Solid Oxide Fuel Cells", to demonstrate the effect of low amounts of electronic conductivity of the electrolyte on fuel cell performance.

With best wishes,

Sincerely yours,

H. S. Isaacs

S. Srinivasan

dva
cc.: I. L. Harry, ERDA
A. P. Fickett, EPRI
attachment

THERMAL EFFICIENCY OF SOLID ELECTROLYTE FUEL CELLS WITH MIXED CONDUCTION

P. N. Ross, Jr.† and T. J. Benjamin
Power Systems Division
United Technologies Corporation
South Windsor, Connecticut 06074

Summary

The effect of mixed anionic and n-type electronic conduction in solid electrolytes on the thermal efficiency of a fuel cell system was analyzed quantitatively. The mixed conduction observed when electrolytes based on ceria are used in H_2/air fuel cell applications lowers the maximum attainable cell thermal efficiency to below 40%. Neither the zirconia nor the ceria based solid oxide electrolytes studied to date can be used in a low temperature (700°C) system that meets simultaneously the requirements on power density and thermal efficiency for electric utility power plants. The material properties required for an advanced fuel cell power plant solid electrolyte were derived in terms of the ionic conductivity and the Schmalzried parameters $P_{\oplus}$ and $P_{\ominus}$: $\sigma_{ion} > 0.033\ (\Omega\ cm)^{-1}$, $P_{\oplus} > 10^{3}$ atm., $P_{\ominus} < 10^{-23}$ atm. at 700°C.

Introduction

Many solid oxide systems have been considered for application as oxide ion conducting electrolytes in high temperature fuel cells. Solid electrolytes of the doped zirconia type have been shown to be suitable for certain fuel cell applications[1-3]. They are purely ionic conductors over wide ranges of temperature and oxygen partial pressures but high temperature (~900°C) are required to obtain useful conductivities and the high temperatures severely limit the materials which can be used in fuel cell fabrication. The doped cerium oxides have been shown to exhibit high ionic conductivities at lower temperatures (700°C). However, recent studies[4-6] have reported that doped cerias are reduced in low oxygen partial pressure atmospheres such as at the fuel cell

† to whom correspondence should be addressed. Present address: United Technologies Research Center, Silver Lane, East Hartford, CT 06108.

anode and significant electronic (n-type) conduction may result when doped cerias are used as fuel cell electrolytes. One of the consequences of mixed conduction is consumption of fuel even at zero total current to compensate for the current drain by electronic conduction, i.e. the cell efficiency will be reduced. The deleterious effect of mixed (ionic and electronic) conduction on the thermal efficiency of a fuel cell system has not been determined quantitatively for any of the ceria electrolytes. Calculation of thermal efficiency will determine whether any of the doped-cerias studied to date will meet the Electric Power Research Institute (EPRI) heat rate for advanced power plants, 7500 Btu/kwh[7] or an overall system thermal efficiency of 45.5%. The thermal efficiency defined by the power generation industry is the ratio of the power delivered to the standard enthalpy of combustion of the fuel and should be distinguished from the efficiency used by electrochemists which is the voltage efficiency, usually defined as the ratio of the power delivered to the total available Gibbs free energy in the fuel.

In the present work, we report the calculations of the performances and thermal efficiencies of ceria-based solid electrolytes and determine their potential as electrolytes for advanced fuel cell power plants. The theory of mixed conduction is also used to establish the properties which a solid electrolyte must possess in order to meet the EPRI systems thermal efficiency. Following the analysis used by Patterson[8] we have chosen to characterize these material properties by the parameters introduced by Schmalzried[9], $P_{\oplus}$, the O_2 partial pressure at which the p-type electronic conductivity equals the ionic conductivity, and $P_{\ominus}$, the O_2 partial pressure at which the n-type electronic conductivity equals the ionic conductivity.

Theory

The reduction of solid electrolytes results in the generation of excess electrons by

$$O^{=} = \frac{1}{2} O_2 (g) + V_O^{=} + 2e^{-} \qquad (1)$$

The electrons created by cation reduction are easily promoted to the conduction band and electronic conduction results. The solid electrolyte can be written as an equivalent circuit as shown in Figure 1. Wagner's theory of mixed conduction[10] can be used to derive equations which describe the voltage, current,

power and efficiency characteristics of the cell shown in Figure 1. For the purposes of this study, only losses within the electrolyte will be considered. Therefore, the anode and cathode will be assumed reversible. Also, the terminal voltage, V_T, is assumed to be equal to the difference in the electrochemical potential of the electrons at the cathode (η_3'') and at the anode (η_3').

$$FV_T = \eta_3'' - \eta_3' \tag{2}$$

In Wagner's general theory, the local charge flux of species i is

$$I_i = -A\,(\sigma_i/Z_iF)\,\nabla\eta_i \;;\; i = 1, 2, 3 \tag{3}$$

where σ_i is the partial conductivity, Z_i is the valence, and $\nabla\eta_i$ is the electrochemical potential gradient of i. In order to obtain η_1 (cations) and η_2 (anions), which are not experimentally measurable, in terms of η_3 (electrons) and μ_{O_2}, the chemical potential of molecular oxygen in the gas phase, further assumptions must be made. Local equilibrium is assumed between neutral atoms, ions, and electrons. Virtual stoichiometry is assumed and the Gibbs-Duhem relation between neutral metal atoms and oxygen anions in the electrolyte is applied. Under these conditions, equation (3) reduced to

$$I_{ion} = -A\,\sigma_{ion}\,(\nabla\mu_{O_2}/2\,Z_2F + \nabla\eta_3/Z_3F) \tag{4}$$

where

$$I_{ion} = I_1 + I_2 \text{ and } \sigma_{ion} = \sigma_1 + \sigma_2 \,.$$

Also,

$$I_e = I_3 = -A\,\sigma_3\,\nabla\eta_3/Z_3F \,. \tag{5}$$

The system is further assumed to be at steady state so that all currents are independent of location in the electrolyte. Following Choudury and Patterson[11], we define a current parameter, r, also independent of location in the electrolyte,

$$r \equiv I_{ion}/I_e \tag{6}$$

At fixed values of μ_{O_2}'', μ_{O_2}', each value of r defines an unique set of V_T and I_{ext}. With the assumptions of steady state and only electrolyte polarization, expressions for V_T and I_{ext} can be written in terms of r, the conductivities, and the chemical potentials. Combining equations (2), (4), (5), (6) with $Z_3 = -1$ results in

$$V_T = \int_{\mu'_{O_2}}^{\mu''_{O_2}} \frac{\sigma_{ion}}{r\,\sigma_3 - \sigma_{ion}} \frac{d\mu_{O_2}}{2Z_2F} \qquad (7)$$

The external current I_{ext} is simply the sum of I_{ion} and I_e, so equations (4), (5), and (6) are used to obtain

$$I_{ext} = \frac{-A}{t} \int_{\mu'_{O_2}}^{\mu''_{O_2}} \frac{[1 + r]\,\sigma_{ion}\,\sigma_3}{(r\,\sigma_3 - \sigma_{ion})} \frac{d\mu_{O_2}}{2Z_2F} \qquad (8)$$

where t is the electrolyte thickness. Equations (7) and (8) have analytical solutions if σ_{ion} and σ_3 are written in terms of μ_{O_2}. For an ideal gas, the chemical potential is related to the partial pressure by

$$\mu_{O_2} = RT \ln P_{O_2} \qquad (9)$$

For a mixed conductor exhibiting only excess electronic conduction and no hole conduction, the ionic and electronic conductivities are related by

$$\sigma_{ion} = \sigma_3 \,(P_{O_2}/P_\theta)^{1/4} \qquad (10)$$

where P_θ is the Schmalzried parameter for electronic conduction and corresponds to the oxygen partial pressure at which the ionic transference number, t_i, is equal to one-half, where

$$t_i = \frac{\sigma_{ion}}{\sigma_{ion} + \sigma_3} \qquad (11)$$

Substitution of equations (9) and (10) into equations (7) and (8) allow integration of V_T and I_{ext}. The final results are

$$V_T = \frac{2RT}{Z_2F} \ln\left[\frac{r - (P'_{O_2}/P_\theta)^{1/4}}{r - (P''_{O_2}/P_\theta)^{1/4}}\right] \qquad (12)$$

and

$$I_{ext} = -\sigma_{ion}\left(\frac{A}{t}\right)(V_T - E_{th}) \qquad (13)$$

where E_{th} is the theoretical open circuit potential in the absence of mixed conduction

$$E_{th} = \frac{RT}{2Z_2F} \ln \frac{P'_{O_2}}{P_{O_2}}$$

The fuel cell power, P, is simply the product of the voltage and the current.

$$P = (V_T)\ (I_{ext}) \tag{15}$$

The voltage efficiency, (η_V), is based on the total Gibbs free energy of the fuel, equivalent to I_{ion} times E_{th}. Therefore,

$$\eta_V = \frac{(V_T)\ (I_{ext})}{(E_{th})\ (I_{ion})} = \left(\frac{V_T}{E_{th}}\right)\left(\frac{r+1}{r}\right) \tag{16}$$

The thermal efficiency, (η_T), of the cell is based on the standard enthalpy of combustion of the fuel

$$\eta_T = \frac{(V_T)\ (I_{ext})}{\Delta H^o \text{ of fuel electrochemically converted}}$$

$$= \frac{9.53 \times 10^{-4}}{\left[\frac{(MW)\ (HHV)}{nF}\right]}\ V_T\ \left(\frac{r+1}{r}\right) \tag{17}$$

where MW is the molecular weight of the fuel (in pounds), n is the number of electrons in the oxidation step, and HHV is the higher heating value of the fuel. If only hydrogen is converted electrochemically, then

$$\eta_T = 0.67\ V_T\ \left(\frac{r+1}{r}\right)$$

Performance characteristics for a mixed-conducting solid electrolyte can be calculated from equations (12), (13), (14), (15), and (17), given values for P_0 and σ_{ion}, by allowing r to take on all values from -1 to $-\infty$. Alternatively, the equations can be used to determine the value of the Schmalzried parameter, P_θ, required to yield the desired value of η_T.

Results

As mentioned above, the EPRI goal for a solid oxide electrolyte fuel cell is a total system heat rate of 7500 Btu/kwh which is equivalent to an overall thermal efficiency of 45.5%. In order to evaluate the required properties of the electrolyte, the efficiency of the electrochemical cell alone must be

separated from the total system efficiency. This separation will depend in general on the overall system design, but it is possible to establish a separation that is reasonably general. We assume a hydrocarbon fuel cell application which may: (a) oxidize the hydrocarbon directly in the fuel cell anode, (b) reform the hydrocarbon to hydrogen and carbon monoxide which is electrochemically oxidized. For the latter case, we define a reformer efficiency as

$$\eta_R = \frac{\Delta H^\circ \text{ of } H_2 \text{ and CO consumed}}{\Delta H^\circ \text{ of fuel into reformer}} \tag{18}$$

This definition of the reformer efficiency takes into account the degree of utilization of the H_2 and CO in the anode. Then the electrochemical cell thermal efficiency is defined as

$$\eta_T = \frac{\text{DC Power delivered by cell}}{\Delta H^\circ \text{ of } H_2 \text{ and CO consumed}} \tag{19}$$

and the inverter efficiency is, as usual,

$$\eta_I = \frac{\text{AC Power out}}{\text{DC Power delivered by cell}} \cdot \tag{20}$$

The overall efficiency, η, is then $\eta_R \eta_T \eta_I$.

Equations (18) and (19) are easily modified for the direct hydrocarbon fuel cell. In this η_R represents the product of the mole fraction of the hydrocarbon that can be electrochemically converted and the degree of utilization of the fuel, or

$$\eta_R = \frac{\Delta H^\circ \text{ of hydrocarbon consumed}}{\Delta H^\circ \text{ of fuel into system}} \tag{21}$$

Using reasonable values for η_R and η_I and $\eta = 45.5\%$, the required value for η_T is at least 50%, even for a direct hydrocarbon oxidation fuel cell.

For the sake of convenience, and comparison with experiment, pure H_2 will be used as the fuel. Since reversibility is assumed for the electrodes, the use of H_2 rather than a hydrocarbon changes only the open circuit potential and the value of P_{O_2} at the anode. It will be shown that these changes are relatively

small and do not affect the conclusions made using H_2 as the fuel. Kudo and Obayashi[4] have presented a complete analysis of cation reduction and the resulting ion-electron mixed conduction for $Ce_{1-x}Gd_xO_{2-(x/2)}$. For the composition described by x = 0.3, $\sigma_{ion} = 0.033$ (ohm-cm)$^{-1}$ and $P_\theta = 3.16 \times 10^{-19}$ atm. at 700°C[4]. Figure 2 is a graphical representation of equations (12), (13), (15), and (17) for this system with air at the cathode and $P_{H_2O}/P_{H_2} = 4$ at the anode (equivalent to the 80% hydrogen utilization). The curves have been plotted using I_{ext} (t/A) so that they are independent of geometry. For comparison, Figure 3 has been calculated for $(ZrO_2)_{0.93}(Y_2O_3)_{0.07}$, at a temperature (820°C) at which the conductivity of yttria-zirconia is the same as the ionic conductivity of gadolinia-ceria at 700°C.

One characteristic of mixed conduction in oxide electrolytes, as Figures 2 and 3 clearly demonstrate, is that the efficiency passes through a maximum with increasing current density, the maximum being located often at very high current density. The performances and thermal efficiencies of fuel cells using different electrolytes can be compared using two different bases: (1) at constant conductivity, and (2) at constant temperature. The comparison at constant conductivity normalizes the electrochemical cells to the same power density in the absence of any electronic conduction in the electrolyte. Since the capital cost of the fuel cell system is scaled by the power density, the comparison of different oxide electrolytes at constant conductivity is equivalent to an approximately constant capital cost basis. Based on present technology for fabricating thin (~ 100 μm), impervious, ceramic layers, 0.033 (ohm-cm)$^{-1}$ is a minimum conductivity needed to provide adequate power density (> 200 WSF) and reasonable capital cost[14]. Table 1 gives a comparison of the results at constant conductivity for several doped cerias against yttria-zirconia and demonstrates clearly that in H_2/air fuel cell applications, none of the doped cerias can provide thermal efficiencies greater than 40%. Table 2 shows the constant temperature comparison at an advanced power plant temperature of 700°C. While lanthanam doped ceria has a maximum efficiency close to 50%, the power density is too low to be of interest, and the efficiencies of the other ceria cells are far below 50%. The comparisons in Tables 1 and 2 of the performances of the yttria-zirconia cell with the doped-ceria cells clearly illustrate the severe efficiency penalty from the degree of electronic conduction occurring in doped cerias in H_2/air fuel cell applications.

One can legitimately question the validity of conclusions derived entirely from performances calculated from a theory. Performance measurements in our laboratory do confirm the essential elements in the theory of mixed conduction. Figure 4 shows a comparison of the experimental and calculated performance curves for a solid electrolyte of the ceria-gadolinia family. The values of σ_{ion} and P_{θ} measured independently for this material were 0.0672 $(ohm\text{-}cm)^{-1}$ and 3.05×10^{-20} atm., respectively. The cell configuration was

$$(1 \text{ atm. air, Pt}) \left|\left| (Ce_{1-x}Gd_xO_{2-x/2}) \right|\right| (\text{Pt, .97 atm. } H_2 + .03 \text{ atm. } H_2O)$$

The close agreement between the measured and calculated performance curves adds to the validity of the analysis of potential electrolyte materials using Wagner's theory of mixed conduction.

Discussion

Using the analysis presented here for the effect of mixed conduction on thermal efficiency, a map of the minimum properties required of oxide materials for use as solid electrolytes in H_2/air fuel cells can be drawn, as done in Figure 5, for ambient pressure cells. It is clear that none of the materials whose properties have been reported in the literature to date meet the requirements for a low temperature (700°C) application. The electronic conduction in the doped cerias is too high to meet efficiency requirements, and the conductivity of the doped zirconias is too low to provide both high power density (low capital cost) and high efficiency. While the map of Figure 5 applies only to H_2/air fuel cells, the general picture is the same for a hydrocarbon fuel cell. Changing the anode gas from a H_2-H_2O mixture to a H_2, CO, H_2O, CO_2 mixture does not result in a significant change in P_{O_2}', since the equilibrium constant for $CO + 1/2\ O_2 = CO_2$ is very close to that for $H_2 + 1/2\ O_2 = H_2O$ for the temperature range of interest[15]. The magnitude of the component of electronic conduction is affected by the value of the ratio of P_{H_2O}/P_{H_2} in the anode, but in the practical range of usage, e.g. 1 to 20, the boundary for P_{θ} in Figure 5 is not shifted significantly.

The total system pressure affects both power density and thermal efficiency. Because the gas pressures are raised to the 1/4 power in equation (12), substantial pressurization is required to produce any significant effect. In the case of the gadolinia-ceria electrolyte, pressurization to 100 atm. increased η_T from 40%

to only 46%, still well below the required efficiency. For yttria-zirconia, the effect of total pressure on the power density at 700°C for $\eta_T > 50\%$ was examined, and it was determined that pressurization within practical limits (~ 10 atm.) did not change the power density by more than 50%, still insufficient power density for use as a low temperature solid electrolyte.

The development of a low temperature solid electrolyte fuel cell satisfying the EPRI requirements for advanced power plants hinges on the discovery of oxides having both fast anion transport and a high resistance to the creation of excess electrons at low oxygen pressure by reaction (1). There is some indication that these two properties are not independent. If we define $\Delta\bar{H}$ as the partial molar enthalpy change for reaction (1), then the equilibrium constant, K, for this reaction will be

$$K = K_o \exp(-\Delta\bar{H}/RT) \tag{24}$$

Following the analysis of Kudo and Obayashi[4], it can be shown that

$$\sigma_e = (e\mu)\,(K_o/[V_o])^{1/2}\,(P_{O_2})^{-1/4} \exp(-\Delta\bar{H}/2RT) \tag{25}$$

where μ is the electron mobility, and $[V_o]$ the total number of oxygen vacancies in the lattice. For a fixed $[V_o]$, which is a function principally of the dopant level, and at a fixed P_{O_2}, the larger the $\Delta\bar{H}$ the smaller the level of electronic conduction. If the purely ionic component of conduction is represented in the usual way

$$\sigma_{ion} = \left(\frac{\sigma_i^o}{T}\right) \exp(-E_i/RT) \tag{26}$$

σ_i^o is a combination of material properties such as the number of anion vacancies, the lattice parameter, and the anion jump frequency, and E_i is the activation energy for oxygen ion conduction. Our survey of the published properties of doped zirconia and doped ceria indicated that the much higher ionic conductivities in doped ceria are a result of much larger σ_i^o values rather than a decrease in E_i. Further, as shown in Figure 6, a correlation was found between σ_i^o and $\Delta\bar{H}$ for doping levels in zirconia and ceria of less than 20 a/o. At higher doping levels, no correlation was found, probably due to vacancy ordering causing deviation from the behavior predicted by equation (26). The correlation of Figure 6 suggests there is a cause and effect relationship between high oxygen ion mobility in the lattice and relatively high volatility of oxygen ions from the lattice. The

values of $\Delta\bar{H}$ and σ_i^o required of a low temperature solid electrolyte are located in the upper right hand corner of Figure 6, assuming that E_i is approximately 0.7 eV. It is clear that the material properties required represent a substantial deviation in material behavior from that observed in the oxides studied to date.

Acknowledgements

The authors gratefully acknowledge the financial support of the Electric Power Research Institute (EPRI), Contract RP114, and the permission to publish this work. We thank Drs. T. Kudo and H. Obayaski of Hitachi Ltd for providing copies of their manuscripts prior to publication.

Table 1: Maximum Thermal Efficiencies at Constant Ionic Conductivity.

System	Ref.	T (°C)	P_θ (atm.)	P · (t/A) (watts/cm)	η_T (%)
$(ZrO_2)_{.93}(Y_2O_3)_{.07}$	12, 13	820	7×10^{-38}	0.0028	50.0
$(CeO_2)_{.82}(Gd_2O_3)_{.18}$	4	700	3.16×10^{-19}	0.0048	40.0
$(CeO_2)_{.67}(La_2O_3)_{.33}$	16	1040	3.91×10^{-15}	0.0030	36.5
$(CeO_2)_{.95}(CaO)_{.05}$	6	800	1.00×10^{-14}	0.0051	30.0
$(CeO_2)_{.95}(Y_2O_3)_{.05}$	5	842	1.13×10^{-13}	0.0050	28.0

Table 2: Maximum Thermal Efficiencies at Constant Temperature (700°C).

System	Ref.	σ_{ion} $(ohm\text{-}cm)^{-1}$	P_θ (atm.)	P · (t/A) (watts/cm)	η_T (%)
$(ZrO_2)_{.93}(Y_2O_3)_{.07}$	12, 13	0.0127	1.00×10^{-44}	0.0015	50.2
$(CeO_2)_{.82}(Gd_2O_3)_{.18}$	4	0.033	3.16×10^{-19}	0.0048	40.0
$(CeO_2)_{.67}(La_2O_3)_{.33}$	16	0.0014	1.34×10^{-26}	0.00017	49.5
$(CeO_2)_{.95}(CaO)_{.05}$	6	0.014	1.00×10^{-17}	0.0021	35.7
$(CeO_2)_{.95}(Y_2O_3)_{.05}$	5	0.0103	5.31×10^{-18}	0.0017	36.

References

1.) Final Report, Project Fuel Cell, Research & Development Report No. 57 (1970), Office of Coal Research, Department of Interior, Washington, D.C.

2.) E. F. Sverdrup, C. Warde and A. Glasser, in "From Electrocatalysis to Fuel Cells", ed. G. Sandstede, Univ. of Washington Press, Seattle and London, 1972, pp. 255-277.

3.) N. Maskalick and C. Sun, J. Electrochem. Soc., 118, 1386 (1971).

4.) T. Kudo and H. Obayashi, J. Electrochem. Soc., 122, 142 (1975); and J. Electrochem. Soc., 123, 415 (1976).

5.) H. Tuller and A. Nowick, J. Electrochem. Soc., 122, 255 (1975).

6.) R. Blumenthal, J. Brugner and J. Garnier, J. Electrochem. Soc., 120, 1230 (1973).

7.) Final Report to the Electric Power Research Institute, Contract RP114, Advanced Fuel Cell Technology Program, 1976.

8.) J. Patterson, J. Electrochem. Soc., 118, 1033 (1971).

9.) H. Schmalzreid, Zeit. Phys. Chem. (Frankfurt), 38, 87 (1963).

10.) C. Wagner, Zeit. Phys. Chem., B21, 25 (1933).

11.) N. Choudhury and J. Patterson, J. Electrochem. Soc., 118, 1398 (1971).

12.) D. Swinkels, J. Electrochem. Soc., 117, 1267 (1970).

13.) J. Dixon, L. LaGrange, U. Merten, C. Miller and J. Porter, J. Electrochem. Soc., 110, 276 (1963).

14.) H. Tannerberger, in "From Electrocatalysis to Fuel Cells", ed. G. Sandstede, Univ. of Washington Press, Seattle and London, 1972, pp. 235-246.

15.) J. Smith and H. van Ness, "Introduction to Chemical Engineering Thermodynamics", McGraw-Hill, Inc., New York, 1959, p. 423.

16.) T. Takahashi, K. Ito and H. Iwahara, Proc. J. Inter. d'Etudes des Piles on Combustile III (Brussels 1965), p. 42.

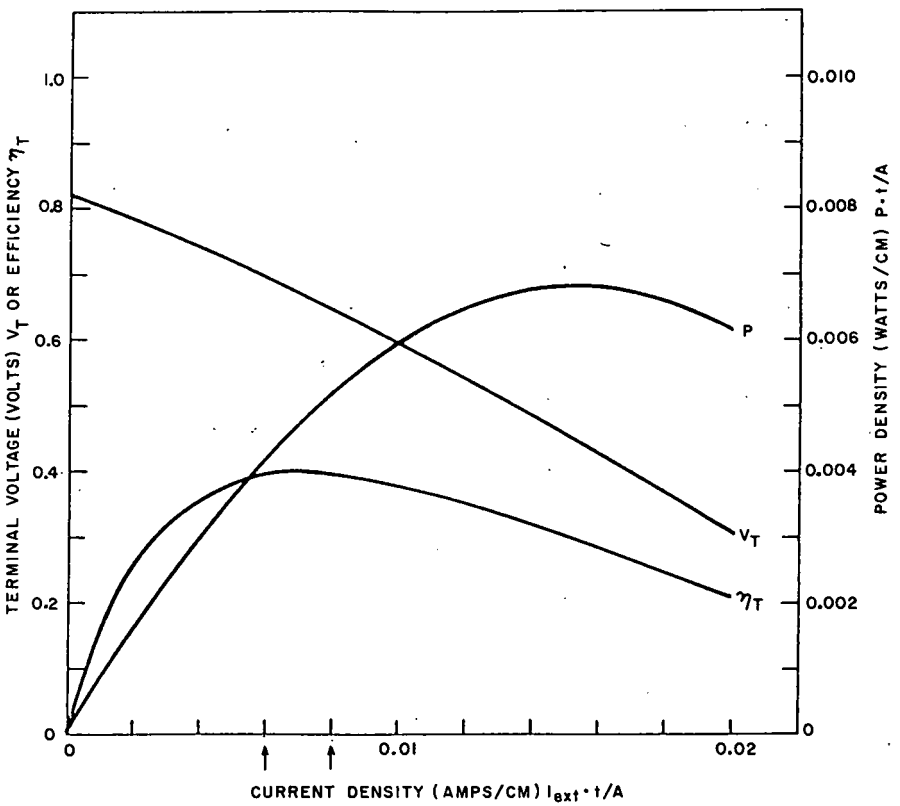
1.0
0.8
0.6
0.4
0.2
0
0.010
0.008
0.006
0.004
0.002
0
0.01
0.02
P
V_T
η_T
TERMINAL VOLTAGE (VOLTS) V_T OR EFFICIENCY η_T
POWER DENSITY (WATTS/CM) P·t/A
CURRENT DENSITY (AMPS/CM) I_{ext}·t/A

Figure 2.

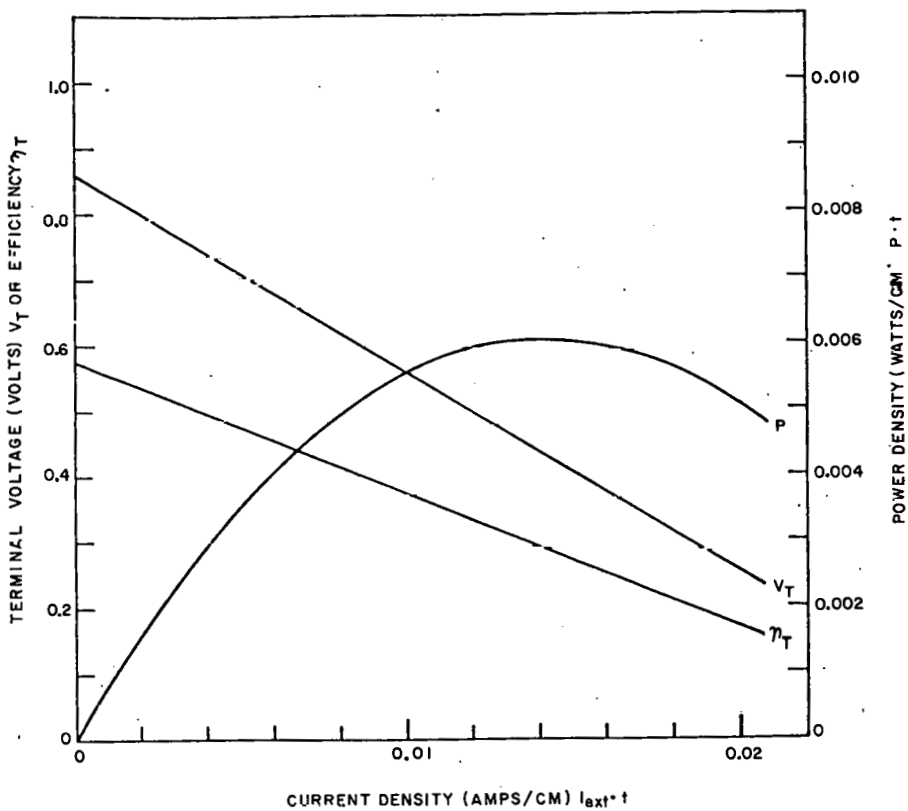
TERMINAL VOLTAGE (VOLTS) V_T OR EFFICIENCY η_T
POWER DENSITY (WATTS/CM^3) P·t
CURRENT DENSITY (AMPS/CM) I_{ext}·t
1.0
0.8
0.6
0.4
0.2
0
0.010
0.008
0.006
0.004
0.002
0
0.01
0.02
P
V_T
η_T

Figure 3.

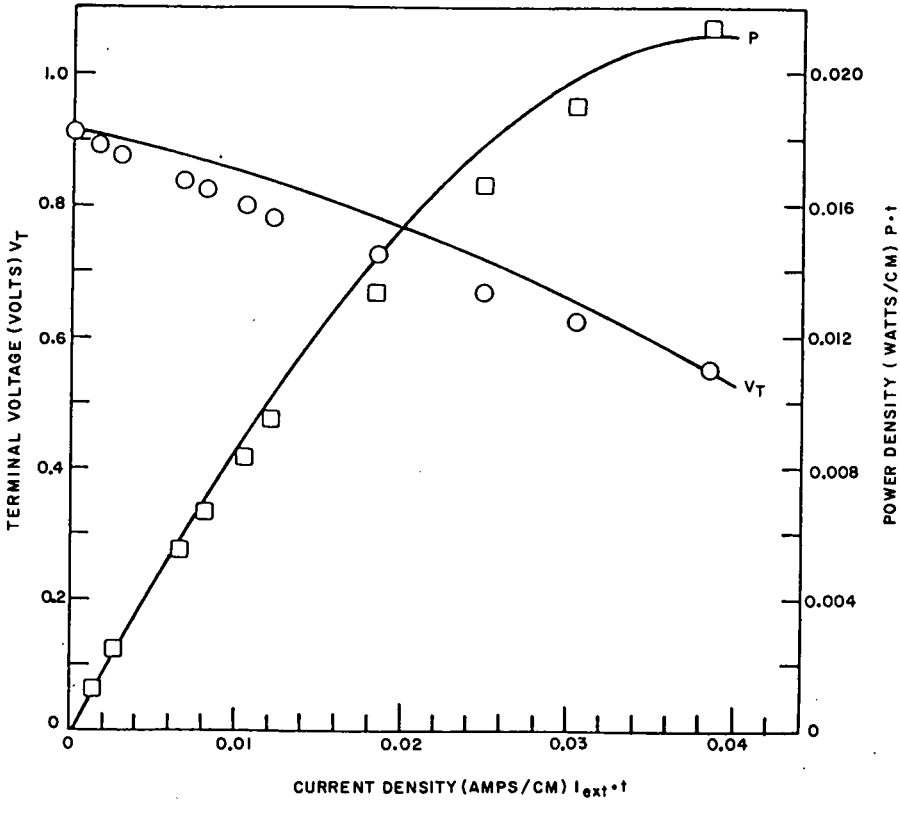
P
V_T
1.0
0.8
0.6
0.4
0.2
0
0.020
0.016
0.012
0.008
0.004
0
0.01
0.02
0.03
0.04
TERMINAL VOLTAGE (VOLTS) V_T
POWER DENSITY (WATTS/CM) P•t
CURRENT DENSITY (AMPS/CM) I_{ext}•t

Figure 4.

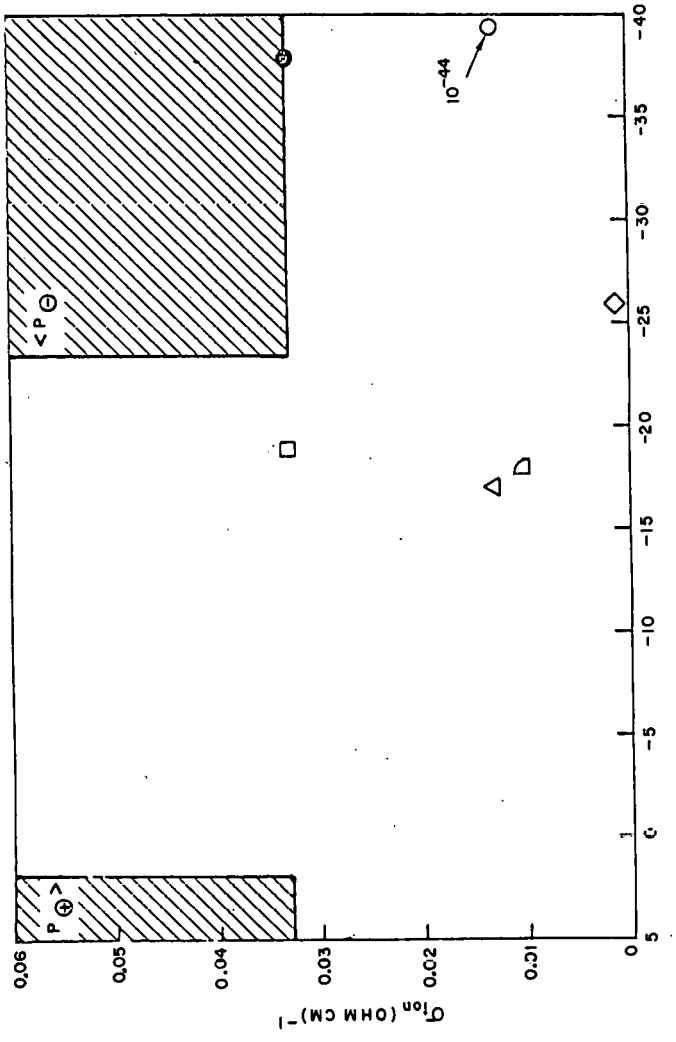
σ_{ion} (OHM CM)$^{-1}$
0.06
0.05
0.04
0.03
0.02
0.01
0
5
1
0
-5
-10
-15
-20
-25
-30
-35
-40
LOG $P_{\oplus}$ OR $P_{\ominus}$
$P_{\oplus}$ >
< $P_{\ominus}$
10^{-44}

Figure 5.

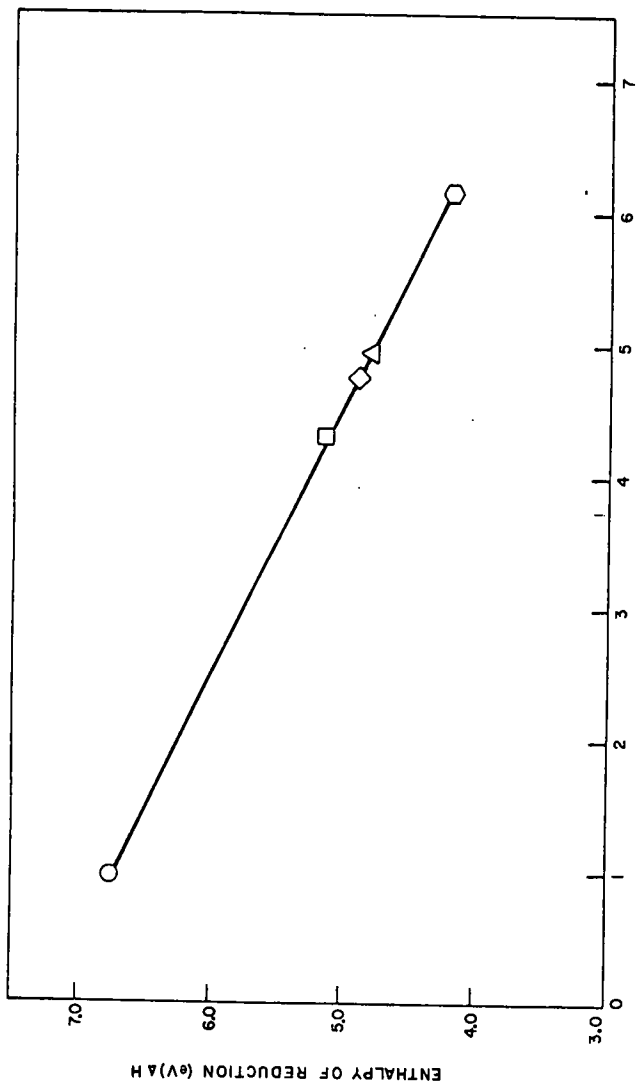

Figure 6.

☆ U.S. GOVERNMENT PRINTING OFFICE:1978—0-714-079/12